



Politecnico di Torino

DIPARTIMENTO DI INGEGNERIA CHIMICA E DEI MATERIALI
Corso di Laurea in Ingegneria chimica e dei Processi Sostenibili

TESI DI LAUREA MAGISTRALE

Transport and Fate of TiO_2 nanoparticles in soil and aquifers

Candidato:
Jacopo De Tommaso

Relatore:
Dr. Tiziana Tosco

Correlatori:
Prof. Alberto Tiraferri
Prof. Natalie Tufenkji

Dicembre 2017

Contents

Sommario	v
1 Introduction	1
1.1 The time's arrow	1
1.2 Nanoscience, Nanomaterials and Nanoparticles	3
1.3 Nanoparticles: diffusion and applications	6
1.3.1 Diffusion of nanoparticles according to CPI	6
1.3.2 Estimating Production Data approach	7
1.3.3 Metallic nanoparticles	7
1.4 TiO ₂ : light and shade	11
1.4.1 The most commonly used nanoparticle	11
1.4.2 Enviromental impact	12
1.4.3 Potential threats	13
1.4.4 Transformation of Nanoparticles in the Environment	13
1.5 Objectives and organization of the thesis	16
1.5.1 Objectives	16
1.5.2 Outline	16
2 Theoretical Background	17
2.1 Colloidal Interactions	17
2.2 DLVO Theory	17
2.2.1 VDW interactions	17
2.2.2 Electrical Double-Layer interactions	19
2.2.3 Born repulsion	23
2.2.4 NON-DLVO Interactions	24
2.3 DLVO and aggregation	25
2.4 Aggregation	27
2.4.1 Fast aggregation	29
2.4.2 Slow aggregation and efficiency of aggregation	31
2.4.3 Critical coagulation concentration	31
2.4.4 Aggregate structure	32
2.5 Colloidal transport in porous media	33
2.6 Deposition	34

CONTENTS

2.6.1	Yao 1971	34
2.6.2	Tufenkji Elimelech 2004	36
2.6.3	Messina, Marchisio, Sethi 2016	37
2.6.4	Convective-diffusion equation and colloid filtration theory	39
3	Material and Methods	43
3.1	Preparation of nanoparticles suspensions	43
3.2	Column Tests	45
3.3	Nanoparticles Characterization	46
3.4	Freeze/Thaw	49
4	Results and Discussion	51
4.1	Nanoparticle properties: Size, Zeta, Stability (TRDLS)	51
4.1.1	10°C experiments	51
4.1.2	Freeze/Thaw Data: EPM	57
4.1.3	Size: Hydrodynamic diameter and Polydispersity	58
4.1.4	DLVO Profiles	62
4.2	Deposition Experiments	65
4.2.1	Role of Salinity and NOM at 10 °C	67
4.2.2	Freeze/Thaw Deposition study	72
4.3	Conclusion and future work	76
4.3.1	Environmental Impact	76
4.3.2	Future work	76

Ai miei nonni, per avermi insegnato l'importanza delle cose semplici.

Sommario

Introduzione

Il mercato globale delle nanoparticelle è in continua evoluzione, già nel 2015 era stimato essere intorno ad 1 miliardo di US \$ ed è tuttora in crescita esponenziale. Alla nanoscala le equazioni di stato dei materiali, e quelle riguardando i loro fenomeni di trasporto (legge di Fourier della conduzione, legge di Fick della diffusione, legge di Newton per la viscosità, *etc.*) possono risultare inesatte. Inoltre, vista lo sviluppo dinamico del mercato e la poliedricità delle sue applicazioni, non esistono tutt'oggi delle definizioni univoche di nanomateriali e nanoparticelle. In linea generale, la definizione del 2011 della commissione europea nel documento "Types and uses of nanomaterials, including safety aspects", è la più accreditata per quanto riguarda i nanomateriali. Le nanoparticelle sono invece generalmente riconosciute essere tutte quelle entità con granulometria tra 1-100 nm. Da un punto di vista scientifico, sarebbe più propriamente corretto riferirsi a nanostrutture piuttosto che a nanofasi o nanoparticelle. In quest'ottica è facile comprendere come, strutture 1D come nanofibers, 2D come nanolayers o nanotubi e strutture 3D come fullereni, dendrimeri o quantum dots, possano tutte essere catalogate sotto il termine nanoparticelle. Soffermandosi sulle loro peculiarità, non dovrebbe quindi stupire il crescente utilizzo delle nanoparticelle in ogni ambito, tecnico e non. Infatti, le proprietà dei materiali alla nano scala sono diverse per due motivi fondamentali:

- **Maggiore superficie specifica.** Visto che superficie scala con il quadrato della dimensione e il volume con il cubo, a parità di dimensione, il rapporto S/V è maggiore per particelle più piccole. Questo comporta profondi cambiamenti rispetto al materiale bulk nelle proprietà elettriche, meccaniche, termiche e può inoltre influenzare la loro reattività chimica.
- **Effetto quantico.** A causa delle dimensioni delle particelle, gli elettroni sono confinati in uno spazio minore, con una minore mobilità. Questo li porta a reagire in maniera diversa a fronte di eccitazioni luminose, andando perciò ad influenzare le proprietà elettriche e magnetiche della materia.

Grazie a superiori proprietà ottiche, catalitiche, termiche, meccaniche ed elettriche, le nanoparticelle trovano impiego sia su grande che piccola scala, da prodotti per

il benessere personale come cosmetici o preparati dermatologici, all'industria automotive, fino a vernici, rivestimenti per superfici autopulenti, materiali da costruzione, ma anche come superconduttori in sistemi di rilevamento innovativi o persino come carrier genetici o nel trattamento del cancro.

L'indice CPI (Nanotechnology Consumer Products Inventory), introdotto per la prima volta nel 2005, ed aggiornato nel 2015, si è imposto nel tempo come cartina al tornasole della nanotecnologia all'interno di prodotti di consumo. Questo catalogo i prodotti a largo consumo in termini di nanoparticelle per prodotto, specificando il tipo di nanomateriale utilizzato e la sua composizione, come dichiarato dal produttore. Tuttavia, come appare chiaro in Fig.1.4, l'approccio CPI qualitativamente, ma non quantitativamente corretto. Infatti, studi di mercato su scala mondiale riescono non solo a quantificare in termini di *tons/yr* le nanoparticelle prodotte, ma anche gli esatti rapporti relativi tra tipi di nanoparticelle in termini massici. Appare quindi evidente come, unendo un approccio euristico (CPI) ed uno algoritmico (studi e prospetti di mercato), si riesca ad inquadrare il problema nella sua totalità. Le nanoparticelle metalliche rappresentano circa il 63 % del totale prodotto e, tra queste, la frazione maggiore (45 %) è occupata dal biossido di titanio $n\text{TiO}_2$. Questo, grazie alla sua capacità di assorbire le radiazioni UV, è largamente presente in cosmetici e lozioni per il corpo. Inoltre, il suo alto indice di rifrazione lo colloca virtualmente in ogni tipo di vernice come pigmento bianco e la sua elevata reattività fotocatalitica ne fa tecnologia consolidata in superfici autopulenti, trattamento di acque reflue e disinfezione di superfici.

Figura 1.4 (b) mostra come, grazie ad un bilancio di massa integrato sul ciclo-vita delle particelle, sia possibile modellare loro flusso, dalla produzione al rilascio/smaltimento. In questo modo ci sia accorge di come proprio a causa della sua larghissima diffusione, il $n\text{TiO}_2$ viene rilasciato in ambiente in quantità considerevoli. Si è stimato che gran parte del biossido di titanio prodotto a livello mondiale finisca, in maniera diretta od indiretta, in ecosistemi acquiferi. La restante parte si ripartisce tra smaltimento in discarica e rilascio nel suolo. Quest'ultimo contributo, è a sua volta costituito da una percentuale maggioritaria di slime biosolidi prodotti in seguito a processi di smaltimento acque reflue. In definitiva, circa il 70% dell' $n\text{TiO}_2$ globalmente prodotto viene rilasciato in, o perlomeno passa attraverso, ecosistemi acquiferi. Per questo motivo, negli anni si è cercato di far luce su quali potessero essere le conseguenze di tale rilascio, sia sull'uomo che sull'ecosistema. Effettivamente, studi *in vivo* ed *in vitro*, dimostrano che il $n\text{TiO}_2$ possa essere potenzialmente dannoso per umani, roditori, pesci, batteri ed altri organismi che ne vengano a contatto. Da qui la necessità crescente di far luce sulla sorte del biossido di titanio una volta rilasciato. Il rischio potenziale associato alle nanoparticelle è fortemente dipendente dalla loro mobilità e dalle trasformazioni fisico-chimiche alle quali possono essere sottoposte. Tra queste, particolare importanza assumono trasformazioni di tipo chimico (es. ossido-riduzioni), fisico (aggregazioni in cluster), biologico (es. reazioni redox mediate da microrganismi viventi) e trasformazioni dovute all'interazione con macromolecole (es. NOM, polisaccaridi, proteine). Alla luce di ciò, gli obiettivi di questo lavoro sono

molteplici:

- Cercare di riprodurre, allo stato dell'arte degli studi in colonna, un ambiente che quanto più possibile simuli quello di rilascio, in termini di forza ionica (IS), eventuale presenza di ioni bivalenti, temperatura, composizione chimica della soluzione, pH, con particolare attenzione alle eterogeneità geochimiche, prima tra tutte la presenza di NOM (natural organic matter).
- Studiare aggregazione e deposizione delle $n\text{TiO}_2$ nel sistema in questione, cercando al contempo di correlarle con il cambiamento delle condizioni ambientali cui sopra.
- Utilizzare due diverse qualità di nanoparticelle di biossido di titanio, in maniera da confrontare il comportamento di una nanoparticella "da laboratorio", con quello di una realmente utilizzata a livello industriale.
- Cercare di riprodurre condizioni climatiche diverse per capire come le nanoparticelle si comportino se sottoposte a cicli di congelamento/decongelamento, con lo scopo di rappresentare un ecosistema acquifero durante un inverno canadese "standard".

Per far ciò si è ricorso a prove di aggregazione e deposizione sotto diverse condizioni di temperatura, salinità e concentrazione di NOM. In particolare, l'aggregazione è stata studiata mediante prove di caratterizzazione del diametro medio, della polidispersità e delle proprietà elettrocinetiche degli aggregati. La deposizione è stata invece investigata conducendo prove in colonna impaccata con sabbia quarzosa. Entrambe, aggregazione e deposizione, sono state studiate in condizioni di temperatura pari a 10 °C ed in seguito a test di congelamento/scongelamento dei campioni di $n\text{TiO}_2$. L'intero lavoro di tesi è stato svolto presso il dipartimento di ingegneria chimica della McGill University di Montreal.

Interazioni energetiche in sospensioni colloidali

Il comportamento delle nanoparticelle all'interno di un ecosistema acquatico, le interazioni tra loro e con l'ambiente stesso, sono regolate da numerosi fattori, quali proprietà morfologiche di bulk e superficie (forma e dimensioni, composizione chimica, carica superficiale ed eventuale presenza di coating), peculiarità chimico-fisiche dell'acquifero (pH, forza ionica (IS), temperatura, composizione ionica, presenza NOM) e caratteristiche idrodinamiche del sistema. In particolare, L'NOM è composto da una grande varietà di composti organici, sia ad alto che a basso peso molecolare, quali acidi organici, carboidrati semplici e complessi, materiale celluloso, proteine, lipidi, *etc...* Proprio a causa della sua virtualmente infinita peculiarità reattiva, sussistono ancora alcuni dubbi circa il suo effetto all'interno di sistemi colloidali. Questo è tuttavia generalmente ritenuto potersi adsorbire sulla superficie delle nanoparticelle, caricandole negativamente

ed amplificando la repulsione energetica dovuta all'EDL, questo in genere porta ad una maggiore mobilità ed alla formazione di aggregati più piccoli. Inoltre, può stabilizzare una sospensione di nanoparticelle, attraverso la complessazione di gruppi acidi carbossilici. Esso è generalmente compreso in una quantità variabile (1 - 20 mg/L) all'interno di ambienti acquiferi, ed è un derivato della decomposizione di materiale animale e vegetale presente nell'ecosistema. All'interno di sistemi colloidali, ovvero miscele formate da una fase continua disperdente e da una sostanza dispersa di dimensioni microscopiche, queste interazioni sono tradizionalmente descritte dalla teoria DLVO. Tali interazioni energetiche si esplicano quindi nei fenomeni di aggregazione e deposizione.

Teoria DLVO

La teoria DLVO classica, descrive la stabilità delle nanoparticelle sospese in una soluzione acquosa, come effetto combinato di interazioni tra forze macroscopiche attrattive di Van der Waals (VDW) e forze repulsive dovute alla presenza del doppio strato elettrico (EDL) (Eq.2.1).

Le interazioni attrattive di VDW tra due corpi provengono dalla somma puntuale di interazioni microscopiche tra ogni molecola di ciascun corpo. Tali interazioni microscopiche (Eq.2.2) sono fondamentalmente interazioni microscopiche intermolecolari *dipolo temporaneo - dipolo indotto* di tipo dispersivo. In linea generale, due corpi che si attraggono a causa di interazioni VDW, presentano un'energia attrattiva del tipo:

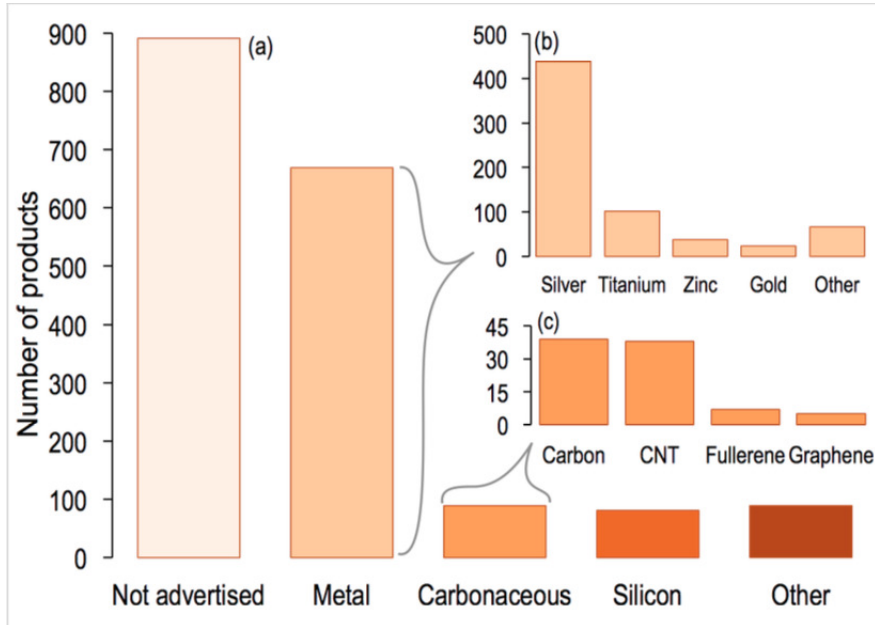
$$\Phi = A \cdot f(h, h/\sigma) \quad (1)$$

dove f è un fattore geometrico, σ è lo spessore dell'oggetto fino al quale le interazioni hanno importanza, h è la distanza di minimo approccio ed A è la costante di Hamaker, che nel caso di una sfera può essere definita come:

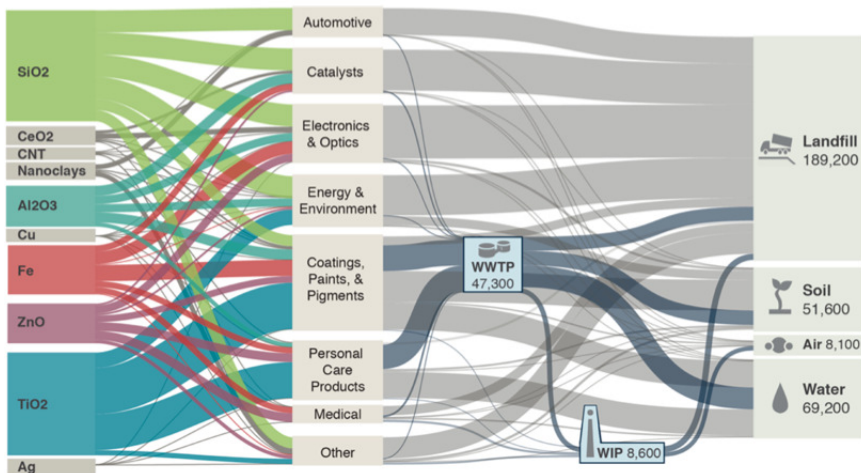
$$A = \pi^2 \rho_N \beta \quad (2)$$

con ρ_N densità molecolare del corpo e β che dipende dalle proprietà magnetiche ed elettriche del materiale. Da un punto di vista pratico, prendendo ad esempio due sfere, interazioni microscopiche di VDW di corto raggio che decadrebbero a $0,2 - 0,3nm$, generano interazioni macroscopiche di lungo raggio, che decadono a $20 - 40nm$. La tabella 2.2 del corpo principale del testo, riporta le espressioni per valutare le interazioni di VDW nella loro forma più recente, e nelle configurazioni geometriche più comuni (sfera - sfera; piano - sfera).

Le forze repulsive di doppio strato elettrico sono sostanzialmente causate da una separazione di carica all'interfaccia solido-liquido di un sistema colloidale. Quando una particella è carica, questa richiama attorno a sé ioni di carica opposta dalla soluzione circostante. Tali ioni si accumulano nell'intorno della superficie carica, disponendosi in una struttura chiamata "doppio strato elettrico". La carica superficiale può avere origini differenti, ma nel caso particolare del nTIO₂, è dovuta alla dissociazione di gruppi superficiali OH⁻ ed H⁺. Questi ioni sono chiamati *ioni che*



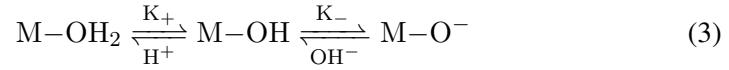
(a) *Composizione dichiarata secondo il CPI. I nanomateriali sono raggruppati in cinque categorie fondamentali: metalli (includono anche gli ossidi metallici), nanomateriali a matrice carboniosa (carbon black, nanotubi di carbonio, fullereni, grafeni), nanomateriali a base silicica (silicone e silice), altri (organici, polimeri, ceramici, etc.) ed i "not advertised".*



(b) *Portata stimata globale massica di ENMs (in tonnellate per anno), dalla produzione allo smaltimento/rilascio. Dati considerati fino all'anno 2010.*

Figure 1: Confronto tra l'approccio CPI e quello Estimating Production Data. Figura da [30] e [34]

determinano il potenziale di prima classe, e di conseguenza l'entità della carica superficiale dipende dal pH della soluzione, come segue:



Dove M è la superficie metallica e K_+ e K_- sono le costanti di protonazione. L'equilibrio mostra come i gruppi idrossili superficiali si possano comportare come acidi o come basi, a seconda che il pH sia rispettivamente basico o acido. In altre parole, a pH acidi, la superficie sarà carica positivamente, e viceversa a pH basici, con il punto a densità di carica superficiale nulla che prende il nome di PZC (point of zero charge). Per quanto concerne il $nTiO_2$, il PZC si colloca attorno a pH 6 - 7, a seconda del diametro medio delle particelle e della loro forma allotropica.

Nonostante sia stato modificato a più riprese, un buon compromesso per visualizzare la struttura del doppio strato è ancora il modello di Stern [95] (Fig.2.2). Questo divide il doppio strato in due sezioni differenti, un layer interno ed uno esterno. La zona interna consiste in un monolayer di controioni, attraverso il cui centro passa un piano chiamato piano di Stern. Viceversa la zona esterna consiste nello strato diffuso, composto dagli ioni in soluzione richiamati sul solido dalla sua carica superficiale. Lo strato diffuso bilancia la carica interna data dalla somma di quella superficiale e quella del piano controionico. La distanza alla quale gli effetti elettrici del doppio strato decadono, è $1/\kappa$, lunghezza di Debye, definita come:

$$\kappa^{-1} = \left(\frac{k_B T \epsilon_0 \epsilon_r}{2q^2 N_A I} \right)^{1/2} \quad (4)$$

dove q è la carica superficiale, N_A il numero di Avogadro, I la forza ionica della soluzione, k_B la costante di Boltzmann, T la temperatura in Kelvin, $\epsilon_{0,r}$ le costanti dielettriche rispettivamente nel vuoto e nel mezzo. La forza repulsiva dovuta al doppio strato elettrico è dovuta ad una situazione di diffusione impedita. Ad esempio, ipotizzando una superficie positivamente carica, il campo elettrico superficiale, impedisce la diffusione degli ioni negativi dallo strato diffuso al bulk e, contemporaneamente, quella degli ioni positivi dal bulk verso la superficie. Sarebbe quindi possibile dimostrare come questa situazione di diffusione impedita, generi una forza sull'interfaccia solido-liquido. Nel caso di due particelle ugualmente cariche che vengono a contatto, questa forza repulsiva risultante dipende da κ , quindi dalla forza ionica IS della soluzione, e dal potenziale superficiale, a sua volta legato principalmente alla concentrazione degli ioni che determinano il potenziale (Tabella 2.2).

Interazioni NON-DLVO

La teoria DLVO classica non riesce tuttavia a descrivere in maniera quantitativamente esauriente prove sperimentali di aggregazione per un nutrito numero di particelle. E' necessario quindi introdurre alcune forze a lungo raggio addizionali,

in maniera da riuscire a spiegare molti dei fenomeni aggregativi. Tra queste, le più importanti sono le forze d'interazione magnetica, sterica, di bridging colloidale, di deplezione ed infine quelle di interazione idrofilica/idrofobica. Indubbiamente, per quanto riguarda il comportamento di nTiO₂ in un ambiente naturale, le forze steriche, quelle di bridging e deplezione, assumono particolare rilevanza.

Le interazioni steriche rappresentano un processo di stabilizzazione della soluzione quando al suo interno sono presenti polimeri o polielettroliti che si adsorbono superficialmente sulle particelle colloidali. Quando una sospensione elettrocratica (per la quale vale la teoria DLVO), presenta anche fenomeni sterici, l'interazione sterica e quella di doppio strato elettrico, possono agire assieme per dare una stabilizzazione *elettro-sterica*, proprio come nel caso dell'NOM. In questo caso, il polielettrolita è sì adsorbito sulla superficie delle particelle, ma porta con sé ancora abbastanza massa molare da riuscire a creare uno spesso ulteriore film superficiale carico sulla sua superficie. Inoltre, quando generalmente la concentrazione del polielettrolita non è tale da permettere un ricoprimento completo delle particelle ($< 50nm$), una stessa frazione della catena polielettrolitica può adsorbirsi su due o più particelle contemporaneamente, destabilizzando *bridging* la sospensione. Allo stesso modo, quando la concentrazione del adsorbente è molto alta e nella sospensione vi è polielettrolita libero, questi può destabilizzare il colloide con flocculazione depletiva.

DLVO ed Aggregazione

Per quanto riguarda le nanoparticelle di biossido di titanio, generalmente tutte le interazioni al di fuori di quelle steriche e DLVO, sono generalmente trascurabili. In quest'ottica, sarebbe teoricamente possibile prevedere l'andamento dei profili di potenziale a partire dalla chimica della soluzione. Ad esempio, andando ad agire sulla forza ionica della soluzione e/o sugli ioni che determinano il potenziale, il profilo del contributo DLVO lentamente shifta tra EDL repulsivo a VDW attrattivo, con quest'ultimo che presenza una buca di potenziale chiamata *buca primaria di potenziale*. Inoltre, considerando il contributo sterico come additivo ed indipendente dagli altri (inesattezza che permette la descrizione qualitativa del sistema), un ricoprimento più spesso diminuisce la profondità della *buca secondaria di potenziale*. La figura 2 aiuta a visualizzare i profili di potenziale al variare della distanza tra le particelle.

Una sospensione colloidale dove agiscono, in prima battuta additivamente, solo le interazioni DLVO e quelle steriche, presenta tre grandezze fondamentali che ne determinano il comportamento. Le già citate buche di potenziale e la barriera energetica H_{barr} . Le buche di potenziale sono buche attrattive all'interno delle quali le particelle aggregano per *coagulazione* o *flocculazione*. Viceversa, H_{barr} è appunto la barriera energetica che le particelle, devono superare per poter formare aggregati. Inoltre H_{barr} è anche discriminante la velocità di aggregazione. In linea generale, ci sono tre condizioni possibili:

- $H_{barr} > 10k_B T$. **Non si ha aggregazione**

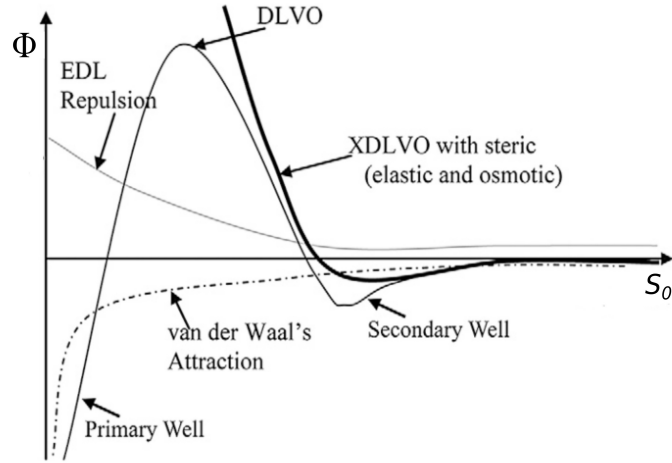


Figure 2: interazioni DLVO e NON-DLVO. Van der Waals (linea tratteggiata), doppio strato elettrico (linea grigia), forze DLVO e forze steriche plottate assieme al variare della distanza tra le particelle. Figura modificata da [98].

- $0 < H_{barr} < 10k_B T$. **Aggregazione lenta o a controllo cinetico.**
- $H_{barr} < 0$. **Aggregazione veloce o a controllo diffusivo.**

Quando la buca secondaria è presente, come ad esempio nel caso dell' nTiO₂, e non è profonda più di pochi $k_B T$, è possibile che le particelle aggregino in una maniera debole come flocculati, facilmente distruttibili introducendo una leggera turbolenza nella sospensione.

Un modo per quantificare l'entità del processo aggregativo, è α_a , ovvero quella probabilità di "sticking" che le particelle della sospensione hanno una volta che si avvicinano tra loro. Nel caso in cui la chimica della soluzione sia favorevole, e quindi H_{barr} sia bassa, α_a è 1 perchè ogni contatto porta alla formazione di un aggregato. Quando invece la barriera energetica è troppo alta, le particelle devono superarla grazie alla propria energia cinetica. Per l'analogia che si viene a creare tra questo processo e lo step di formazione del complesso di transizione all'interno di una reazione chimica, questa condizione si chiama a cinetica controllante, come se H_{barr} fosse un'intrinseca energia di attivazione. Nel caso a cinetica controllante, α_a può essere definito come:

$$\frac{1}{\alpha_a} \approx \frac{1}{2\kappa a} \exp(H_{barr}/kT) \quad (5)$$

dove κ è la lunghezza di Debye ed a è il raggio della particella nell'ipotesi in cui la

sospensione sia formata da particelle circa monodisperse. Tale formulazione suggerisce come α_a sia strettamente correlata con la chimica della soluzione. Quando IS è alta, H_{barr} è bassa a causa della compressione del doppio strato elettrico. Viceversa, diminuendo la forza ionica, la barriera energetica diventa importante e quindi gradualmente diminuisce anche la velocità di aggregazione. In altri termini, lavorando sulla IS e sulla concentrazione di ioni che determinano il potenziale, ovvero sulla densità di carica superficiale del solido, è possibile regolare la velocità del processo aggregativo, e quindi muoversi tra $\alpha_a(fast)$, sempre vicino ad 1, ed $\alpha_a(slow)$, sempre minore di 1. Quella concentrazione di elettrolita per la quale $H_{barr} = 0$, è la CCC, cioè concentrazione critica di coagulazione, definita come:

$$CCC \propto \frac{1}{z^6 A_{121}^2} \tanh\left(\frac{ze\phi_\delta}{4k_B T}\right) \quad (6)$$

Dove ϕ_δ è il potenziale allo strato di Stern e A_{121} la costante di Hamaker che descrive l'interazione tra due particelle "1" nel mezzo "2". Questo dimostra come CCC dipenda sia da z , valenza dello ione disperso, che da ϕ_δ , potenziale di Stern.

Deposizione e Teoria della filtrazione in un sistema colloidale

Una volta all'interno di un mezzo poroso, è possibile modellare il trasporto delle nanoparticelle utilizzando l'equazione di advezione-dispersione. Le particelle sono ovvero trasportate attraverso advezione e dispersione nel fluido, ed a loro volta si scambiano con il grano solido. Questo scambio in massa netto per unità di tempo si esplica attraverso attachment e detachment delle particelle sul collettore e dipende dalla concentrazione di colloidale adeso e sospeso. Così come l'aggregazione può essere teoricamente divisa in contatto e formazione di un aggregato primario con efficienza di formazione pari proprio al coefficiente di sticking α_a , allo stesso modo è possibile visualizzare la deposizione di particelle colloidali su una superficie come un processo multi-step. Il primo step consiste nel trasporto delle particelle sospese dal bulk del liquido fino al grano solido, il collettore, quell'oggetto con dimensioni molto maggiori di quelle delle particelle, sul quale esse si vanno a depositare. Il secondo comprende l'eventuale deposizione delle particelle sul collettore stesso. Analogamente al processo aggregativo, il secondo step è governato da un'efficienza di deposizione α_d , che rappresenta la frazione efficiente di particelle che rimangono adese al collettore dopo il contatto. Il primo step, quello di trasporto, è definito da una seconda efficienza, η_o , efficienza al contatto, definita come il rapporto tra la velocità overall con la quale le particelle si depositano sul collettore, diviso il trasporto convettivo di particelle verso l'area d'impatto del collettore. Il prodotto tra queste due efficienze da η l'efficienza alla rimozione, un'efficienza di processo che tiene conto delle efficienze dei due meccanismi in serie.

Trasporto e deposizione di una particella su un collettore, sono descritti, nella loro forma più generale, come divisi in tre step fondamentali:

-
- **Intercettamento.** Quando una particella sospesa, seguendo la linea di flusso del liquido, viene a contatto con un collettore a causa delle loro reciproche dimensioni.
 - **Sedimentazione per gravità.** Quando le particelle hanno una densità molto diversa rispetto a quella del fluido, esse tenderanno a modificare la loro traiettoria rispetto alle linee di flusso. Questo effetto le porterà ad impattare sul collettore secondo traiettorie dettate dal campo gravitazionale, da qui il nome del meccanismo in questione.
 - **Diffusione Browniana.** Tutte le particelle, in maniera proporzionale alle proprie dimensioni ed alle interazioni con il fluido, impattano il collettore muovendosi di moto Browniano.

L'equazione di trasporto delle particelle in un mezzo poroso, nella sua forma euleriana, risulta essere [120]:

$$\frac{\partial C}{\partial t} + \nabla \cdot (vC) = \nabla \cdot (D \cdot \nabla C) - \nabla \cdot \left(\frac{D \cdot F}{k_B T} C \right) \quad (7)$$

Dove C è la concentrazione di particelle, t è il tempo, D è il tensore di diffusione, v è la velocità delle particelle indotta dal mezzo nel quale sono sospese, T è la temperatura assoluta ed F è il vettore delle forze esterne che, in questo caso, sono rappresentate dalla forza gravitazionale e dalle forze colloidali, ovvero le forze generate da interazioni DLVO e NON-DLVO. I termini a sinistra dell'uguale rappresentano rispettivamente l'accumulo (spesso trascurabile) ed il trasporto convettivo. Invece i termini a destra dell'uguale rappresentano il trasporto indotto dalla diffusione e dalle forze esterne. L'equazione di trasporto non ha una soluzione analitica, tuttavia è possibile, utilizzando un'approccio numerico, ricavare η_0 e da questa, tramite un approccio sperimentale, il parametro semiempirico α_d . Per fare ciò è necessario ricorrere a prove in colonna riempita di materiale granulare poroso ed al cui interno si inietta una sospensione con una data concentrazione di particelle C_0 , per un tempo t_0 . Scegliendo opportunamente la lunghezza d'onda λ , è possibile monitorare in continuo l'effluente della colonna in termini di concentrazione di nanoparticelle. Perciò, iniettando la sospensione desiderata con una velocità d'approccio costante, è possibile ottenere curve di breakthrough, dalle quali ricavare il valore medio di C/C_0 , con C concentrazione delle particelle in uscita dalla colonna. In questo modo, all'interno della teoria CFT, è possibile correlare le efficienze α_d ed η_0 , come:

$$\alpha_d = -\frac{2d_c}{3(1-f)\eta_0 L} \ln(C/C_0) \quad (8)$$

dove L è la dimensione caratteristica del mezzo filtrante, f è la porosità del letto, d_c è il diametro nominale del collettore e C/C_0 è la concentrazione di particelle eluite, normalizzata su quella delle particelle filtrate in condizioni di *clean bed*

filtration, all'inizio della curva di breakthrough. Negli anni, numerose soluzioni analitiche e numeriche, sono state proposte per ricavare η_0 e quindi, in maniera semi-empirica, ricavare α_d . Tra queste, le più accreditate tutt'oggi probabilmente sono quella di Tufenkji-Elimelech del 2004 [108] e quella elaborata da Messina Marchisio Sethi [115] nel 2016:

La definizione di tutti i termini comprendenti le equazioni, del loro significato fisico, delle assunzioni necessarie alla derivazione e delle condizioni al contorno utilizzate, si possono ricercare nelle sezioni 2.5.3 e 2.5.4 del corpo principale di tesi.

Materiali e Metodi

Due tipi di nTiO₂ sono state utilizzate per studiarne il trasporto in colonna sotto diverse condizioni fisicochimiche. Le particelle rappresentano due tipologie diverse: il biossido di titanio, le P25 (Evonik) sono infatti largamente diffuse e studiate e rappresentano il termine di confronto classico per qualunque studio su scala di laboratorio. Viceversa, le CoRI C provengono direttamente dal "Coating research institute" in Belgio, e sono rappresentative di particelle effettivamente impiegate in ambito industriale nella preparazione di vernici e smalti per superfici. Le P25 sono composte da anatasio e rutilo in rapporto 80/20, con un diametro nominale dichiarato di 21nm ed un'area superficiale BET di 50 m²/g. Le CoRI C sono invece formate interamente da anatasio, con un diametro nominale dichiarato di 5-15nm. Entrambe le particelle sono state utilizzate sospendendole in soluzioni di NaCl a diversa forza ionica (1-100 mM) ed in MHRW (acqua riconstituita volta a simulare la chimica di un'acqua superficiale), aggiungendo una quantità variabile di NOM per averne una concentrazione finale nel campione tra 0 - 20 mg/L. Il pH dei campioni, così come quello degli elettroliti, è stato bufferato fino a circa 8, in modo da essere rappresentativo di un'acqua in ambiente naturale.

Come materiale collettore per il riempimento della colonna, si è scelto di utilizzare sabbia di quarzo super pura con diametro nominale dichiarato di 256 nm. Questa, sebbene rappresenti una qualità di suolo "ideale", privo da impurezze, è considerata essere lo stato dell'arte per prove in colonna, ed un buon compromesso per minimizzare le interazioni esterne indesiderate, focalizzandosi solo sul trasporto dovuto a meccanismi di natura energetica (DLVO, NON-DLVO) e fisica (straining). Una puntuale descrizione dei materiali e della loro eventuale preparazione e/o condizionamento, fa fede alla sezione 3.1 del corpo principale.

Il trasporto e la deposizione delle nanoparticelle sono stati indagati mediante studi in colonna. Questa è stata opportunamente impaccata con sabbia di quarzo precedentemente citata, con una porosità di colonna pari a 0,43. Ciascuna prova in colonna consiste in diversi step:

- Impaccamento della colonna con sabbia pre-condizionata per almeno 12 ore in elettrolita. L'eluente dalla colonna è collegato ad uno spettrofotometro

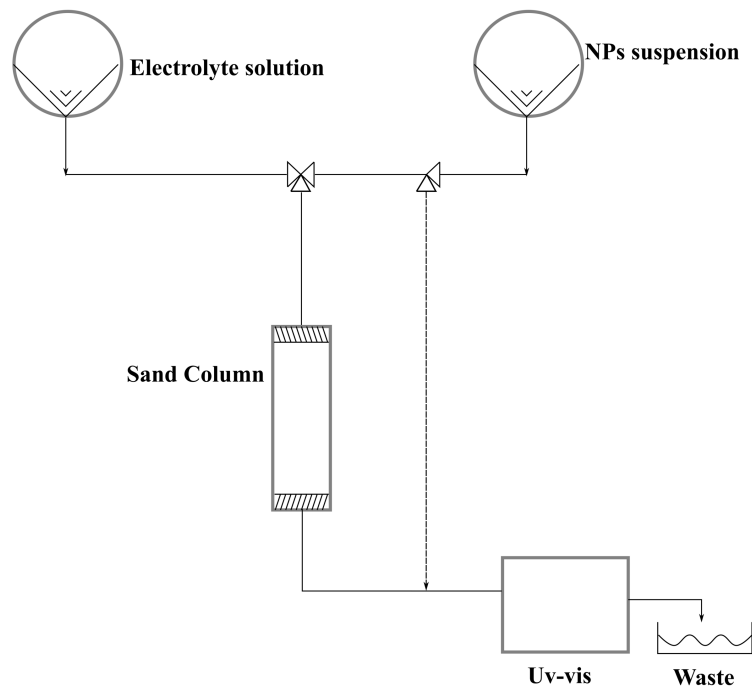


Figure 3: Studi in colonna. Layout del sistema

UV-visibile che, alla lunghezza d'onda di 270 nm, misura in continuo l'adsorbanza, e quindi la concentrazione C , delle particelle in uscita dalla colonna.

- Lavaggio della colonna con almeno 12 PVs (volume di vuoto in colonna non occupato dal fluido) dell'elettrolita opportuno. In questo modo ci si assicura che la colonna si equilibra.
- A velocità di approccio costante pari a $7,510^{-3}$ m/s, iniettare 1,3 PVs di elettrolita, seguiti da 3,7 PVs di sospensione campione. Questa presenta la chimica desiderata e contiene 5 mg/L di $n\text{TiO}_2$. Infine, dopo aver iniettato altri 2,5 PVs di elettrolita, la C_0 viene rilevata attraverso una misura di by-pass, cioè iniettando direttamente nello spettrofotometro, la sospensione campione.
- Lavaggio dei tubi con DI e 0,1 NaOH.

Tutti i test sono eseguiti a 10°C in frigo. I test vengono ripetuti in tre condizioni, che differiscono tra loro per il modo nel quale i campioni vengono trattati prima di essere pompati in colonna. Il primo modo, da qui chiamato test a 10°C , prevede

semplicemente la preparazione del campione immediatamente prima della prova, seguita dal test in colonna. Il secondo consiste nel sottoporre campioni ad un ciclo F/T (congelamento/scongelo), attuato per 24 ore in un range di temperature tra $-10\text{ }^{\circ}\text{C}$ e $+10\text{ }^{\circ}\text{C}$, in maniera da simulare le condizioni di temperatura di un inverno canadese mite. Perciò stesso, i campioni sottoposti a questo test, sono stati preparati e poi iniettati in colonna dopo 24h. Il terzo modo prevede la preparazione dei campioni in contemporanea con quelli trattati con F/T. A differenza dei primi, questi vengono stoccati in frigo per 24h, fungendo quindi da sospensioni di controllo per le prove di trasporto dei campioni sottoposti al ciclo termico. La figura 3 rappresenta uno schema esemplificativo del sistema. In maniera da confermare e comprendere a pieno i risultati degli studi di deposizione, ogni condizione di lavoro investigata in colonna, è stata ulteriormente caratterizzata in termini di analisi dimensionale e proprietà elettrocinetiche delle particelle (zeta potential e mobilità elettroforetica). Durante ogni test, l'inflow e la sospensione filtrata tra 2 e 2,6 PVs, sono stati immediatamente collettati ed analizzati con un DLS (Zetasizer Nano ZS). Questo, investendo la sospensione con una radiazione laser, permette di caratterizzarla in termini di distribuzione dimensionale (diametro idrodinamico e polidispersità) e mobilità elettroforetica. Ogni misura è stata ripetuta almeno due volte. Inoltre, per corroborare ulteriormente i risultati ottenuti, ed al contempo offrire un punto di vista diverso sulla stabilità delle soluzioni colloidali sotto diverse chimiche di soluzione, sono stati condotti test TRDLS (Time-resolved DLS), ovvero test DLS condotti su un intervallo di tempo più lungo (circa 16 ore), e misurazioni ogni 15 minuti. In questo modo è possibile controllare la stabilità delle particelle in differenti condizioni di pH, IS e concentrazione NOM, soprattutto nei primi 90/120 minuti, che rappresentano l'intervallo di tempo nel quale generalmente esse sono effettivamente sottoposte alle prove sperimentali di filtrazione.

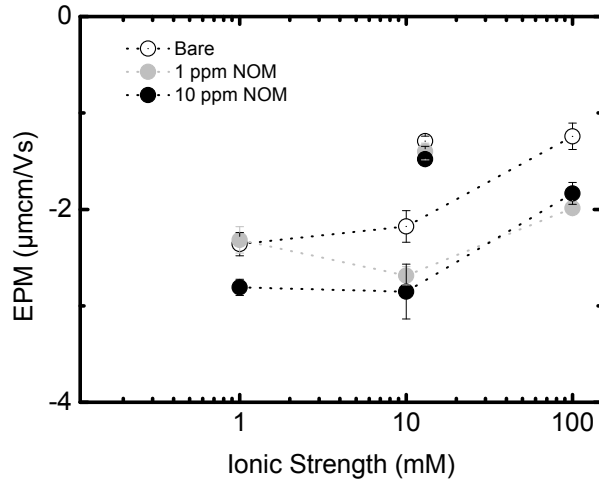
Risultati ed Osservazioni

In linea di massima, è possibile dividere i test in tre famiglie fondamentali: Prove in colonna a $T = 10\text{ }^{\circ}\text{C}$; Prove in colonna in seguito a congelamento/scongelo e prove di caratterizzazione in termini granulometrici ed elettrocinetici. Per quanto riguarda le prove a $10\text{ }^{\circ}\text{C}$, il trasporto di entrambe, CoRI C e P25 è stato investigato in un NaCl 1 - 100 mM o MHRW, ed in presenza di NOM in concentrazione 0 - 10 mg/L. Per quanto concerne le prove di trasporto dopo i cicli F/T, CoRI C è stato studiato solo in MHRW, in presenza di 1 - 10 mg/L NOM, mentre il P25 è stato testato in MHRW, NaCl 1 - 100 mM, in presenza di 0 - 20 mg/L di NOM. Il pH è controllato in tutte le prove, aggiustato ad 8 tramite 0,1 M NaOH quando necessario.

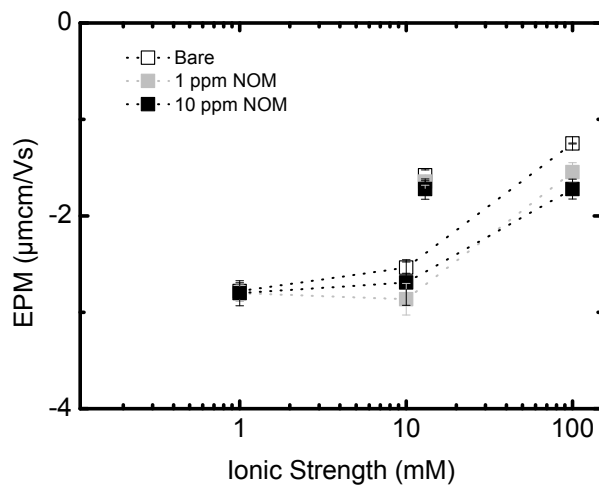
Prove di caratterizzazione

Le figure 4.1, 4.2 e 4.3 sono rappresentative dei test TRDLS condotti. Già a partire da questi esperimenti di carattere preliminare, è possibile ricavare alcune informazioni interessanti sull'effetto di NOM/IS/valenza ioni, sulla stabilità della sospensione colloidale. La Figura 4.1 sembra sottolineare l'effetto stabilizzante dell'NOM. Infatti, le P25 sembrano essere stabilizzate dalla presenza di NOM, in un modo che risulta essere proporzionale alla forza ionica della soluzione, ed anche alla valenza degli ioni disciolti. Questo perché, come dimostrato in letteratura, a forze ioniche maggiori, corrispondono strutture adsorbite più compatte e coese. Questo può essere dovuto sia da un cambiamento della forma intrinseca dell'NOM, da lineare a sferico, in modo da permettere una quantità adsorbita maggiore a parità di massa, sia da una compressione degli EDL intorno alle $n\text{TiO}_2$, che a sua volta diminuisce quindi le repulsioni elettrostatiche tra NOM e le particelle stesse, permettendo all'NOM, ora sferico, di ricoprire aree maggiori. La figura 4.2 comincia invece a dare qualche informazione sulla differente stabilità delle due $n\text{TiO}_2$ a parità di chimiche di soluzione, con le CoRI C che risultano essere generalmente più grandi, polidisperse ed instabili.

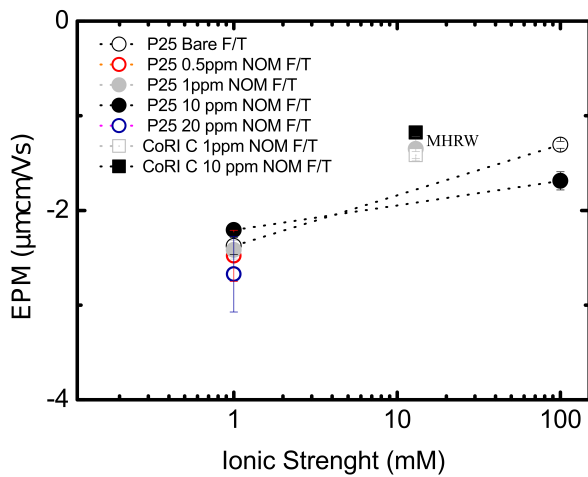
L'effetto stabilizzatore dell'NOM è ulteriormente corroborato dalle prove di mobilità elettroforetica, riportate in figura 4. Questa riporta la mobilità elettroforetica delle sospensioni, ed è da riferirsi indistintamente all' inflow o all' outflow. Nelle prove a 10°C , le sospensioni sono già leggermente cariche negativamente a causa del pH che è leggermente superiore al pzc . Ciò stante, l'adsorbimento dell'NOM aumenta in valore assoluto la stabilità colloidale delle particelle. Inoltre, come previsto dalla teoria DLVO aumentando la forza ionica, la soluzione tende all'elettro-neutralità. L'azione reciproca di IS ed NOM, è anche qui ben evidenziata. Difatti, nonostante a pH 8 l'adsorbimento dell'NOM dovrebbe essere teoricamente sfavorito come confermato da studi precedenti, è probabile che la concentrazione di NOM sia così alta che tutte le particelle siano completamente ricoperte entro IS pari a 10, e perciò stesso, aumentando IS si ottiene come unico effetto quello di comprimere sempre più l'EDL, cambiando drasticamente la pendenza delle curve di mobilità elettroforetica. Come previsto dalle serie di Hofmeister sull'effetto che la valenza ionica ha all'interno della destabilizzazioni di sospensioni colloidali, l'effetto degli ioni Ca^{2+} ed Mg^{2+} dell'MHRW, è dominante rispetto a quello di NaCl, producendo, a parità di IS, una maggiore elettro-neutralità della sospensione. Quanto detto è applicabile per entrambe P25 e CoRI C. Per quanto riguarda i test su campioni sottoposti a F/T, il loro EPM e la loro caratterizzazione dimensionale (tabella 1) danno qualche informazione che verrà successivamente confermata dalle prove di trasporto in colonna. Ad esempio, sono da sottolineare l'alta polidispersità di entrambi i tipi di particelle, le dimensioni degli aggregati, ben oltre l'ordine di grandezza sia della sensibilità macchina che del caso standard a $T = 10^\circ\text{C}$ (Tabelle 4.1 e 4.2) e l'ambiguo comportamento dell'NOM. Questi sembra infatti in qualche modo destabilizzare la sospensione in un range di concentrazione tra 0,5 - 10 mg/L.



(a) P25



(b) CoRI C



(c) CoRI C

Figure 4: Mobilità elettroforetica per P25 e CoRI C a $T = 10^\circ\text{C}$ e F/T (a) nTiO_2 P25 in 1, 10, 100 mM NaCl e MHRW; tal quali e ricoperte con 1 e 10 mg/L NOM. (b) nTiO_2 CoRI C in 1, 10, 100 mM NaCl e MHRW; tal quali e ricoperte con 1 and 10 mg/L NOM. (c) nTiO_2 P25 in 1 o 100 mM NaCl, tal quali o ricoperte con 0,5 - 20 mg/L NOM. nTiO_2 CoRI C in MHRW ricoperte con 1 - 10 mg/L NOM. pH fissato a $7,9 \pm 0,1$.

Table 1: Sommario degli esperimenti di aggregazione e deposizione P25 e CoRI C sottoposti a FT. I valori relativi alle prove DLS sono quelli dell'effluente dalla colonna. Non sono stati rilevate differenze significative rispetto a quelli della soluzione iniettata. Dove i valori di Alpha e C/C_0 non sono riportati, i valori delle prove DLS si riferiscono a quelli della sola sospensione influente. Valori medi di almeno due misurazioni. Z. avg. è il diametro idrodinamico delle particelle. I. mean è il picco dimensionale di distribuzione e PDI la polidispersità della soluzione. * Le condizioni di Physical straining fanno fede a quelli di [159]. ** Dati non disponibili.

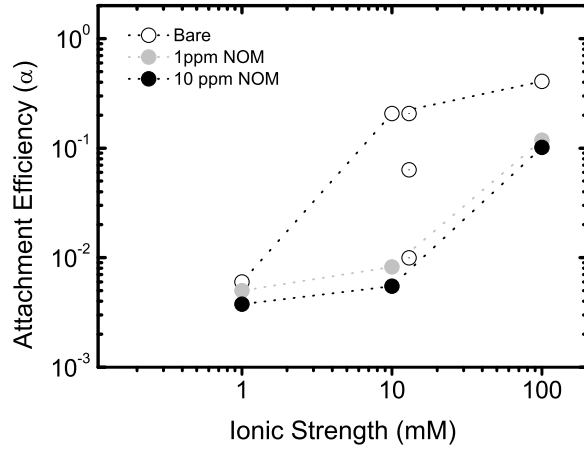
Electrolyte	IS (mM)	EnP	NOM (mg/L)	C/C_0	α_d^{TE}	I. mean (nm)	PDI	z-avg (nm)	P. straining* $\frac{dp}{dc} > 0,003$
NaCl	1	P25	0	$0,98 \pm 0,02$	$0,002 \pm 0,001$	166 ± 24	$0,19 \pm 0,01$	148 ± 10	NO
	100			$0,02 \pm 0,01$	$0,438 \pm 0,001$	126 ± 158	1 ± 0	3657 ± 931	YES
NaCl	1	P25	0,5	$0,94 \pm 0,01$	$0,007 \pm 0,001$	219 ± 14	$0,33 \pm 0,01$	249 ± 8	NO
NaCl		P25	1	$0,83 \pm 0,05$	$0,022 \pm 0,007$	152 ± 113	1 ± 0	4492 ± 2441	YES
MHRW	13	P25	1	$0,82 \pm 0,04$	$0,020 \pm 0,003$	156 ± 10	$0,22 \pm 0,08$	155 ± 5	NO
NaCl	1	P25	10	$0,71 \pm 0,04$	$0,041 \pm 0,005$	182 ± 29	$0,96 \pm 0,07$	1483 ± 336	YES
	100			$0,02 \pm 0,01$	$0,437 \pm 0,001$	248 ± 98	$0,82 \pm 0,177$	1181 ± 398	YES
MHRW**	13	P25	10	$0,73 \pm 0,01$	$0,016 \pm 0,001$				-
NaCl	1	P25	20	$0,92 \pm 0,01$	$0,016 \pm 0,001$	225 ± 5	$0,21 \pm 0,02$	225 ± 3	NO
MHRW	13	CoRI C	1	$0,47 \pm 0,01$	$0,095 \pm 0,001$	87 ± 20	1 ± 0	3225 ± 400	YES
MHRW	13	CoRI C	10	$0,41 \pm 0,01$	$0,104 \pm 0,001$	110 ± 30	1 ± 0	4651 ± 1000	YES

Studi di Deposizione in colonna

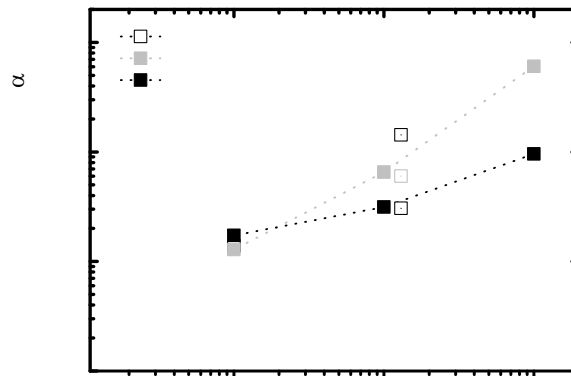
Per quantificare la tendenza alla deposizione dei due tipi di $n\text{TiO}_2$ presi in studio, due tipologie di test in colonna sono stati effettuati, uno $T = 10^\circ\text{C}$ ed uno dopo il ciclo F/T, con il relativo campione di controllo. Alcune curve rappresentative di breakthrough per i test condotti dopo F/T sono 7, altre curve di breakthrough sono invece reperibili nella sezione 4.2 del testo principale. Da queste, nell'intervallo di tempo tra 1,9 e 2,1 PVs, si ricava C/C_0 e quindi, utilizzando l'equazione 8, dove il calcolo di η_0 segue la correlazione ??, si sono calcolate le α_d raffigurate in figura 5, in modo da avere uno strumento semi-empirico per la comparazione dei meccanismi di trasporto sotto diverse condizioni sperimentali.

(a) e (b) di figura 5 sono singolarmente in accordo qualitativo con quanto ci si sarebbe aspettato dalla teoria e dagli studi in letteratura, oltre che con gli esperimenti relativi all'EPM delle particelle sospese. All'aumentare della forza ionica, ad una concentrazione di NOM fissata, a causa dell'affievolimento dei fenomeni repulsivi legati al doppio strato, corrisponde una progressiva crescita dell'efficienza di deposizione (Figura 6). Perciò, aumentando IS sia ha una densità di carica meno negativa sia sul collettore che sulle particelle, in maniera proporzionale anche alla valenza degli ioni disciolti (MHRW). Confrontando invece le efficienze di deposizione delle due particelle, risulta chiaro come in media le CoRI C, a parità di condizioni, abbiano efficienze molto più vicine all'unità. Non è possibile cercare una risposta a questa differenza utilizzando solo la teoria DLVO/NON-DLVO. Infatti, guardando ad esempio ai relativi valori EPM, questi non sono così drasticamente diversi tra CoRI C e P25. E tuttavia, osservando i valori di diametro idrodinamico, polidispersità ed intensità del picco di distribuzione (Tabelle 4.1 e 4.2), si capisce come ci sia un significato fisico dietro la maggior deposizione di CoRI C. Praticamente ogni prova di filtrazione relativa al CoRI C, è accompagnata da physical straining. Tale meccanismo si verifica quando le particelle formano aggregati così grandi, che non riescono, statisticamente, a passare attraverso i pori più piccoli. Una volta che le particelle restano intrappolate tra i pori, è molto difficile che riescano ad uscirne, e per la fisica del sistema particella-poro-collettore, e per la debolezza delle forze di trascinamento in questa zona.

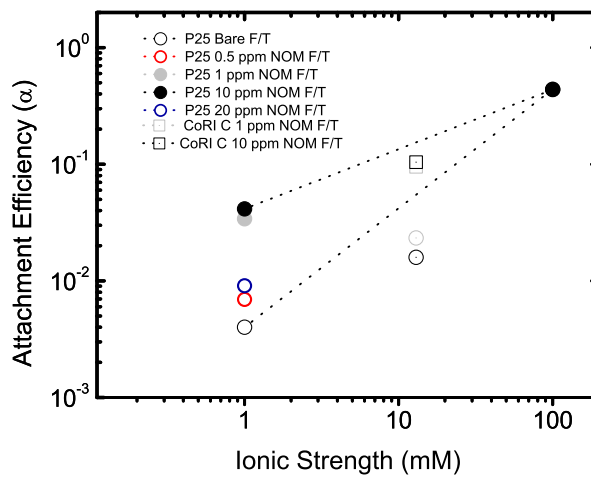
La Figura 5 raffigura anche il già citato effetto dell'NOM sul sistema. Tuttavia questo effetto sembra essere meno marcato sul CoRI C rispetto al P25. Considerando che le CoRI C sono particelle commerciali, si può immaginare come la loro composizione dichiarata 100 % anatasio, sia solo tale. Da qui si può dedurre, forti di studi di letteratura che imputano la stabilità intrinseca delle $n\text{TiO}_2$ all'eventuale presenza di impurezze, come, fissata una stessa IS, le CoRI C possano essere meno negativamente cariche. Il gap tra i PZC dei due tipi di nanoparticelle, potrebbe essere il motivo per il quale, anche 10 ppm di NOM non sono abbastanza per stabilizzare stericamente le CoRI C. Inoltre, visto che la teoria classica della filtrazione, utilizzata per il calcolo di α_d , non tiene conto della presenza eventuale di straining. Visto che questi non è generalmente compreso nel calcolo di α_d all'interno della teoria CFT, il trend delle curve di deposizione, ed i relativi valori di



(a) P25 10°C

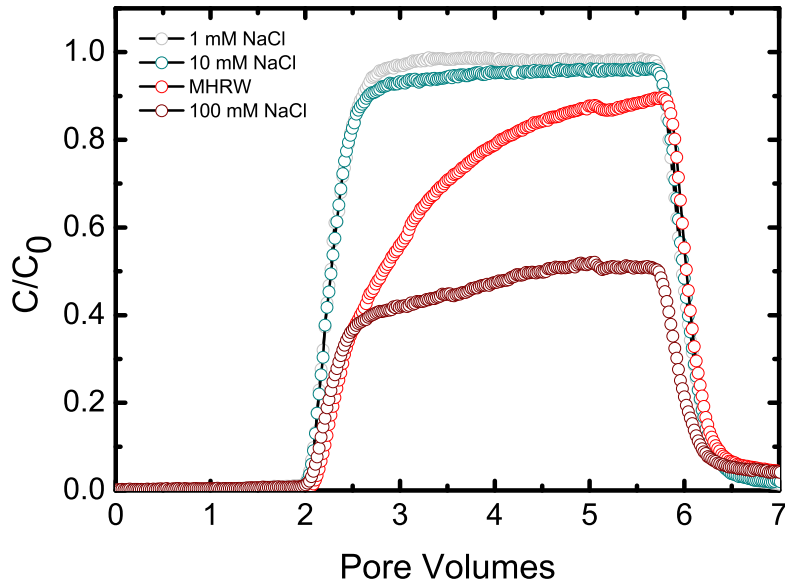


(b) CoRI C 10°C

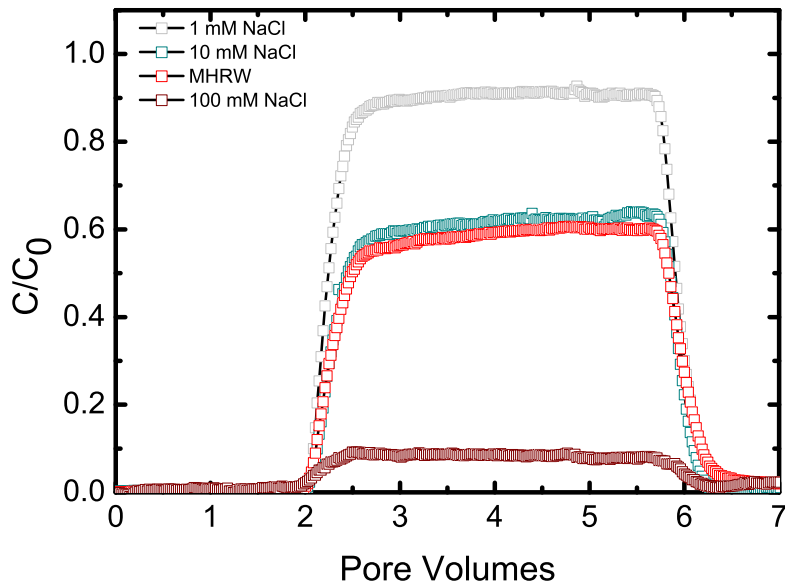


(c) P25 & CoRI C. F/T

Figure 5: α_d calcolate usando Eq.2.47. (a) P25 e (b) CoRI C a $T = 10^\circ\text{C}$. (c) F/T P25 e CoRI C. I simboli aperti con il punto, rappresentano l'MHRW. Condizioni sperimentali che fanno riferimento agli stessi di Fig.4.9 e Fig.4.10 del corpo principale.



(a) P25



(b) CoRI C

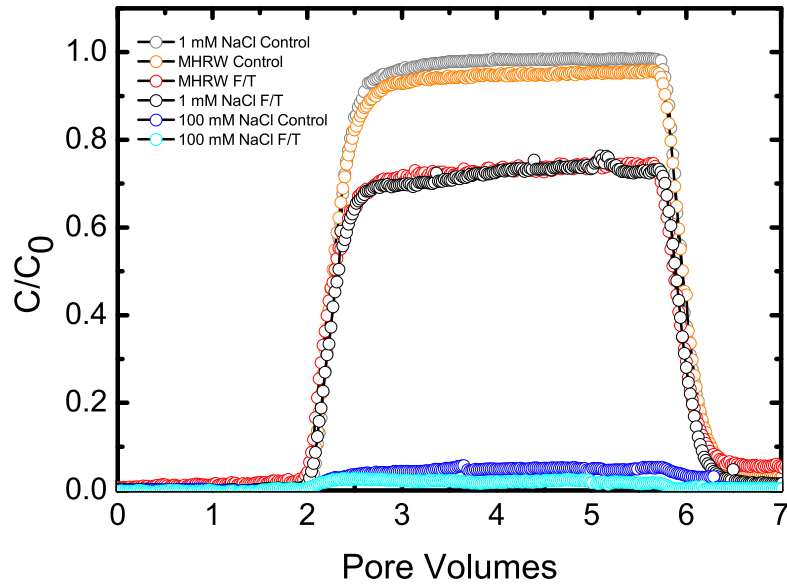
Figure 6: Representative particle breakthrough curves for 10°C series. Experiments conducted in a column packed with clean quartz sand, at $\text{pH } 7,9 \pm 0,1$, $T = 10^\circ\text{C}$, approach velocity $7,5E-05 \text{ m/s}$, mean grain diameter $d_c 256 \text{ nm}$, porosity $f 0,43$. (a) P25 coated with 1 mg/L NOM , suspended in 1, 10, 100 mM NaCl and MHRW. (b) CoRI C coated with 1 mg/L NOM , suspended in 1,10,100 mM NaCl and MHRW.

α_d , sono da ritenersi solo a scopo di interpretazione qualitativa delle osservazioni sperimentali. Infine (c) rappresenta le curve di deposizione per i test in colonna condotti dopo aver sottoposto le particelle a congelamento/scongelo.

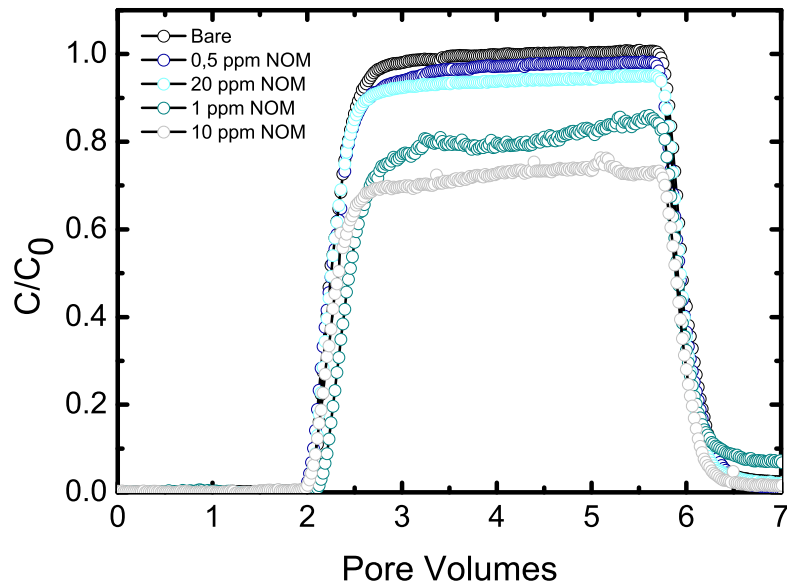
Figura 5 (c) presenta i risultati delle prove di trasporto in seguito a F/T. In linea generale, il test F/T diminuisce/aumenta (a seconda della concentrazione di NOM) notevolmente la ritenzione di entrambe le particelle rispetto al caso di $T = 10^\circ\text{C}$ e rispetto alle prove in colonna dei campioni di controllo. Non c'è praticamente eluizione per il P25 disperso in 100 mM NaCl, qualunque sia la sua concentrazione di NOM. Inoltre, lo straining è qui rilevante sia per P25 che per CoRI C (tabella 1 e Figura 7). In particolare, la deposizione da straining appare qui dominante nel caso di CoRI C. Questo permette di comprendere come mai le CoRI C appaiano praticamente non influenzate dalla presenza di NOM, nonostante questi abbiano comunque un piccolo, ma non trascurabile, effetto sulla loro EPM. Per quanto riguarda le P25, è interessante notare l'effetto dell'NOM sulla loro mobilità. Quando queste si trovano all'interno di una soluzione di 100 mM NaCl o MHRW, l'NOM sembra leggermente aumentarne la mobilità. Tuttavia, quando formano una sospensione colloidale con 1 mM NaCl, sembrano essere al contempo stabilizzate e destabilizzate, a seconda di che concentrazione di NOM si usi. Infatti, operando tra 0,5 - 20 mg/L NOM, la ritenzione aumenta, nell'ordine: $10 > 1 \gg 20 > 0,5 \gg 0$ mg/L NOM. Inaspettatamente il sistema è più mobile in assenza di NOM, con una maggiore tendenza alla deposizione nell'intervallo 1 - 10 mg/L NOM. Questo fenomeno va letto nell'effetto che la temperatura, ed il cambiamento dello stato della materia hanno, su termodinamica e cinetica del meccanismo di adsorbimento dell'NOM sulle particelle in sospensione. Una bassa temperatura favorisce la termodinamica del fenomeno ma ne ostacola fortemente la cinetica. Per questo è probabile che, a 0,5 mg/L le particelle non siano completamente rivestite a causa della cinetica lenta e della bassa concentrazione, questo può essere promotore di un fenomeno di flocculazione bridging, che rimane però circoscritto a pochi weak bridge-spots. Aumentando poi la concentrazione di NOM, tale fenomeno diventa sempre più importante, fino al punto in cui, presumibilmente ad una concentrazione di NOM tra 10 e 20 mg/L, quasi tutte le particelle sono ricoperte. A questo punto il sistema comincia ad essere leggermente stabilizzato da un punto di vista sterico, e ciò spiegherebbe come mai il valore di α_d relativo a 20 mg/L, sia molto vicino a quello del caso bare. Questo risultato è molto interessante perché apre uno spiraglio completamente nuovo, e sull'effetto dell'NOM, e sull'influenza che le condizioni atmosferiche stagionali possano avere sulla mobilità e quindi la potenziale pericolosità delle nTIO₂.

Lavoro futuro

Mi piace pensare come questo lavoro possa essere un punto di partenza per un focus puntuale e sistematico sul trasporto ed il comportamento delle nTIO₂ in ambiente naturale. Gran parte della letteratura precedente si soffermava sul comportamento del P25, un tipo di nanoparticelle "da laboratorio", molto facili da maneggiare e



(a)



(b)

Figure 7: Representative particle breakthrough curves for F/T series. Experiments conducted in a column packed with clean quartz sand, at $\text{pH } 7,9 \pm 0,1$, $T = 10^\circ \text{C}$, approach velocity $7,5E-05 \text{ m/s}$, mean grain diameter $d_c 256 \text{ nm}$, porosity $f 0,43$. (a) P25 coated with 10 mg/L NOM, suspended in 1, 100 mM NaCl and MHRW; Test and Control. (b) P25 in 1 mM NaCl, coated with 0 - 20 mg/L NOM. Control not reported.

caratterizzare, ma come visto, con peculiarità totalmente diverse da quelle delle CoRI C. Sono inoltre fiducioso del fatto che anche altri tipi di particelle "commerciali", abbiano comportamenti totalmente diversi. Passi in avanti vanno fatti in quest'ottica, cioè lentamente spostare l'attenzione da scala di laboratorio a quella industriale. Infine, come visto, test ad ampio spettro, sotto diverse condizioni climatiche/ambientali, risultano imprescindibili in quanto piccoli cambiamenti delle condizioni a contorno (Temperatura, pH, IS, tipo di ioni disciolti, *etc.*) hanno un impatto enorme sulla mobilità del sistema.

Chapter 1

Introduction

The interest in nanoparticles and nanotechnology has been dramatically growing in the last years. The nanoparticles are increasingly used in several industrial fields and, therefore, in several aspects of every-day life. The increasing amount of produced volumes is accompanied by many questions about nanoparticles fate and potential threats. Besides, at the end of their life-cycle, the nanoparticles likely end up in water and soil. This aspect, along to the transformations that may occur once the particles are released, stresses the importance of a fully understanding of nanoparticles transport and fate. In particular, the effects of adsorbed natural organic matter (NOM) and temperature on nanoparticles, have found to be significant in order to completely understand the behaviour of nanoparticles in the environment. Since the mobility of nanoparticles greatly influences their potential risk, this work will mainly try to find out which is the role played by NOM and freeze/thawing cycle on $n\text{TiO}_2$ transport and deposition.

1.1 The time's arrow

The history of nanoparticles begins in the ancient world. They were naturally produced by weathering, volcano eruptions, wildfires or biological processes [1, 2]. Even if unknowingly, they have been widely use for their optical properties in luster and glass technology [3, 4]. For instance Figure 1.1 displays iridescence under specular reflection due to a double layer of silver nanoparticles smaller (5-10 nm) and bigger (5-20nm) respectively in the inner and outer layer. The light is differently scattered by the two layers [5] because of a phase shift due to the interphase distance of 430nm [4]. The very first scientific modern document about the subject is "The Bakerian Lecture: Experimental Relations of Gold (and other metals) to light" (M. Faraday 1857). Here, the author, talking about gold, says:

"known phenomena appeared to indicate that a mere variation in the size of its particles gave rise to a variety of resultant colours."

1.1. THE TIME'S ARROW

Back then, the increasing curiosity about nanoscience was founded in the quantum size effect [5]. Namely, the idea of manipulating electronic, magnetic and optical features with size [6, 7]. That led to a systematic work on photocatalytic properties and opened the pathway to nanoscience as we know it today. The Chronological Table 1.1 shows some relevant milestones. It appears how over the years the research has been focused not only on composition but also on size, size distribution, shape, surface properties, spatial distribution of the particles.

Table 1.1: Chronological table of nanotechnology. Modified Table from [14]

Year	Remarks	Country/People
~1300 BC	Discovery of soluble gold	Egypt and China
~ 300 AD	Lycurgus cup	Alexandria or Rome
1618	First book on colloidal gold	F. Antonii
1676	Book published on drinkable gold that contains metallic gold	J. von L. Kunckel (Germany)
	in neutral media	
1718	Publication of a complete treatise on colloidal gold	Hans Heinrich Helcher
1857	Synthesis of colloidal gold	M. Faraday (Great Britain)
1902	Surface plasmon resonance (SPR)	R. W. Wood (USA)
1908	Scattering and absorption of electromagnetic fields by a nanosphere	G. Mie (Germany)
1931	Transmission electron microscope (TEM)	M. Knoll and E. Ruska (Germany)
1937	Scanning electron microscope (SEM)	M. von Ardenne (Germany)
1959	Feynman's Lecture on "There's Plenty of Room at the Bottom"	R. P. Feynman (USA)
1960	Microelectromechanical systems (MEMS)	I. Igarashi (Japan)
1960	Successful oscillation of a laser	T. H. Maiman (USA)
1962	The Kubo effect	R. Kubo (Japan)
1965	Moore's Law	G. Moore (USA)
1969	The Honda-Fujishima effect	A. Fujishima and K. Honda (Japan)
1972	Amorphous heterostructure photodiode created with bottom-up process	E. Maruyama (Japan)
1974	Concept of nanotechnology proposed	N. Taniguchi (Japan)
1976	Carbon nanofiber	M. Endo (Japan)
1976	Amorphous silicon solar cells	D. E. Carlson and C. R. Wronski (USA)
1980	Quantum hall effect (Nobel Prize)	K. von Klitzing (Germany)
1982	Scanning tunneling microscope (STM)	G. Binnig and H. Rohrer (Switzerland)
1986	Atomic force microscope (AFM)	G. Binnig (Switzerland)
1986	Three-dimensional space manipulation of atoms demonstrated	S. Chu (USA)
1987	Gold nanoparticle catalysis	M. Haruta (Japan)
1990	Atoms controlled with scanning tunneling microscope (STM)	D. M. Eigler (USA)
1991	Carbon nanotubes discovered	S. Iijima (Japan)
1992	Japan's National Project on Ultimate Manipulation of Atoms and Molecules begins	
1995	Nano-imprinting	S. Y. Chou (USA)
1996	Nano sheets	T. Sasaki (Japan)
2000	National Nanotechnology Initiative (NNI)	
2003	21st Century Nanotechnology Research and Development Act	
2005	Nanosciences and Nanotechnologies: An action plan, Europe	

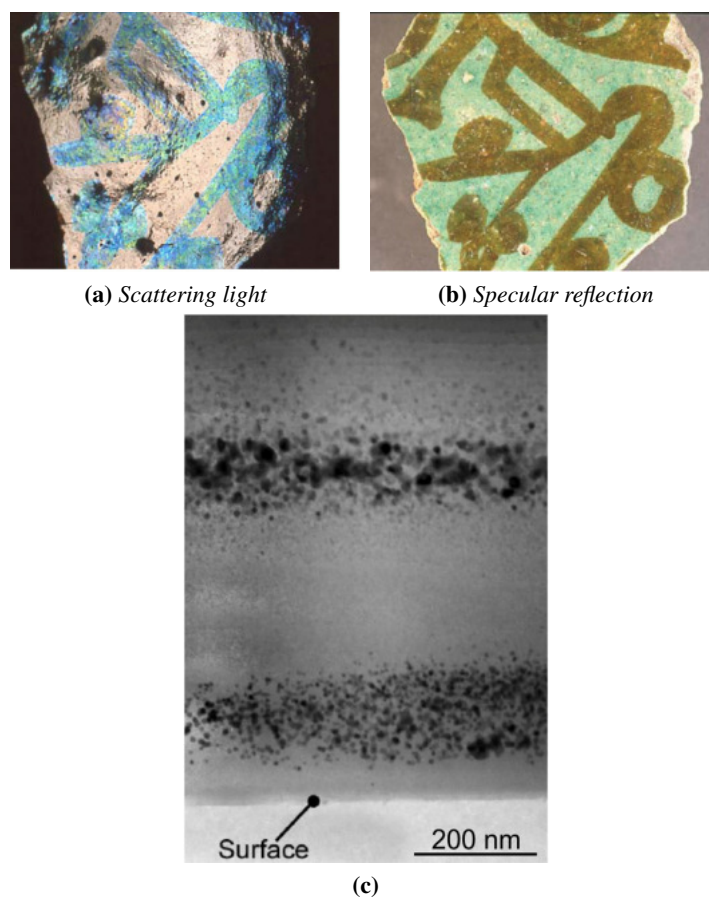


Figure 1.1: Photograph of a medieval piece of glazed ceramic. Observed by (a) Scattered light and (b) Specular reflection. (c) TEM image of the double layer of silver nanoparticles. Pictures from [5]

1.2 Nanoscience, Nanomaterials and Nanoparticles

In the recent past the nanotechnology global market has been drastically growing. In the 2015 it was estimated being around 1 Trillion US dollars [8, 9] and the newest market outlook reports put forward a flourishing situation in the next years [10]. The nanoscience is, in its simplest definition, "the study of objects with structural elements in the size range of 1-100 nm" [11]. However the definition of nanoscience and its own entities, the nanomaterials, is quite more complex because they combine biology, chemistry, physics, medicine with engineering [12]. The nanomaterial definition is not unique and often different definitions do not match each other [13, 16]. According to ISO, a nanomaterial is a material with any external dimension in the nanoscale or having internal structure or surface structure in the nanoscale. Nanomaterials work within a continuum/discrete size range. This

means that they may have different physical, chemical and biological properties from bulk materials.

It would be spontaneous to think about the objects we are referring to as "particles" or "phases", but it is necessary to think about them as "structures" [11]. The ISO did not offer the possibility of such categorization, it appeared then reasonable, to harmonize the terminology. In 2011 the European commission published a Staff Working Paper called "Types and uses of nanomaterials, including safety aspects" that reflects the true nature of nanomaterials. According to the document: "Nanomaterial means a natural, incidental or manufactured material containing particles, in an unbound state or as an aggregate or as an agglomerate and where, for 50 % or more of the particles in the number size distribution, one or more external dimensions is in the size range 1 nm - 100 nm". For the reasons mentioned above it is convenient to define the nanomaterials as particles or phases or as structures. For instance, the European commission [16] divides into:

- **Inorganic non-metallic nanomaterials:** titanium dioxide (TiO_2), silicon dioxide (SiO_2), zinc oxide (ZnO), aluminum hydroxides and aluminium oxo-hydroxydes, diiron trioxide, triiron tetraoxide, cerium dioxide (CeO_2), zirconium dioxide (ZrO_2), calcium carbonate (CaCO_3), indium tin oxide (ITO), antimony tin oxide (ATO), disbismuth trioxide (Bi_2O_3), nickel monoxide (NiO), disilver oxide (Ag_2O), etc.;
- **Metals and Metal alloys:** gold (Au), silver (Ag), Platinum (Pt) and palladium (Pd) alloy, copper (Cu) nanopowders, iron (Fe) nanoparticles, nickel (Ni), cobalt (Co), aluminium (Al), zinc (Zn), manganese (Mn), molybdenum (Mo), tungsten (W), lanthanum (La), lithium (Li), rhodium (Rh), etc.;
- **Carbon-based nanomaterials:** fullerenes (C_{60}), carbon nanotubes (CNT, SWCNT, MWCNT), carbon nanofibers (CFN), carbon black and graphene flasks;
- **Nanopolymers and dendrimers:** polymer nanoparticles, polymer nanotubes, nanowires and nanorods, polyglycilmethacrylate (PGMA) fibres, nanocellulose, nonostructured polymer-films, polyacrylonitrile nanostructures (PAN), dendrimers;
- **Quantum dots;**
- **Nanoclays;**
- **Nanocomposites;**

However, in this way it would be complicated to understand the key role that the shape plays. Therefore we can also refer to nanomaterials as divided into [15]: monodimensional (1D) structures such as nanolayers, two-dimensional (2D) structures like nanofibers, nanowires, organic or inorganic nanotubes, or three dimensional (3D), for examples fullerenes, vesicles, buckyballs, dendrimers or quantum dots.

Nanoparticles don't have a standard and unified definition, not even a legal and operative one like those of nanomaterials [13, 16]. Figure 1.2, for example, shows the relation between nanoparticles and nanomaterials in general according to the ISO. Here they are clearly different, but, for example, in the SCCP (Scientific Com-

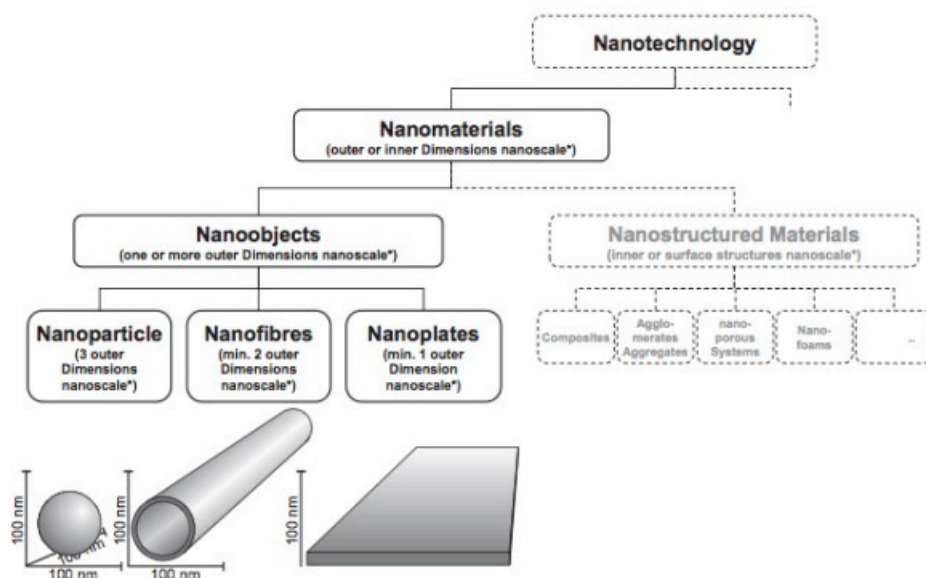


Figure 1.2: The ISO definition of nanoobjects. Figure from [18]

mittee on Consumer Products) the two match up perfectly. Even if in Table 1.2 there are the most acknowledged definitions, the scale of nano is something where the bulk-phase equations of state could be inapplicable and the phenomenological equations of transport (Fourier's Law of conduction, Fick's Law of species transport, Newton's Law of viscosity, *etc*) may be fallacious. For this reason, the way the nanoparticles are defined, it really depends on their application. Hence, it is common to encompass all the 0D building blocks [17] as out-and-out nanoparticles, in accordance with ISO. At the same time, it is also allowed, although slightly improper, to use the terms 1D, 2D and 3D "nanoparticles" instead of the more correct "nanomaterials".

The properties of materials at the nanoscale are different for two main reasons [19]:

- **Surface Area:** an increasing in surface-to-volume ratio due to the a decreasing of the geometrical dimensions of the particles, lead to have larger surface area [20, 21]. In this way there is a dispersion enhancing, that is to say, a given mass of nanomaterial will have more particles exposed to the surface than a same mass but made up of bigger particles. This behaviour might influence the chemical reactivity and affect mechanical, electric and

1.3. NANOPARTICLES: DIFFUSION AND APPLICATIONS

Table 1.2: definition of nanoparticles by various organizations: International Organization for Standardization (ISO), American Society of Testing and Materials (ASTM), National Institute of Occupational Safety and Health (NIOSH), Scientific Committee on Consumer Products (SCCP), British Standards Institution (BSI), and Bundesanstalt für Arbeitsschutz und Arbeitsmedizin (BAuA). modified Table from [14]

Association	Nanoparticle
ISO	A particle spanning 1-100 nm (diameter)
ASTM	An ultrafine particle whose length in 2 or 3 places is 1-100 nm.
NiOSH	A particle with diameter between 1 and 100 nm, or a fiber in the range 1-100 nm.
SCCP	At least one side is in the nanoscale range.
BSI	All the fields or diameters are in the nanoscale range.
BAuA	All the fields or diameters are in the nanoscale range.

thermal properties [19].

- **Quantum Effect:** Because of the size of the particles, the electrons are confined and their restricted movements make the material acts differently when excited by the light. At very small size ($d < 100nm$), the Quantum effect modifies electrical and magnetic behavior of matter [20].

1.3 Nanoparticles: diffusion and applications

1.3.1 Diffusion of nanoparticles according to CPI

Since their commercialization, the nanoparticles have found a relevant role in most technology fields. It is possible to find them everywhere, from personal care products such as cosmetic and dermatological goods ([22–25]) to biology and medicine tools, for example as drug and gene delivery ([26, 27]), or even for the treatment of cancer ([28, 29]). Figure 1.3 gives an insight on the spreading of nanoparticles into the global market. It seems now reasonable to introduce the CPI index. CPI stands for (Nanotechnology) Consumer Products Inventory and was created by the Woodrow Wilson International Center for Scholars and the Project on Emerging Nanotechnologies in the year 2005. It was originally thought as freely accessible database of "consumer products with nano-claims" but since the last update in 2015, it has become the "most frequently resource showcasing the the widespread applications of nanotechnology in consumer products" ([30]). The CPI takes in count seven product descriptors [31]:

- Nanomaterial Composition.
- Nanomaterial Shape and size.

- Coating.
- Nanomaterial location: The location within each product (bulk, surface, in suspension *etc.*).
- Nanomaterial function.
- Potential exposure pathways.
- How much we know: the amount of information that is available to corroborate the manufacturer's claim that the product contains nanomaterials.

Even though the CPI appears to be the most trustful and reliable source to quantify the number of nanoparticles in commercial products and their relative composition, it still have some issues. It has to be clear that the CPI works in terms of nanoparticles per product but it doesn't take in count neither the actual volume of production, nor the production volume of each product. For example, according to [30] the most popular advertised nanomaterials are the silver nanoparticles, present in 400 products more than the 2nd most widespread (TiO_2). However the global annual production of silver nanoparticles represents only 2% of that of TiO_2 [32,33]. That is something cannot be explained only with the CPI approach.

1.3.2 Estimating Production Data approach

The CPI is a litmus test of nanoparticles scattering. Figure 1.4 shows how the CPI approach is qualitatively, but not quantitatively, correct. Figure 1.4 (b) represents a result of a market study through eight world macro-regions [34]. Working synergically on marketing studies [32, 35, 36] prospects (the *tons/yr* of nanoparticles produced) and CPI (where to find them) it is possible to have a clear overall picture. The overview indicates that in both CPI and Future Markets studies, metallic nanoparticles represent the most fraction (63%). They cover a number of around 700 products over 1120 and constitute 200000 *tons/yr* over a total estimate amount of 319000 *tons/yr* [33]. They are mostly present as suspended in fluids (e.g., water, skin lotion, oil, car lubricant), as surface-bound particles (e.g., hair curling and flat irons, textiles). Besides, in terms of reference market, they are widely intended for purpose of catalysis, electronic and optics, coatings, paints and pigments, personal care products and medical.

1.3.3 Metallic nanoparticles

Metallic nanoparticles have a large number of useful features, as summarized below:

- **Optical Function:** When a small metallic nanoparticles is excited by light, the conduction electrons, begin then to oscillate coherently. It leads to a displacement of the conduction electron charge cloud relative to the nuclei.

1.3. NANOPARTICLES: DIFFUSION AND APPLICATIONS

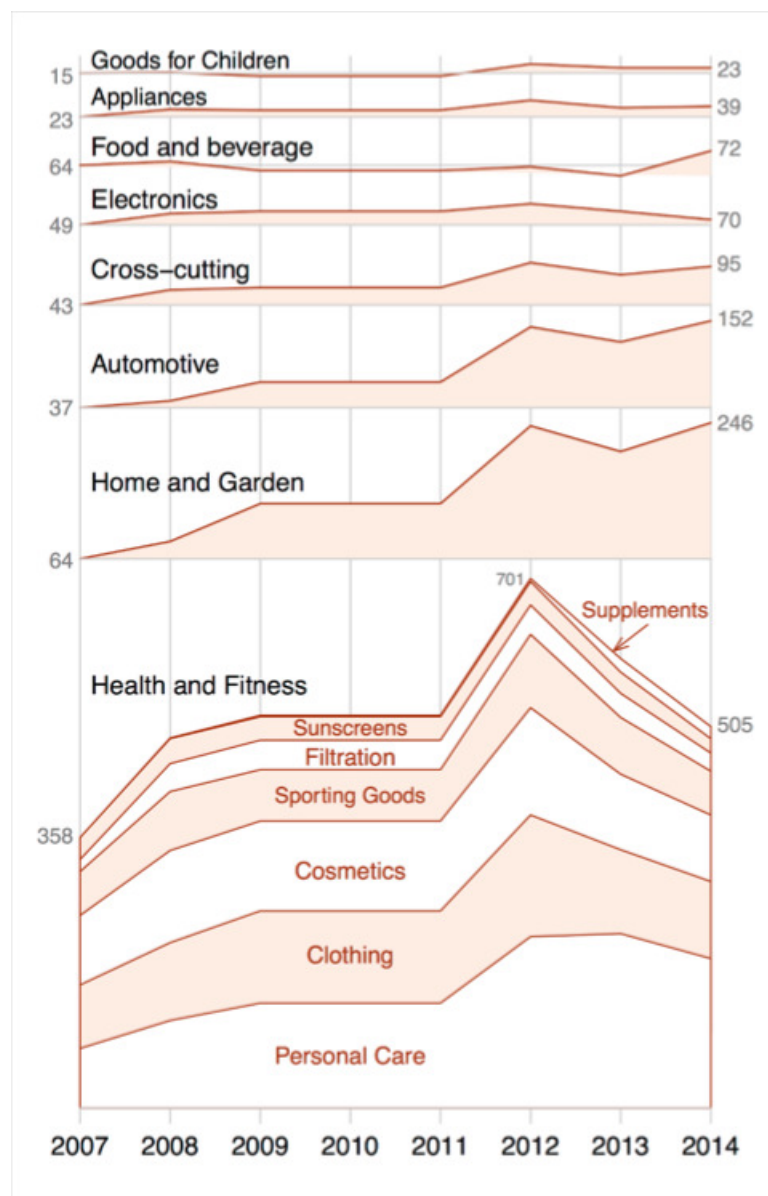
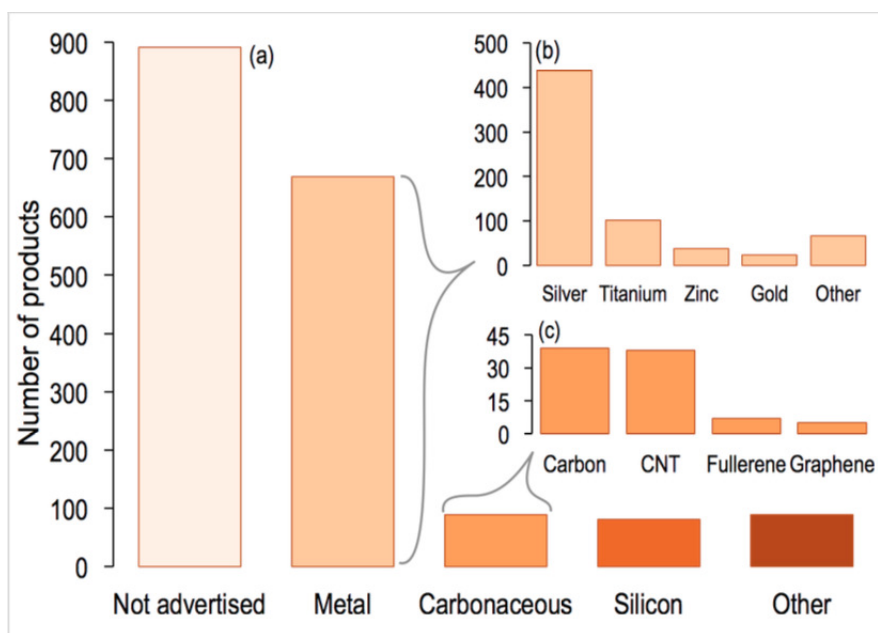
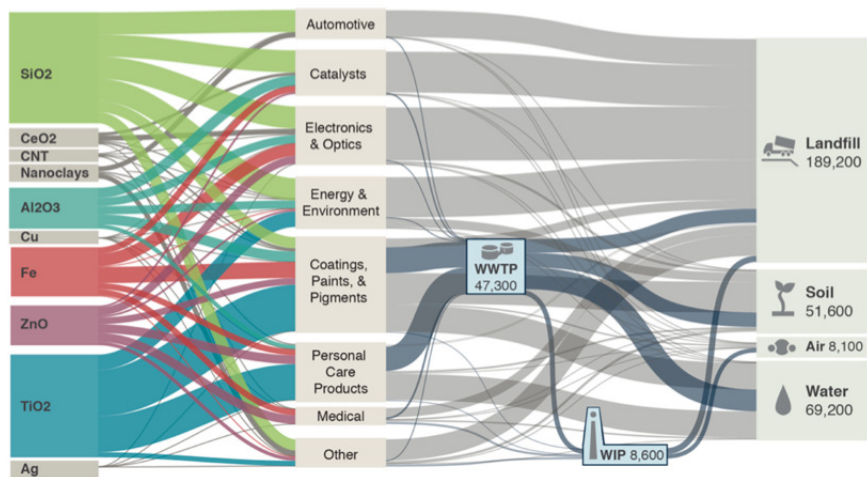


Figure 1.3: Average number of products containing nanoparticles over time (since 2007) in each major category and in the Health and Fitness subcategories. Figure from [30] without modifications.

1.3. NANOPARTICLES: DIFFUSION AND APPLICATIONS



(a) Claimed composition of nanomaterials listed in the CPI, grouped into five major categories: not advertised, metal (including metals and metal oxides), carbonaceous nanomaterials (carbon black, carbon nanotubes, fullerenes, graphene), silicon-based nanomaterials (silicon and silica), and other (organics, polymers, ceramics, etc.).



(b) Estimated global mass flow of ENMs (in metric tons per year) from production to disposal or release, considering high production and release estimates as of 2010. From [34] without modifications.

Figure 1.4: Comparison between CPI and Estimating Production Data approaches.

In general, the collective oscillation of electron, is called "Plasmon Resonance". Plasmon resonance is strictly related to the dielectric constant of the particles. Particles, which, in turn, depends on shape and size of the particles [37]. I.g., it is possible to obtain different colours by controlling size and shape of the particles are used in.

- **Catalyst function:** Reaction efficiencies can be enhanced since the specific surface area of such nanoparticles is large compared with existing particles [14]. To fulfill the several requirements of both heterogeneous and homogeneous catalysis, the transition-metal nanoparticles are widely utilized [38, 39]. In heterogeneous applications, the problems have historically been the lacking of selectivity and the understanding of mechanistic aspect, whereas the homogeneous catalysis has been suffering by thermal stability and the impossibility of removal of the catalyst from the reaction media. The bridge between the high activity and selectivity of the homogeneous and the workability of the heterogeneous, is being built through the use of nanoparticles. They can work directly in homogeneous systems or as heterogenized homogeneous particles by fixation onto a heterogeneous support such as silica, alumina, other oxides or carbon [43]. Because of a very large surface area [40–42], nanoparticle activity is very high even under mild conditions [38]. They are also well soluble in classic solvents and, besides, shape and size play a key and certain role in the catalytic steps. At the end, they bring both selectivity and efficiency to heterogeneous catalysis miming the metal surface activation and catalysis at the nanoscale [43], and feasibility to homogeneous catalysis. The actual applications cover a wide range of reactions, i.g., Oxidation, Hydrogenation, Water-gas shift, Olefin hydrogenation, Nitrile hydrogenation, Photoinduced electron transfer, *etc.*
- **Thermal function:** When the particle diameter is small (less than 10 nm), the melting point is also lower than a bulk metal [14]. The change is due to a much larger surface-to-volume ratio than bulk materials. The surface area is related to both size and shape of the particles. This property can find several applications in precision engineering. For instance, low boiling point nanoparticles, can be utilized to make electronic wiring.
- **Electrical function:** The superconductivity transition temperature gets higher for smaller particles [44]. The superconductivity phase transition temperature is that, below which, the material shows the characteristics of superconductivity in terms of the enhancement of electron transfer. This it means that, using nanostructures, it is possible to work in high temperature conditions and therefore obtain high-temperature superconductivity materials. This feature finds application in in designing novel electrochemical sensing systems [45]

- **Mechanical function:** Mechanical characteristics (i.g., hardness and elastic modulus, interfacial adhesion and friction, movement law) improve within the size of nano [46]. These properties can also influence the tribological properties of lubricated systems [47]. Mixing nanoparticles with metals or ceramic can bring to a composite with improved [48] or even different characteristics [49] than polymer composite.

1.4 TiO_2 : light and shade

1.4.1 The most commonly used nanoparticle

As explained above, metallic nanoparticles are extensively and heavily present in both mass-market industry and research industry with around 200 *ktons/yr*. The main functions of metallic nanoparticles in 1.3.3 have been noted in both precious and transition metals. The nanosized titanium dioxide, as TiO_2 aggregates consisting of an n number of primary particles $n\text{TiO}_2$, represents around the 45 % nanoparticles world's supply [33]. $n\text{TiO}_2$ is known for its ability to absorb UV radiation and it is therefore included in personal care products (e.g., cosmetics, dermatological products, *etc.*) [22, 50–52]. It can be also found as white pigment in virtually any kind of paint because of its high refractive index [53, 54], and more importantly, it is the state-of-art of photocatalysis [55](1.5). Besides, because of its photo-assisted reactivity, it is an established technology in wastewater purification [60, 61] . Additionally, $n\text{TiO}_2$ appears promising in disinfection [56], self-cleaning surfaces [57] and even in cancer treatment [58].

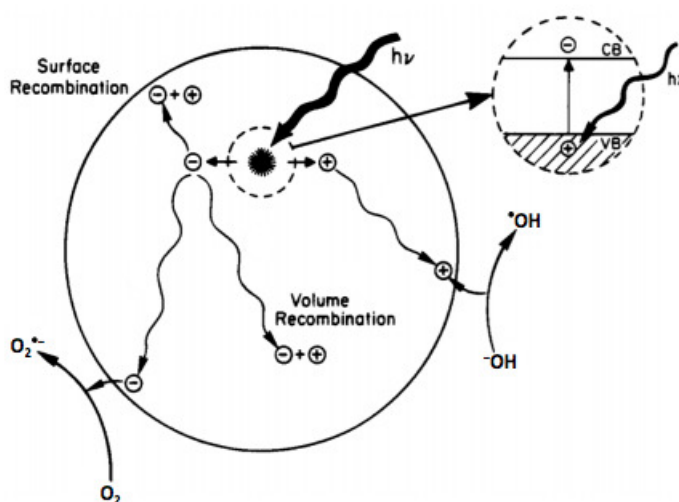
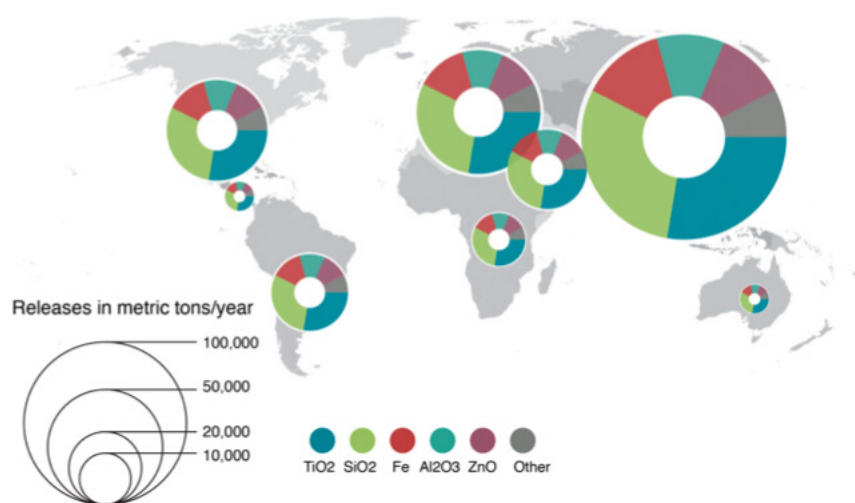
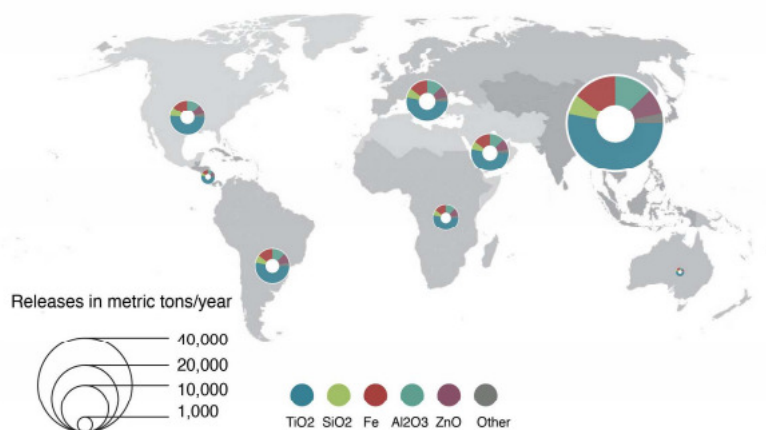


Figure 1.5: Energy band diagram and photosensitization of $n\text{TiO}_2$. Figure from [59] without modifications.



(a) Air, water, soil, and landfills.



(b) Water.

Figure 1.6: ENM releasing. (a) Regional distribution of estimated ENM release to all compartments: air, water, soil, and landfills. (b) Regional distribution of estimated ENM release to water. Modified figure from [33].

1.4.2 Environmental impact

Using a time-integrated mass balance approach it is possible to develop a release estimate scenario [33] to model the engineered nanoparticles (ENP) flow from production to either dispose or release. After their life, and according to their residence time in a given application, ENP can end up in air, water, soil and landfills [33]. Fig.1.6 displays the regional distribution of ENM and the relative percentage of each most widespread nanoparticles. The studies [33] and [34] quantify these relative percentage and the regional emissions.

Our particles of interest, the $nTiO_2$, constitute the main contaminant in water and soils. 36000 *tons/yr* [33] over 88000 *tons/yr* end up in water, as waste water treatment plants (WWTP), direct release to water from swimming or other direct water contact, or both of them. Rough estimates [33] says that 5% and 10% of the total amount of TiO_2 is released to water body respectively via stormwater and via swimming, the rest is from WWTP. By contrast, 26000 *tons/yr* of $nTiO_2$ contaminate the soil [33]. However, the most part of those is from biosolids produced during wastewater treatment as sludge solids. In the final analysis, almost the 70% of the whole produced volume of titanium dioxide, goes to, or at least pass through, a water environment. Which begs the question : are $nTiO_2$ harmful for either the environment or the living organisms?

1.4.3 Potential threats

ENM release can occur at the manufacturing, consumption and disposal stages of particle life [51, 62]. They may have an unforeseen impact on human and environmental health. In particular, both *in vivo* and *in vitro* studies have indicated that $nTiO_2$ could potentially be harmful to humans ([63–66]), rodents ([67–70]), fish ([71–73]), bacteria ([74–76]) and other organisms ([76, 77]). Because of their commercial relevance and potential toxicity, a growing interest has been increasing around the environmental fate of $nTiO_2$. Once it is released into an aquatic environment its level of public health risk associated depends on its mobility and transformation in this ecosystem. The goal of my work has been the study of behaviour of $nTiO_2$ in soil and groundwater.

1.4.4 Transformation of Nanoparticles in the Environment

Because environmental systems are dynamic and stochastic, the risks associated with the release of ENP in the environment are strictly linked to the physiochemical changes and incidental coatings of nanoparticles, as well to the subsequent reactions after their releasing [78]. Figure 1.7 illustrates the principal kinds of transformation that may occur once ENP are released. There are 4 main types of transformations:

- **Chemical transformations.** Reduction and oxidation are coupled processes in natural systems and great number of ENP may be composed of or contain compounds that undergo reduction, oxidation, or both in aquatic and terrestrial environment. For instance, that is the case of metal nanoparticles like silver and iron, or also metal sulfides and metal selenides, susceptible to oxidation [78] and major constituents of quantum dots. Natural waters and aerated soils are predominantly oxidizing environments, while carbon-rich sediments and groundwater may be reducing environments due to depletion of oxygen. Moreover, sunlight-catalyzed redox reactions may affect ENP coatings, oxidation state, generation of reactive oxygen species (ROS), and persistence [78]. For instance, many ENP ($nTiO_2$, CNTs) are congenitally

1.4. TiO_2 : LIGHT AND SHADE

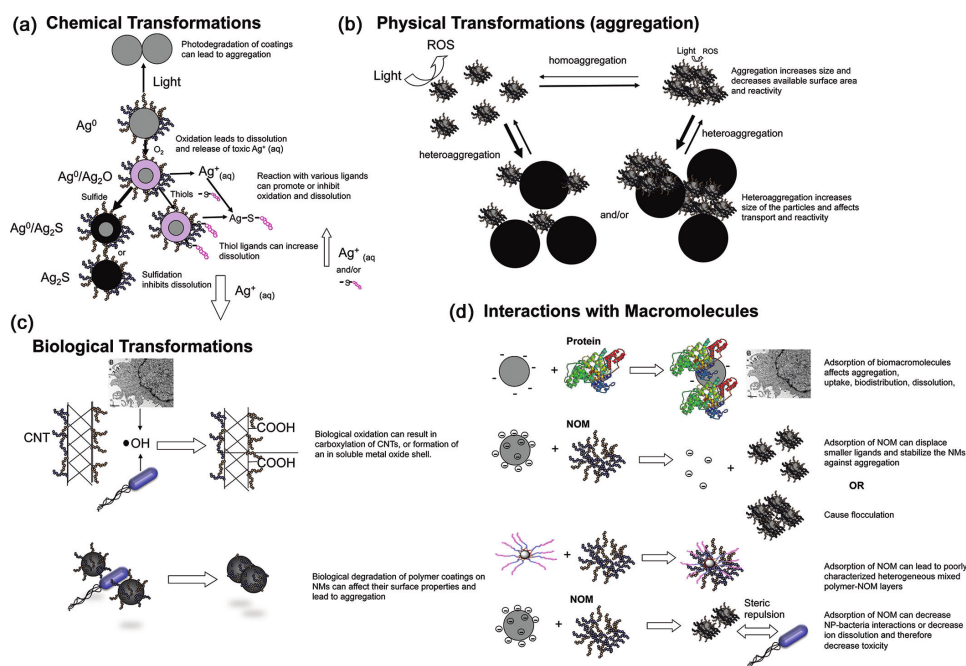


Figure 1.7: (a) Representative chemical transformations of metal nanoparticles and the potential impacts on their behavior and effects in the environment. AgNPs are used to exemplify the types of transformations that may occur. The magnitude of arrows approximately correlates with potential for these processes to occur as determined from the limited data available on these processes. (b) Effects of physical transformations including aggregation and heteroaggregation on the reactivity and transport of nanoparticles. The magnitude of arrows approximately correlates with potential for these processes to occur as determined from the limited data available on these processes. (c) Biologically mediated transformations of nanoparticles and their coatings, and the subsequent impact on fate, transport, and effects. Arrows do not indicate the relative potential for these processes to occur due to the limited data currently available for that assessment. (d) Effects of nanoparticle interactions with macromolecules such as proteins and natural organic matter. Adsorbed macromolecules can affect aggregation, nanoparticle-biointeractions, bio-uptake, and fate, transport, and effects in the environment. Arrows do not indicate the relative potential for these processes to occur due to the limited data currently available for that assessment. Figure from [78] without modifications.

photoactive, potentially producing ROS if exposed to sunlight. Furthermore, some nanoparticles may be affected by dissolution and sulfidation. These processes can change surface properties, toxicity and persistence. Finally, adsorption of macromolecules or organic and inorganic ligands on ENP surfaces can significantly modify their surface chemistry and resulting behavior in biological and environmental systems.

- **Physical transformations.** Aggregation of ENP reduces the surface area to volume effects on their reactivity. The increasing in aggregate size also influences their transport in porous media, sedimentation, reactivity, uptake by organisms, and toxicity. This mechanism is a key topic in this work and will be further explored in the second chapter.
- **Biologically mediated transformations.** Redox reactions are fundamental to growth in all biological systems. These reactions take place in the cytoplasm, cell wall, cell membrane, and extracellularly via redox-labile enzymes and cytochromes or through ancillary intracellular ROS production such as hydroxyl radicals or H₂O₂ [78]. Biologically mediated transformations of both the ENP core and the coatings are possible. These processes may modify surface charge, aggregation state, and reactivity of nanoparticles, which ultimately can affect their transport, bioavailability, and toxicity.
- **Macromolecule ENP interactions.** This is probably the most critical biotransformation of ENP and it includes the adsorption of an endless number of biomacromolecules in living cells (e.g., proteins) and in the environment (e.g., Natural organic matter, polysaccharides). Hence, the nanoparticles may be deeply transformed through their interaction with biomacromolecules which can coat and thereby transform their outer surfaces. Besides, the adsorption is often irreversible, determining EPM properties (e.g., size, surface charge and composition), environmental behavior and biological response. The behavior and impacts of ENP greatly depend on the types and amounts of these biological and environmental components attached to their surfaces. For instance, the NOM can adsorb as mono or multilayer, depending on the particle properties and the conditions (e.g., pH and ionic strength) during interaction. NOM coatings on ENP will affect the attachment to surface, and therefore the ENP aggregation. The actual effect played by NOM on ENP transport and fate has yet to be explored. However, chapters 2, 3 and 4 will further explore this aspect, giving some insights about that.

1.5 Objectives and organization of the thesis

1.5.1 Objectives

The work start from the legacy of a considerable amount of studies [79–82]. The object of my research has also been to study the nTiO₂ behaviour, trying to simulate, as best as possible, a natural subsurface environment with all its significant physical and geochemical heterogeneities, including the presence of natural organic matter (NOM). So, ultimately, I aimed to understand the aggregation and deposition trend of nTiO₂ under certain condition of Ionic Strength (IS), Temperature, groundwater chemistry, NOM, in a given supposed-to-be lab groundwater system. The questions I investigated about, were:

- How do the surrounding conditions influence the mobility of nTiO₂ ?
- Is there any difference between two kind of commercial nTiO₂ ?
- How do the nTiO₂ behave in groundwater during a "standard" winter in Canada ?

1.5.2 Outline

The second chapter gives an insight on the state-of-art in both aggregation and deposition theories. Besides, it explains how the colloidal interactions come from and how it is possible to modify them. The reasons why nanoparticles draw or repulse each other and the role of polyelectrolytes. The third chapter fully outlines the nominal material properties and the test procedures step-by-step. It also contains information about the laboratory equipment, their operating conditions and the methods adopted to carry out the measurements. The fourth chapter focuses on the results of aggregation and deposition studies of two different kind of nTiO₂, under several physiochemical condition. It draws attention on the effect of IS, natural organic matter concentration and temperature onto nanoparticles transport and fate in a natural aquatic environment.

Chapter 2

Theoretical Background

2.1 Colloidal Interactions

In an aquatic environment, nanoparticles behave governed by particle-specific properties (e.g., size and shape, chemical composition, surface charge and coating), surrounding solution conditions (e.g., pH, ionic strength IS, namely the concentration of all ions present in solution, ionic composition, presence of NOM) and hydrodynamic conditions [62, 79]. How the particles interact with each other and with environmental surfaces is determined by such factors. Talking about nanoparticles mobility in aquifers, means talking about the aggregation and deposition processes of a colloidal system. These interactions have traditionally been described by the Derjaguin-Landau-Verwey-Overbeek (DLVO) theory of colloidal stability. The theory takes in count the interplay of two main forces: the Van der Waals attractive forces and the double layer repulsive forces. The DLVO gives "the most basic account of colloidal stability" [11] but it is often only a starting point to the description of a colloidal system. This chapter will be initially focused on DLVO theory, non-DLVO theory and specific interactions. After, there will be an insight on the aggregation and deposition processes, with a brief description of the most recent theories.

2.2 DLVO Theory

2.2.1 VDW interactions

The classical DLVO theory [83] describe the stability of nanoparticles suspended in an aqueous environment as the effect of Van der Waals (VDW) and electrical double-layer (EDL) interactions. According to the classical DLVO theory, the *net* interaction potential between two surfaces determines the behaviour of the system and is the sum of two contributions:

$$\Phi_{net} = \Phi_{VDW} + \Phi_{EDL} + \Phi_{Born} \quad (2.1)$$

2.2. DLVO THEORY

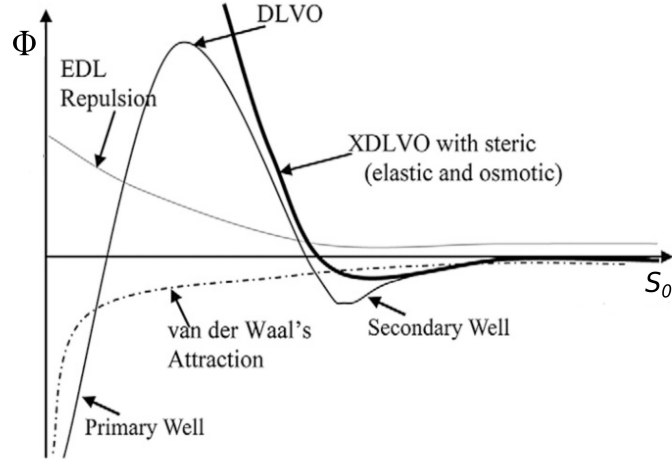


Figure 2.1: DLVO and NON-DLVO interactions. Van der Waals force (dashed line), electrostatic double layer (EDL) force (gray line), total Derjaguin-Landau-Verwey-Overbeek (DLVO) forces, and elastic force plotted together to find total potential as a function of separation distance. Extended Derjaguin-Landau-Verwey-Overbeek (XDLVO). Modified figure from [98].

Where Φ indicates the potential energy [J] and VDW, EDL, Born, respectively represent Van der Waals, electrical double-layer and Born interactions. VDW forces result from three type of interactions and each one characteristic for a certain class of compounds. At the molecular level, the Φ_{VDW} between two molecules is as follow:

$$\Phi_{VDW} = -\frac{\beta_{dip-dip} + \beta_{ind} + \beta_{disp}}{r^6} \quad (2.2)$$

where $\beta_{dip-dip}$ depends on the magnetic dipole moments of the molecules; β_{ind} depends on the permanent dipole of the first molecule and the molecular polarizability of the second molecule; β_{disp} depends on the first ionization potential of molecules and their molecular polarizability [11]. Unless the molecules are very light or very polar, The dispersion interactions are predominant. I.g., the oscillation of the electron clouds of all molecules produces strong *temporary* dipole moments. These, in turn, induce strong dipole moments in in the surrounding molecules. The more electron populated molecules are, the more dispersion forces will be relevant because the asymmetry in charge distribution. In 1937 Hamaker [84] hypothesized that summing the microscopical energies between all the molecules in one body with all those in the other body, could result in the VDW interactions between two object in the macro scale. For example, in the case of two macroscopic spheres of

equal radii a , a distance of closest approach h , with $h \gg a$, the integration over the whole surface brings to :

$$\Phi(h) = -\frac{Aa}{12h} \quad (2.3)$$

where A is the Hamaker constant, given by:

$$A = \pi^2 \rho_N \beta \quad (2.4)$$

where ρ_N is the molecular density of the spheres. It appears how, switching from micro to macro scale, the potential dependence on the distance of separation has changed. Therefore, inverse sixth power molecular interaction, generate inverse first power interaction for macroscopic particles. I.g, short radius effects (r^6) approximately decay at $0, 2 - 0, 3nm$ but their macro level effect is up to $20 - 40nm$. It is possible to trace every interaction equation form back to a common form :

$$\Phi = A \cdot f(h, h/\sigma) \quad (2.5)$$

where f is a geometrical factor and σ is the object thickness within which the interactions take place. For instance, when $\sigma \gg h$, the f factor is evaluable with the Derjaguin approximation. Table 2.2 summarizes the interactions in their most recent version. These equations are based on the linear superposition approximation (LSA) method that applies for low surface potentials and symmetric electrolytes [85]. The LSA both overcomes the Derjaguin approximation condition ($\kappa a > 10$) and it is a compromise between the constant-charge approximation (CCA) and the constant-potential approximation (CPA). Table 2.2 also introduces the effect of a medium between the particles. In the situation of two particles of similar ("1") or different ("1" and "2") composition, the Hamaker constants are modified as follow [89]:

$$A_{121} = (A_{22}^{1/2} - A_{11}^{1/2})^2 \quad (2.6)$$

$$A_{123} = (A_{22}^{1/2} - A_{11}^{1/2})(A_{33}^{1/2} - A_{22}^{1/2}) \quad (2.7)$$

Where: A_{123} describes the interaction for the deposition of a nanoparticle "1" onto a surface "3" when suspended in a medium "2"; A_{121} is the Hamaker constant for the aggregation of two particles "1" suspended in the medium "2". Besides, the Hamaker constants A_{ii} ($i = 1, 2, 3$) are those for the interaction in vacuum and are easily available for both organic [91] and inorganic [90] materials.

2.2.2 Electrical Double-Layer interactions

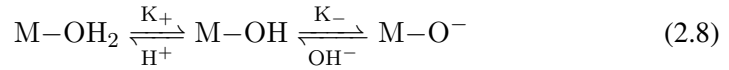
The electrical double layer forces arise from a charge separation at aqueous interface. When a particle carries a surface charge, that gathers an excess on counterions (ions of opposite charge) in the proximity of the surface. The structure formed in the vicinity of the interface is termed an "electrical double layer" [11], described

2.2. DLVO THEORY

by its surface charge density σ_s , its surface potential relative to the bulk solution ψ_s and the concentration and potential profile, $\psi(x)$ and $C_i(x)$, where x is the distance from the interface. There are several origins of surface charge, such as:

- Preferential absorption/desorption of lattice ions.
- Specific absorption of ions.
- Ionization of surface functional groups.
- Isomorphic substitution.

The nTiO₂ case study, may be treated as constant potential surfaces with OH⁻ and H⁺ as surface ions. These ions are called *first class potential-determining ions*. They come from a mismatched atomic combination of the surface oxygen atoms that perturbs the balance of charge [92]. It so may be possible that the oxygen surface atoms carry an unbalanced partial charge. The entity of the charge depends on the *pH* of the solution in contact with the particles.



Where M is the metal surface and K_+ and K_- are the protonation constants. Reaction 2.8 shows that the surface hydroxyl groups have an amphoteric behaviour, they can act as acid or basic groups, respectively when the particles are exposed to high and low *pH*. In other words, the value of *pH* whose corresponding surface charge density is zero is called the point of zero charge (PZC). As widely known [11, 93, 94], the PZC of nTiO₂ is around 6-7, depending on average diameter of the particles and their allotropic form [93]. Figure 2.2 summarizes the milestones in EDL theory. Nowadays the Stern model [95] is still acknowledged as a good theoretical compromise to describe and understand the double layer structure. In this method the double layer consists of an inner and an outer portion. The inner portion contains a monolayer of counterions, trough which passes a plane called *Stern plane*. The difficult quantitative description of the inner layer leads to consider everything before the diffuse layer, as "solid". In view of this, it may seem reasonable to mix up ψ_δ and ψ_s , where ψ_δ is the potential at $x = H$, Stern plane. In these terms, the diffuse layer charge balances both the actual surface charge and that into the stern layer. The effect of the double layer onto the surrounding area decays in a distance of $1/\kappa$. $1/\kappa$ is the Debye distance, given by:

$$\kappa^{-1} = \left(\frac{k_B T \epsilon_0 \epsilon_r}{2q^2 N_A I} \right)^{1/2} \quad (2.9)$$

where q is the elementary charge, N_A is the Avogadro's number, I is the ionic strength, k_B is the Boltzmann constant, T is the absolute temperature, ϵ_0 is the

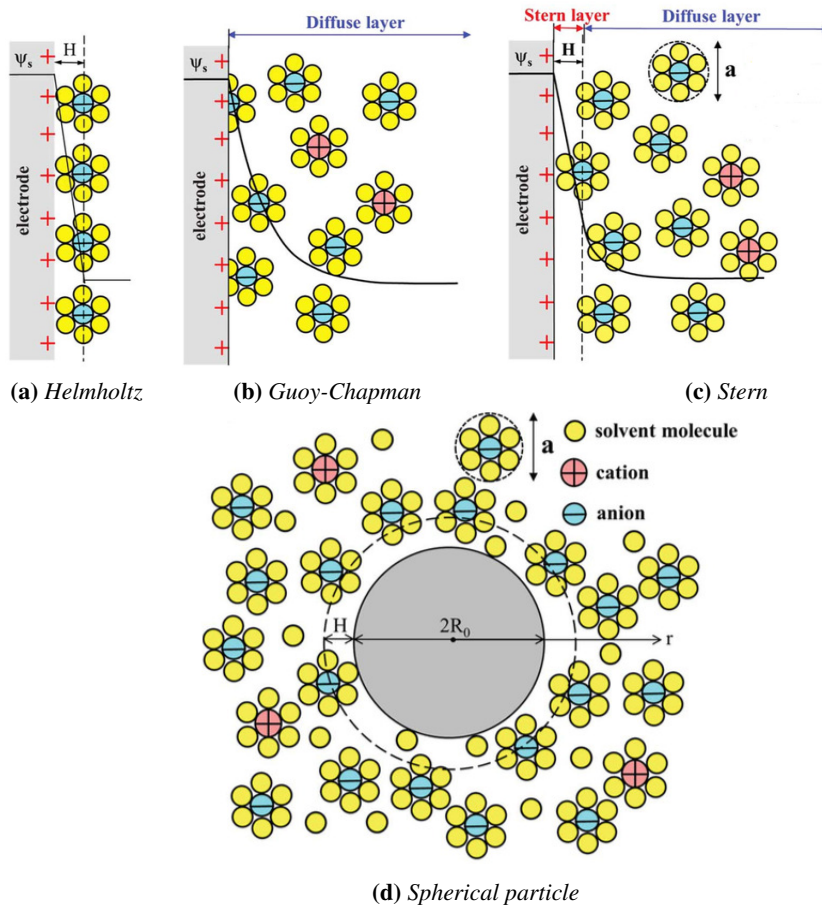


Figure 2.2: Schematic representation of electrical double layer structures according to: (a) the Helmholtz model, (b) the Gouy-Chapman model, and (c) the Gouy-Chapman-Stern model. The double layer distance in the Helmholtz model and the Stern layer thickness are denoted by H while ψ_s is the potential at the electrode surface. (d) Schematic of the EDL structure forming near a cylindrical or spherical electrode particle with radius R_0 . Modified figure from [96].

2.2. DLVO THEORY

dielectric permittivity in vacuum, ϵ_r is the relative permittivity of solution. In turn, I is the ionic strength, given by:

$$I = \frac{1}{2} \sum_i z_i^2 c_i \quad (2.10)$$

where z_i is the valence of the ion of type i , c_i its concentration expressed in mol/L and i runs over all types of ions in solution. In a colloidal system, κ is often used instead of the same I to characterize the solution. The reason behind the Φ_{EDL} , potential of repulsion between two particles, is not so intuitive. In its simplest version, the problem is that of two charged flat plates, at a distance $2b$. Each plate bears an electric double layer and, whatever are its boundary conditions, the potential profile $\psi(x)$ is:

$$\psi(x) = C_{ost} \cdot \psi_\delta e^{-\kappa x} \quad (2.11)$$

and when $\frac{zF}{RT} |\psi_\delta| < 2$, the exact profile of the resulting $\psi(x)$ between the plates is:

$$\psi(x) = \psi_\delta \frac{\cosh \kappa x}{2 \cosh \kappa b} \quad (2.12)$$

The Figure 2.3 gives an overlook of the situation. There, it is furthermore clear what is the role of the chemistry of the solution. As seen in Equation 2.12, the potential between the surfaces depends on both κ and ψ_δ . In turn, κ depends on the I (Equation 2.9) and it would be possible to demonstrate that ψ_δ mostly depends on the concentration of the *potential determining ions*. The increasing of concentration of any ions, can push the double layer against the surface of the solid but working with the *potential determining ions*, modifies the ψ_δ . Outside the common area, on both the sides, the profile of $\psi(x)$ follows the Equation 2.11 and goes to zero moving away from the surface to the bulk. There is, therefore, a delta of potential between the bulk solution outside the shared area, and the midway between the two plates. It would be possible to demonstrate that, just like the Van't Hoff osmotic pressure formula, a prevented ions diffusion situation create an additional membrane force. In the case of double layers bearing surfaces, the ions of opposite sign of the surface, would move from right outside the inner plane to the bulk and, viceversa, the same sign ions would migrate from the bulk to the interface. Both of these diffusion are prevented by the electrical double layer presence. The generated force can be imagined as a pressure over an area. For this reason, the delta of pressure is given by:

$$P(x^*) - P_{bulk} = 2RTC_{bulk} \cosh \left(\frac{zF\psi(x^*)}{RT} \right) - 1 \quad (2.13)$$

where x^* is a random x coordinate. Here is the origin of the repulsion interactions due to the EDL. It appears clear that if x^* is the midway between the plates, the additional force created is the actual repulsion force we are looking for. The

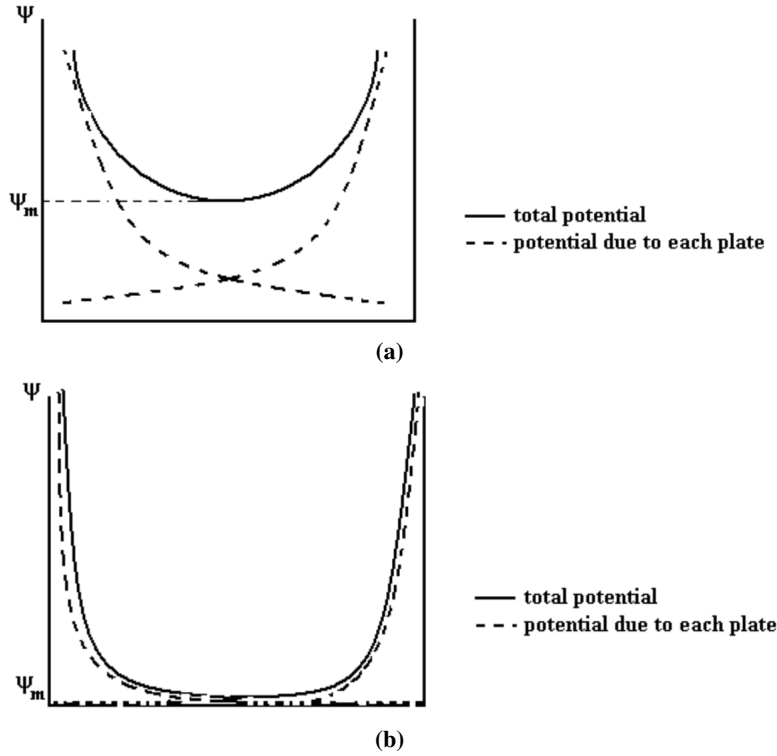


Figure 2.3: Potential profile between two surface bearing electric double layers with an increasing Ionic Strength from (a) to (b).

interaction potential caused by this force looks like:

$$\Psi_{EDL} = 64 \frac{RT}{\kappa} C_{bulk} \tanh^2 \left(\frac{zF\psi_m}{4RT} \right) e^{-\kappa 2b} \quad (2.14)$$

where ψ_m is the midway potential and can be calculated with Equation 2.12. The real case scenario of two spheres is not analytically determinable for every dimension of particles and distances between them. However, the Table 2.2 shows some widely used equations for the most commonly encountered geometries.

2.2.3 Born repulsion

The Born repulsion takes in account the impossibility of a physical interpenetration between the crystal planes of the particles. Each nucleus of each particle is surrounded by an electronic cloud. For this reason, when the particles approach more than 17 – 18nm, they find an infinitive repulsive force that keep them separated. An estimation for Born repulsion alone, was proposed by [97]:

$$\Phi_{Born} = \frac{A\delta_c^6}{7560} \left[\frac{4d_p + h}{(d_p + h)^7} + \frac{3d_p - h}{h^7} \right] \quad (2.15)$$

2.2. DLVO THEORY

where d_p is $2a$ and δ_c is the collision diameter, usually estimated equal to 0,5 nm [89].

2.2.4 NON-DLVO Interactions

Classical DLVO forces alone are not sufficient to accurately predict aggregation behavior [98]. To match experimental data for various type of aggregating primary particles, additional short-range forces are considered. The most important are steric [87, 99], magnetic [100], bridging [101], depletion [102] and hydrophilic/hydrophobic [103] forces. The steric interaction is important to describe the repulsion between particles with adsorbed layers of polymers or surfactants. They can be use to model the effect of polymer or poly-electrolyte coatings or natural organic matter (NOM) into an aqueous environment. Let us suppose the thickness of the coating is δ and, in its simplest form, the coated particles are assumed to be electrical neutral. Therefore, the steric interaction is a stabilization process that occurs when two coated particles advance nearer. They carry polymer sheathes that may overlap each other. When this happens, two phenomena can take place. As long as the distance S_0 between the surface of the bare particles is within δ and 2δ , they will tend to slightly interpenetrate and then repulse each other. The interpenetration causes a decreasing of the chemical potential of the solvent in the zone of overlap. The potential mismatch between the shared area and the bulk, is manifested as an osmotic pressure difference. As showed before, it is possible to see the osmotic pressure as a repulsion force over the interaction zone. This additional force can be seen as an additional osmotic potential [104] to the Eq. 2.1:

$$\begin{aligned} \Phi_{osmotic} &= 0 & S_0 \geq 2\delta \\ \Phi_{osmotic} &= \frac{4k_B T \pi a}{\nu_1} \varphi_p^2 \left(\frac{1}{2} - \chi \right) \left(\delta - \frac{S_0}{2} \right)^2 & \delta \leq S_0 \leq 2\delta \\ \Phi_{osmotic} &= \frac{4k_B T \pi a}{\nu_1} \varphi_p^2 \left(\frac{1}{2} - \chi \right) \delta^2 \left(\frac{S_0}{2\delta} - \frac{1}{4} - \ln \left(\frac{S_0}{\delta} \right) \right) & S_0 < \delta \end{aligned} \quad (2.16)$$

where χ is the Flory-huggins solvency parameter, φ_p is the volume fraction of polymer within the brush layer, ν_1 is the volume of solvent molecule and a the radius of the bare particle. However, if the brushes are compressed beyond $S_0 = \delta$, there is a supplementary repulsion force due to an elastic recoil. The elastic recoil (ER) potential is given by [104]:

$$\begin{aligned} \Phi_{ER} &= k_B T \left[\left(\frac{2\pi a}{M_w} \varphi_p \delta^2 \rho_p \right) \left(\frac{S_0}{\delta} \ln \left(\frac{S_0}{\delta} \left(\frac{3 - S_0/\delta}{2} \right)^2 \right) \right. \right. \\ &\quad \left. \left. - 6 \ln \left(\frac{3 - S_0/\delta}{2} \right) + 3 \left(1 + \frac{S_0}{\delta} \right) \right] \quad S_0 < \delta \end{aligned} \quad (2.17)$$

In the above, M_w is the molecular weight of the polymer and ρ_p is its density. The steric interactions, both the osmotic and the elastic recoil terms, might be linearly

superimposed to the classical DLVO interactions(2.1). However, it has been noted that the steric and the electrostatic double layers are not independent [11] because the two of them may act in concert to produce *electro-steric stabilitation*. For instance, this may happen following the adsorption of a polyelectrolyte. In that situation, the polyelectrolyte is attached to particle surface of opposite charge but it still brings enough molar mass and charge to create a thick charged layer at the surface. Therefore, it is possible to calculate the Φ_{net} as (Fig. 2.1):

$$\Phi_{net} = \Phi_{VDW} + \Phi_{EDL} + \Phi_{Born} + \Phi_{osmotic} + \Phi_{ER} \quad (2.18)$$

Nevertheless, there is no fully predictive model for the effective colloidal interaction potential for electro-steric stabilization [99] and, furthermore, there is a likely superimposition of electrostatic and spheric components. For instance, the osmotic overlap parameters would theoretically be a function of the solvent's dielectric constant and ionic strength. Nowadays, only semi-empirical models, such as that in Table 2.2 may be able to take into account the mutual influence between double and polymer layer. In addition to steric stabilization, polymers and polyelectrolyte can influence colloidal behaviour in at least two other ways. For very heavy polymers, in very low concentrations ($< 50ppm$), the same polymer can be adsorbed onto two or more particles and so linking them [11]. This is a destabilization process know as *bridging* flocculation. Conversely, the presence of free polymer into the dispersion may lead to another attraction mechanism. This is called *depletion* flocculation and may be caused by a chemical incompatibility between adsorber and adsorbate or, most likely, by an high polymer concentration. When the polymer already occupies the whole available surface, the centers of mass of the free polymer molecules are excluded from a zone near the already coated surface. For this reason, there will be an osmotic pressure difference [11], in the shape of an additional attractive potential. Figure 2.4 resumes the types of situation that can occur in the presence of a polymer. Some complementary interactions are summarized below in Table 2.1: The listed interactions are not relevant to this work and therefore will not be discussed in detail. For any details the text [106] is suggested.

2.3 DLVO and aggregation

After the explanations of all the mechanisms that may likely influence the nanoparticles behaving in water, the Φ_{net} might appears like:

$$\Phi_{net} = \Phi_{VDW} + \Phi_{EDL} + \Phi_{Born} + \Phi_{osmotic} + \Phi_{ER} + \Phi_{bridging} + \Phi_{depletion} + \Phi_{oth.} \quad (2.19)$$

where $\Phi_{oth.}$ refers to those in Table 2.1. Since for nTiO₂ everything but DLVO plus steric interaction is usually negligible in most of the work conditions, Figure 2.1 is a faithful picture of what is going on. It might be theoretically possible to predict the trend of the curves. For example, increasing the IS or the surface charge density, the

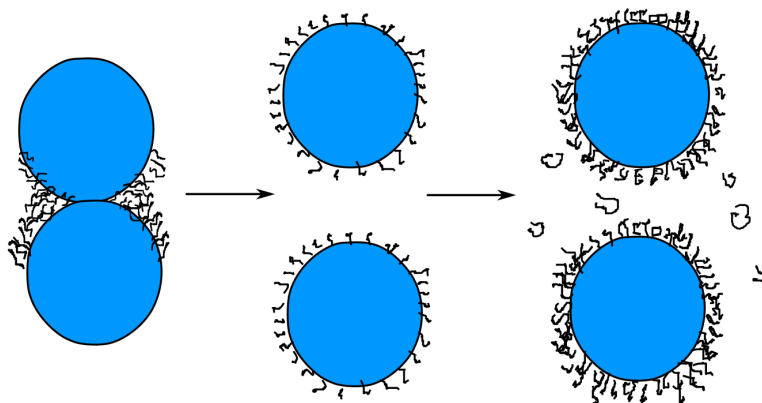


Figure 2.4: Polymers on colloidal dispersion. The concentration of polymer increases from left to right. Depletion and Bridging flocculation correspond, respectively, to high and low concentration of polymer. The steric stabilization occurs for a medium concentration.

DLVO contribute shifts from a EDL shape to a VDW shape, respectively for very low and very high IS values. Besides, considering the steric contribution separate from others, thinner coatings give a deeper secondary well. Then the question arises: "How can be DLVO theory useful to predict and understand nanoparticles aggregation and deposition"?

When the stability behaviour of a colloid is described by DLVO theory, it is an *electrostatic* colloid. An electrostatic colloids presents three significative features in DLVO coordinates: a *primary minimum*; a *secondary minimum* and an *energy barrier* H_{barr} . Both the primary and secondary minimum are attractive wells and represent aggregation in its broadest sense. The aggregation there is respectively termed aggregation as *coagulation* and aggregation as *flocculation*. By contrast, the H_{barr} is the "potential energy barrier" to aggregation [11]. It is the energy the particles have to overcome to be able to aggregate. The particles move under brownian motion, whose average energy is $k_B T$. Besides, the H_{barr} not only influences whether the particles aggregate or not, but also the rate of the process [89]. There are three possible conditions:

- **No aggregations in the primary minimum.** When $H_{barr} > 10k_B T$ no aggregation is possible into the primary minimum.
- **Slow aggregation.** When $0 < H_{barr} < 10k_B T$ nanoparticles aggregation is "slow" or "reaction-limited". The related solution chemistry conditions are to be considered unfavorable and the related energy interactions are repulsive.
- **Fast aggregation.** When $H_{barr} < 0$ nanoparticles aggregation is "fast" or "diffusion-limited". The related solution chemistry conditions are to be con-

Table 2.1: NON DLVO for sphere-sphere interaction. LR as long-range interaction, SR as short range interaction. A is constant that depends on the degree of surface hydration, it is in the range of $3 - 30 \text{ mJ/m}^2$; B is a constant, describes the "degree of hydrophobicity" and is in the order of $20 - 100 \text{ mJ/m}^2$; k_B is the Boltzmann constant $1,3805 \times 10^{-23} \text{ J/K}$; λ_{hyd} is the decay length, in the order of $0,6 - 1,1 \text{ nm}$; λ_{phob} is the decay length, in the order of $1 - 2 \text{ nm}$; k_1 is the first Helfrich bending modulus of the surface, it has been found that $k_1 \rightarrow \infty$ if the membrane surface bears any charge.

Interaction	Range	Nature of interaction	Expression	Reference
Hydration	SR	Repulsive	$\Phi_{Hydration} = +A \exp(-S_0/\lambda_{hyd})$	[11]
Hydrophobic	LR	Attractive	$\Phi_{Hydrophobic} = -B \exp(-S_0/\lambda_{phob})$	[11]
Magnetic	LR	Attractive	Not reported	[105]
Undulation	SR	Repulsive	$\Pi(S_0) \approx \frac{(k_B T)^3}{2k_1 S_0^3}$	[11]

sidered favorable and the absence of repulsive energy barriers allows every particle to aggregate into the primary energy well.

However, when the secondary energy well is less than a few $k_B T$, the particles might not need a high energy level to aggregate. That's how the flocculation works. The nanoparticles may aggregate in a "weak" way, and form then flocks that could be easily broken by stirring. For this reason, everything aggregates in the primary minimum, because of the depth of the well, is considered to be irreversibly aggregated, whereas particles in the secondary well are reversibly aggregated. The effect of the secondary well is particularly relevant into sterically stabilized colloidal system. The steric interactions influence the depth of the secondary well and then the probability the particles have to be retained there. For instance, in the case of $n\text{TiO}_2$ into a $n\text{TiO}_2\text{-NaCl}_{aq}$ -sand system and in presence of Suwannee River humic acid (SRHA), representing the NOM, the H_{barr} has found been to be significant ($> 25k_B T$) at all conditions [89]. However, the experiments have shown aggregation, explained by the presence of a secondary minimum due to the SRHA's electrostatic and/or steric repulsive interactions [107].

2.4 Aggregation

There are two ways to classify the aggregation processes [11], either with respect to the process by which the particles group together or to the sticking probability when they come close one another. In the first place, the particles get attached by brownian motions or convection. Aggregation by the brownian diffusion is always present and it is termed *perikinetic*. However, when the particles grow approximately more than $1 \mu\text{m}$, the second mechanism, that of shearing motion, becomes

2.4. AGGREGATION

Table 2.2: Key Equations To Evaluate Particle-Particle and Particle-Surface Interactions. Where: a_p is the particle radius; e is the electron charge $1.602 \times 10^{-19} C$; F_{ST} is the steric force; h is the surface-to-surface separation distance; k_B is the Boltzmann constant $1,3805 \times 10^{-23} J/K$; l the film thickness; s the distance between polymer chains on a surface; T is the absolute temperature; Φ_{EDL} is the electrical double-layer interaction energy; Φ_{ST} is the steric interaction energy; Φ_{VDW} is the van der Waals interaction energy; z is the counterion valence; Γ_i is the dimensionless surface potential for particle or collector, $\Gamma_i = \tanh [(ze\psi_i)/(4k_bT)]$; ϵ_0 is the dielectric permittivity in vacuum, $8,85 \times 10^{-12} F/m$; ϵ_r is the relative permittivity of solution; κ is the inverse Debye length; λ is the characteristic wavelength; ψ is the surface potential. Modified table from [79].

Geometry	Interaction	Expression	References
• -	EDL	$\Phi_{EDL} = 64\pi\epsilon_0\epsilon_r a_p (k_B T / ze)^2 \Gamma_1 \Gamma_2 \exp(-\kappa h)$	[85]
• -	VDW	$\Phi_{VDW} = \frac{A_{123} a_p}{6h(1+14h/\lambda)}$	[86]
• -	STERIC	$F_{ST}(h) = 2\pi a_p \left(\frac{k_B T}{s^3}\right) \frac{8l}{5} \left[\left(\frac{2l}{h}\right)^{5/4} - 1\right] + \frac{8l}{7} \left[\left(\frac{h}{2l}\right)^{7/4} - 1\right]$ $\Phi_{ST} = -\int_{\infty}^h F_{ST}(h) dh$	[87, 88]
• - •	EDL	$\Phi_{EDL} = 64\pi\epsilon_0\epsilon_r \left(\frac{a_1 a_2}{a_1 + a_2}\right) (k_B T / ze)^2 \Gamma_1 \Gamma_2 \exp(-\kappa h)$	[85]
• - •	VDW	$\Phi_{VDW} = -\frac{A_{121} a_1 a_2}{6h(a_1 + a_2)(1+14h/\lambda)}$	[86]
• - •	STERIC	$F_{ST}(h) = 2\pi \left(\frac{k_B T}{s^3}\right) \frac{8l}{5} \left[\left(\frac{2l}{h}\right)^{5/4} - 1\right] + \frac{8l}{7} \left[\left(\frac{h}{2l}\right)^{7/4} - 1\right]$ $\Phi_{ST} = -\int_{\infty}^h F_{ST}(h) dh$	[87, 88]

dominant. This latter kind of aggregation is named *orthokinetic*. Regarding the probability of sticking, as briefly anticipated, under favorable solution chemistry conditions and if the first contact between the particles occurs when they physically crash into each other, the process is termed *diffusion-limited aggregation*. In such a case, the sticking probability is 1 because every contact ends up being an aggregate. Vice versa, under unfavorable solution chemistry conditions the H_{barr} might be quite high. Here the particles have to cross the barrier by means of thermal motion. Such a process of aggregation is thus called *reaction-limited aggregation* because of the analogy between the H_{barr} and the analogous activation energy for a chemical reaction. It is also possible, even if less precise, to divide the aggregates into homoaggregates and heteroaggregates. This nomenclature refers only to the morphology and the composition. Homoaggregates will be, thus, those formed by an NP-NP attachment. They can be usually found in laboratory suspensions to study the energy interactions between particles. A real environment system contains, in turn, a large number of natural particles that can eventually interact with the released ENP. The two of them can form an heteroaggregate. To understand the particle-particle interactions becomes imperative to fully study understand the mobility and the transport. Aggregation and deposition have to be seen as two linked and associated phenomena. I.e., an increase in size due to aggregation may also change the mobility through a porous media and the intrinsic mechanism of deposition [62, 108]. Figure 2.5 gives us an overview of how the aggregation state could deeply influences the nanoparticle environmental interactions.

2.4.1 Fast aggregation

As introduced above, the rapid aggregation is characterized by Brownian diffusion only. In 1916 Smoluchowsky [110] theorized that the "number of collision occurring per unit volume per unit time is proportional to the square of the number concentration of particles in the dispersion n ", namely:

$$-\frac{dn}{dt} = k_r n^2 \quad (2.20)$$

where n is number of aggregates per unit of volume, and k_r is the rate constant of the process. It is possible to demonstrate that, for a pure *orthokinetic* aggregation mechanism:

$$k_r = \frac{4k_B T}{3\mu} \quad \text{with} \quad \frac{4}{3} \approx \frac{(a_i + a_j)^2}{a_i a_j} \quad (2.21)$$

where μ is the viscosity of the medium and $a_{i,j}$ are the radii of particles. However, the solution describes properly only a situation with no *perikinetic* aggregation, with no lubrication forces, no dependence on different particles shape and a very dilute system. With that in mind, it has to be noted that, according to the Smoluchowsky solution (Equation 2.21), the k_r isn't influenced by the particle size. That's the reason why the predicted rate constant diverges from the theory for very high shear rates. For high shear rates, the particles grow more than the theory can predict and the factor "4/3" is not a constant anymore.

2.4. AGGREGATION

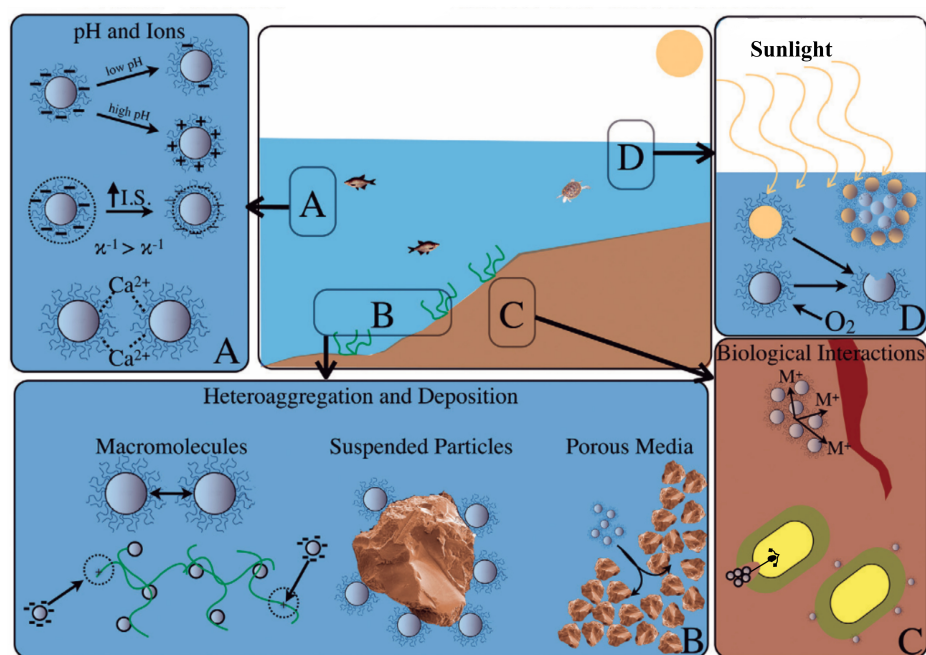


Figure 2.5: The effect of the aggregation on the nanoparticles behaviour. Possible scenarios in an aqueous environment. (A) pH and ions. Increasing acidity can lead to charge neutralization at the point of zero charge. Increasing ionic strength reduces the size of the electrostatic double layer and repulsive forces. Certain ions (e.g., Ca^{2+}) can bridge [109] functional groups of natural compounds (NOM) on the surface of nanoparticles. (B) Heteroaggregation. Macromolecules present in the environment coat nanomaterials leading to a steric effect. Larger macromolecules trap NPs in a mesh or gel causing stabilization or destabilization. Nanoparticles also associate with other particles such as clays or biocolloids. Nanoparticles ow through porous media depending on their aggregation state. (C) Biological interactions. Cells activate phagocytosis mechanisms depending on if a particle is aggregated or not. Nanoparticles containing metals aggregate at the surface of organisms and release metal ions at varying rates. (D) Transformations. Oxidants or sunlight degrade particle coatings or the particles themselves. Aggregated photoactive NPs only have the outside particles active. Modified figure from [98].

2.4.2 Slow aggregation and efficiency of aggregation

The rate of slow aggregation was described by Fuchs first [111]. He, under the same Smoluchowsky hypothesis of pure Brownian motion of the particles, theorized a relation for the aggregation rate constant under unfavorable conditions:

$$k_r = \frac{2k_B T}{3\mu} \left[\int_{2a}^{\infty} \frac{1}{r^2} \exp\left(\frac{\Phi_{net}}{k_B T}\right) \right]^{-1} dr = \frac{k_r(fast)}{W} \quad (2.22)$$

where r is a coordinate fixed in the centre of a given "target" particle. and W is given by [111]:

$$W = \int_{2a}^{\infty} \frac{1}{r^2} \exp\left(\frac{\Phi_{net}}{k_B T}\right) dr \quad (2.23)$$

but a good approximation has been found in presence of a significative energy barrier [112]:

$$W \approx \frac{1}{2\kappa a} \exp(H_{barr}/kT) \quad (2.24)$$

W is then defined as (N. of total collisions)/(N. of effective collisions) and is termed *stability ratio*. Under the presence of a significative energy barrier, the k_r for fast and slow aggregation differs each other for a factor $1/W$. This factor is that "sticking probability" or, more properly, the efficiency of aggregation α_a . Bearing in mind the Smoluchowsky hypothesis listed above, it should be also emphasised that with high shear rate, even if the calculated value of α_a was zero, aggregation could occur. This deviation is the same would be possible to find under fast aggregation conditions. There, the calculated attachment efficiency should always be close to one. Despite that, an intense shear rate could bring lubrication forces to dominate the mechanism and therefore decrease the possibility of attachment.

2.4.3 Critical coagulation concentration

The Equation 2.24 suggests that the α_a is strictly related with the chemistry of the solution. At high salt concentration, the H_{barr} is low because of the compression of the electrical double layer. For this reason, the aggregation rate k_r is constant since the aggregation is in the fast regime. Conversely, when the IS decreases, the aggregation rate dramatically decreases as well. As explained before, the H_{barr} depends on the IS of the solution and also on the surface charge density. Hence, the $\alpha_a(fast)$ is always close to one, whereas the $\alpha_a(slow)$ can be modified working on both the IS and the surface charge density. Therefore, the threshold between slow and fast aggregation is very sharp and it is defined by a given electrolyte concentration. I.e., the electrolyte concentration for which the H_{barr} goes to zero, determines the transition between the two aggregation behaviour. This concentration is called critical coagulation concentration (CCC), defined as:

$$CCC \propto \frac{1}{z^6 A_{121}^2} \tanh\left(\frac{ze\phi_\delta}{4k_B T}\right) \quad (2.25)$$

2.4. AGGREGATION

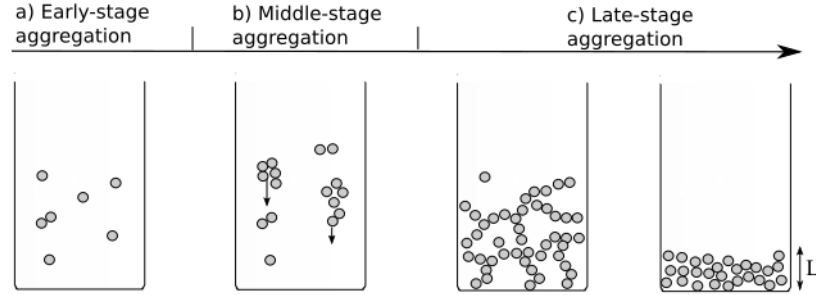


Figure 2.6: Aggregate structure evolution over time. a) Doublet formation. b) Flocks, fractal structures, coalescence, sedimentation. c) Gel, colloidal crystal, sediment layer, deposited layer. Modified figure from [11].

This means that the CCC depends on both the stern potential and the valence z of the electrolyte. it is hence valid:

$$CCC \propto \frac{1}{z^n} \quad (2.26)$$

where with sufficient accuracy:

$$n \propto 0,5|\phi_\delta|^{0,49} \quad (2.27)$$

Here, substituting value of ϕ_δ reasonably high ($> 100mV$) or low ($< 20mV$), it could be shown how the value of n is in between 2 to 6 [113].

2.4.4 Aggregate structure

The process of aggregation starts when pairs of *primary particles* collide to form a doublet. This kind of aggregation is that completely described by the Smoluchowsky theory of aggregation 2.20 and it is termed early-stage aggregation. However, since shape and structure of the aggregates are relevant in their mobility, would be interesting to study how aggregates grow and take different structures. It is helpful to think of three aggregation processes [11]: Early-stage, middle-stage and late-stage aggregation. Fig.2.6 displays the three processes. Early-stage is that of the doublet formation and it always present under every condition of aggregation. When the doublets start to grow, they can form fractal structures. Hence, each piece of the structure has the exact same geometry of the structure itself. The late stage is characterized by a gradual sedimentation into layers. These sediments will have a self-similar structure at any grade of magnification. If the assumption of

fractal geometry is reasonable, the number of aggregates is proportional to L , the characteristic length of the aggregate, as follow:

$$n_p = L^{d_p} \quad (2.28)$$

with d_p fractal dimension. d_p depends on the aggregation rate and the density of the fractal structure. The higher the d_p , the more compact the structure is. The maximum d_p occurs to be for spherical particles that aggregates into larger spheres. Here $d_p = 3$. By contrast, $d_p = 1$ refers to linear aggregates. Besides, d_p values of $\approx 1,8$ and $\approx 2,5$ correspond respectively to fast and slow aggregation.

2.5 Colloidal transport in porous media

When the particles are transported in a porous media, both physical and physiochemical mechanisms contribute to the filtration of colloids. These interaction processes usually result in dynamic deposition and release phenomena, with different behaviours in the early and advanced stages of deposition. Initially, since very few particles are attached on the surface of the grain, their deposition don't influence the total interaction energy between particles and solid grains. This phase is termed clean-bed filtration and does not take into account possibility of detachment and may be described by the classical filtration theory. When a significant amount of particles is already attached on the solid surface, the solid "collector" surface is to be considered as porous medium plus deposited particles. Therefore, the advanced stages of deposition are likely influenced by the kinetic of the deposition process as well. It is possible to identify 4 main mechanisms of colloidal transport:

- **Straining.** It is a complex advanced stage mechanism of filtration that occurs when the ratio of particle to soil grain diameter exceed a limit value. When that happens, colloid transport occurs only in the larger pores, wheres the smallest ones are clogged by entrapped larger particles. The straining is influenced by both physical and physiochemical factors, such as particle and porous medium properties.
- **Clean-bed filtration.**
- **Ripening.** When particle-particle interaction is attractive, the deposited particles slowly drawn the "fresh feed" particles approaching the grain. The attachment kinetic is progressively increasing and this leads to an higher concentration of particles near the solid grain. With time, this mechanism may cause a clogging of the porous medium.
- **Blocking.** Conversely, when particle-particle interaction is repulsive, the deposited particles stand in the further deposition of suspended particles in the vicinity of the collector surface. The effect is a decline in the attachment rate

with an increasing concentration of deposited particles, together with a partial release of deposited particles. This mechanism is usually observed when a significant barrier exists in particle-particle interaction energy profiles.

2.6 Deposition

As seen in the previous section, The aggregation process is broadly made on two separated steps, a contact and an eventually an attachment. In this perspective, aggregation and filtration are similar. In both of them may be found a "sticking" coefficient that tell us whether the contact lead or not to an adhesion. As a matter of fact, in its broadest possible way, deposition may be viewed as a two-step process [114, 115]. First, the transport of the suspended particle from the bulk of the suspension to the solid-liquid interface (collector); and second, the particle adhesion to the collector surface. Just like in aggregation, the second step is governed by an attachment coefficient α_d that represents the fraction of attached particles over the total amount coming in contact with the collector. However, In this case there is another efficiency, termed single collector contact efficiency, η_0 . The latter is obtained as the ratio of the overall rate of particle deposition onto the collector, I , to the convective transport of upstream particle towards the projected area of the collector [108]. The product of η_0 and α_d gives the single collector removal efficiency η , which takes in account the two steps of transport and attachment [79].

2.6.1 Yao 1971

The classical colloid filtration theory (CFT) describes the early stages of colloid deposition. According to that, the transport of colloidal particles from the bulk fluid to the proximity of the grain surface is typically described by three mechanisms: interception, gravitational sedimentation, and Brownian diffusion [114]. Figure 2.7 illustrates the situation. In turn, the "attachment" step is controlled, as reported above, by surface interaction forces, such as those of the DLVO theory. Transport by *interception* occurs when a suspended particle, moving along the streamline, comes into contact with the grain because of its own size. However, if the density of the particles is greater than that of the water, they will tend to move through a different trajectory. This behaviour is caused by the effect of the gravitational field and it is hence called *gravitational sedimentation*. Finally, every particle, proportionally with its size, moves because of its interaction with the medium. This last mechanism is *Brownian diffusion*. The very first equation to quantify the single-collector contact efficiency η_o was proposed by YAO in 1971 [114]. He determined an analytical solution under several assumptions. First of all, the CTF equation may be solved to get the single-collector efficiency if only one transport mechanism is operative. Besides, the steady state, Stoke equation for a laminar flow around spheres, Einstein's equation for the diffusion coefficient of the suspended particles $D_{bm} = \frac{kT}{3\pi\mu d_p}$, $C = C_0$ at $z \rightarrow \infty$ but $C = 0$ at

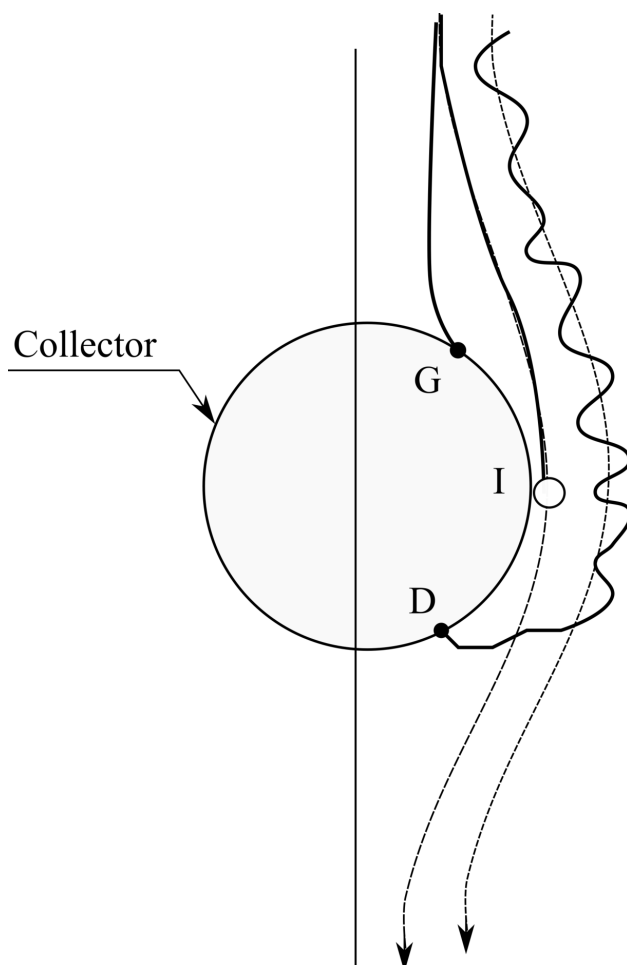


Figure 2.7: *Transport mechanism in classical CFT. Interception, gravitational sedimentation and Brownian diffusion. The dashed line is the streamline and the continuous line is the particle trajectory. Modified figure from [114].*

2.6. DEPOSITION

$z = (d + d_p)/2$ and no influence on the flow pattern by the deposition within the pores, are assumed. This approach leads to consider η_0^{Yao} as a simple summation of three partial efficiencies:

$$\eta_0^{Yao} = \eta_D + \eta_I + \eta_G \quad (2.29)$$

with the diffusion term developed by Levich [116] at high Peclet numbers ($N_{Pe} > 70$) and the sedimentation and interception terms from [117], as follow:

$$\eta_D = 4,04Pe^{-2/3} = 0,9 \left(\frac{kT}{\mu d_p v_o} \right)^{2/3} \quad (2.30)$$

$$\eta_I = \frac{3}{2} \left(\frac{d_p}{d} \right)^2 \quad (2.31)$$

$$\eta_G = \frac{(\rho_p - \rho)gd_p^2}{18\mu v_o} \quad (2.32)$$

with v_o the fluid velocity. The first right-hand side term of the Eq.2.29 considers the mutual influence of advection and brownian diffusion, the second term takes into account the deposition rate due to advection and the last term that to gravity. However, the Yao's model presents several inaccuracies. First of all, the additivity is clearly an oversimplification because it ignores the interplay of the mechanisms when none dominates the others. Besides, the Equation 2.38 itself doesn't take in account the influence of the viscous interactions and the universal VDW forces. Moreover, the assumptions made to analytically solve the CTF equation turned to be too restrictive [114], in particular that of laminar flow around the particles.

2.6.2 Tufenkji Elimelech 2004

Despite the discrepancies between the model and the experimental tests, Equation 2.29 remains a milestone in filtration theory and the point of starting to develop every other more accurate prediction. In order to overcome the limits of the Yao's theory, it has to be considered the retarding effect of hydrodynamic interaction (viscous) on the particle velocity, but also that of DLVO forces. Just like The η_0^{Yao} , the TE correlation equation for the single-collector contact efficiency assumes the η_0^{TE} as sum of three individual contribution:

$$\eta_0^{TE} = \eta_D + \eta_I + \eta_G \quad (2.33)$$

and, moreover, the single-collector contact efficiency can be expressed as a function of four dimensionless groups:

$$\eta_0^{TE} = \eta_0^{TE}(N_R, N_{Pe}, N_{VDW}, N_{gr}) \quad (2.34)$$

where definition and physical meaning of these parameters can be found in Table 2.3. The factors within the sum of Equation 2.33 are, in their turn, power functions

of multiple dimensionless parameters [124], for example $\eta_I = aN_R^b N_{Pe}^c N_{VDW}^d$. The TE solution is therefore obtained by performing a multiple linear regression analysis between the relevant dimensionless parameters and the corresponding single-collector contact efficiency. How to get, step-by-step, the solution and how to progressively "turn off" each term of the sum, can be found in [108]. Hence, the overall single-collector contact efficiency for deposition in saturated porous media can now be written as the sum of the individual contributions for each transport mechanism [108]:

$$\eta_0^{TE} = 2,4A_s^{1/3} N_R^{-0,081} N_{Pe}^{-0,715} N_{VDW}^{0,052} + 0,55A_S N_R^{1,675} N_A^{0,125} + 0,22N_R^{-0,24} N_G^{1,11} N_{VDW}^{0,053} \quad (2.35)$$

The Equation 2.35 predicts with accuracy the transport behaviour in natural and engineered aquatic system such as [108] : sandy aquifers, riverbank filtration, engineered water treatment systems. Numerical solutions fits the TE equation under a wide range of conditions (e.g., particle diameter d_p , grain diameter d_c , fluid approach velocity U , Hamaker constant A , particle density ρ_p , absolute temperature T , porosity of the bed f). The main drawback [125] of this model is that, accounting for two single acting transport mechanisms (gravity and advection) and one mixed term due to the interaction of Brownian diffusion and advection, there may be an overestimation of the rate of particle deposition under some particular conditions. For very small or very big particles and/or for very low approaching velocities, the model could predict a single collector contact efficiency higher than one, that is clearly not physically possible [79]. The problem will be pointed out on the second boundary condition (Equation 2.44). As explained above, that condition is the analogous of the Yao's, that is $C = C_0$ very far from the collector. However, due to different geometry, the same condition is not correct in case of very low N_{Pe} [126]. As shown in Table 2.3, a very low N_{Pe} means either low velocity or low diameter of the collector. Furthermore a low N_{Pe} means, in other hands, an overestimation of the η_D . Has been later [127] clarified that also large N_{Pe} could lead to an overestimation, but this time, on the η_G contribution.

2.6.3 Messina, Marchisio, Sethi 2016

In order to overcome the two main limitations described above, namely the simplification assumption of additivity and the overestimation of the collector efficiency (i.e., greater than one) either for low approach velocities or very small particles, a new solution of the colloidal transport problem has been proposed. This model [115] considers the different filtration processes jointly and mutually interacting. Unlike the TE Eulerian approach, The Messina Marchisio Sethi (MMS) model utilizes an hybrid Eulerian-Lagrangian approach where the Lagrangian approach is used only for null diffusion cases ($N_{Pe} \rightarrow \infty$). Therefore: van der Waals and hydrodynamic forces are supposed to balanced each other according to the Smoluchowky-Levich approximation; no external forces but the gravity are

Table 2.3: Dimensionless parameters in TE particle filtration theory. Where d_p is the particle diameter, d_c is the collector diameter, U the fluid approach velocity, D_{bm} is the bulk diffusion coefficient according to Stokes-Einstein equation, A is the Hamaker constant, k_B is the Boltzmann constant, T is the absolute temperature of the fluid, a_p is the particle radius, ρ_p is the particle density, ρ is the medium density, μ is the absolute fluid viscosity, γ is $(1 - f)^{1/3}$ and g is the gravitational acceleration. Modified Table from [108].

Parameter	Expression	Physical meaning
N_R	$\frac{d_p}{d_c}$	Steric number or Aspect ratio
N_{Pe}	$\frac{U d_c}{D_{bm}}$	Peclet number
N_{VDW}	$\frac{A}{k_B T}$	Van der Waals number. Van der Waals interaction energy over the particle's thermal energy
N_{gr}	$\frac{A}{12\pi\mu a_p^2 U}$	Attraction number. It represents the interplay between van der Waals attraction forces and fluid velocity on particle deposition rate due to interception
N_G	$\frac{2 a_p^2 (\rho_p - \rho) g}{9 \mu U}$	Gravity number; ratio of Stokes particle settling velocity to approach velocity of the fluid
A_S	$\frac{2(1-\gamma^5)}{2-3\gamma+3\gamma^5-2\gamma^6}$	Porosity-dependent parameter

considered and the geometry is that of a single spherical collector in a cylindrical domain. The main feature of this approach is to divide the whole phenomenon of filtration into three [115] fundamental processes that can occur alone or together as completely new mechanisms and not as simple addition among them. Hence, the particles can come into contact by advection (A), gravity (G) and Brownian diffusion (D). The Interception processes we found in Equations 2.33 and 2.29 can be now seen as the combination between advection and a new mechanism due to the steric size of the particles. The latter is termed steric effect (S) and can be only act as the increase of deposition due to finite-size particles, in the presence of any other transport mechanism [115]. With this in mind, the proposed correlation for η_0^{MM} is :

$$\begin{aligned} \eta_0^{MM} = & \eta_0^A + \eta_0^{AS} + \eta_0^G + \eta_0^{GS} + \eta_0^D + \eta_0^{DS} + \eta_0^{AG} + \eta_0^{AGS} \\ & + \eta_0^{AD} + \eta_0^{ADS} + \eta_0^{DG} + \eta_0^{DGS} + \eta_0^{AGD} + \eta_0^{AGDS} \end{aligned} \quad (2.36)$$

Hence, using a hierarchical procedure, from single transport mechanism to double and three combined transport mechanisms, each η_0 has been estimated. The step-by-step solution and procedure, can be found elsewhere [115]. Thus, in case of non-null advection [115] the single collector efficiency can be determined by:

$$\begin{aligned} \eta_0^{MM} = & 1,5062N_R^{1,9834} + N_G(1 + 6,0187N_R^2) \\ & + N_{Pe}^{-1}(7,5609 + 4,9534N_R) \\ & + N_G^{0,8741}(0,0442 + 0,1220N_R^{0,4210}) \\ & + N_{Pe}^{-0,6338}(2,9352 + 2,7480N_R^{0,3737}) \\ & + N_G^{0,6550}N_{Pe}^{-0,3450}(0,9461 + 1,1626N_R^{0,3737}) \\ & + N_G^{0,5873}N_{Pe}^{-0,2565}(-0,6740 - 0,7119N_R^{0,5438}) \end{aligned} \quad (2.37)$$

where The N are the dimensionless number of Table 2.3. In Equation 2.37 may be found the three terms introduced by Yao's solution (Equation 2.29). The Yao's keystone η , i.e., η_D , η_I , η_G respectively correspond to η_0^{AD} , η_0^{AS} and η_0^G . As expected, these terms are the most important ones. However, and here the difference with the former correlations, the pure diffusion term η_0^D is a key term as well. In particular, this is the dominant one at very low N_{Pe} and is what allow to overcome the overestimation rate of deposition issue (i.e., $\alpha_d > 1$). In the end, despite the fact that MMS doesn't take in account other external interactions than the gravity, it is a good compromise to predict the deposition behaviour of nanoparticles into a natural or artificial aquatic environment, also over a wider operative range.

2.6.4 Convective-diffusion equation and colloid filtration theory

The transport and deposition of a colloidal particles in an homogeneous porous media may be modelled by the classical convective-diffusion equation. Its first

2.6. DEPOSITION

form is that proposed by [114]:

$$\frac{\partial C}{\partial t} + v\nabla C = D_{bm}\nabla^2 C + \left(1 - \frac{\rho}{\rho_p}\right) \frac{mg}{3\pi\mu d_p} \frac{\partial C}{\partial z} \quad (2.38)$$

Where C is the local concentration of the suspended particles, v is the velocity of the fluid, t is the time, D_{bm} is the diffusion coefficient of the particles into the medium, ρ and ρ_p are medium and particles densities, respectively, μ is the viscosity of the fluid, m and d_p are mass and diameter of the particles, g is the gravitational acceleration and z is the spacial coordinate. The equation is derived from a mass balance of C for a one-dimensional flow in a packed column. From left to right: the first term on the left-hand side is the accumulation; the second term accounts for the convective transport; the terms on the right-hand side describe the effect of diffusion and gravitational settling on the system. In time, the most common general form of the convective-diffusion equation, has become [120]:

$$\frac{\partial C}{\partial t} + \nabla \cdot (vC) = \nabla \cdot (D \cdot \nabla C) - \nabla \cdot \left(\frac{D \cdot F}{k_B T} C \right) \quad (2.39)$$

where D is the particle diffusion tensor and F includes both colloidal and gravitational forces; that is :

$$F = F_{col} + F_G \quad (2.40)$$

where F_G is the gravitational force and F_{col} the colloidal force derived from the total interaction potential Φ_{net} according to the DLVO theory:

$$F_{col} = -\nabla\Phi_{net} \quad (2.41)$$

The DLVO forces are also considered in the F term, whereas the viscous effect are taken into account in the velocity v vector and into the diffusion tensor D . A more exhaustive description of this dependence can be found elsewhere [120–122]. For instance, the TE model starts from this approach, using the equation in a nondimensionalized form [120]:

$$\frac{\partial C^*}{\partial \theta} = a_1(H, \theta) \frac{\partial^2 C^*}{\partial H^2} + a_2(H, \theta) \frac{\partial C^*}{\partial H} + a_3(H, \theta) C^* \quad (2.42)$$

With $C^*(H, \theta)$ dimensionless concentration distribution of particles around a spherical collector; H dimensionless surface-to-surface separation distance between a particle and the collector; θ the tangential coordinate and the $a(H, \theta)$ variable coefficients derived during the integration of the Equation 2.39. The Equation 2.42 goes with the following boundary conditions [120]:

$$C^*(H = 0, \theta) = 0 \quad (2.43)$$

$$C^*(H \rightarrow \infty, \theta) = 1 \quad (2.44)$$

$$\left(\frac{\partial C^*}{\partial \theta} \right)_{\theta=0} = 0 \quad (2.45)$$

The first condition is that of the perfect-sink model, that is, all particles reaching the collector are immediately immobilized and therefore removed from the dispersed phase. The second condition is the analogous as Yao, $C = C_0$ for $z \rightarrow \infty$. However, The Tufenkji Elimelech (TE) equation no longer uses the isolated sphere geometry but The Happel's sphere-in-cell model [123]. In this model, the porous medium is an ensemble of identical spherical collectors, each surrounded by a fluid shell of thickness b . The particular feature is also that b is chosen so that the overall porosity of the porous medium is maintained for the single collector:

$$b = a_c(1 - f)^{-1/3} \quad (2.46)$$

where a_c is the radius of the collector. That's the reason why the Equation 2.44 has to be taken outside the Happel's fluid shell. Finally, the third boundary condition arises from the symmetry around the forward stagnation path [124]. The filtration Equation 2.42 can be numerically solved. There is no analytical solution for the convective-diffusion equation, regardless its form. For this reason, it is not possible to get the actual single-collector *removal* efficiency η under a wide range of working condition. But still, the classical colloid filtration theory permits to obtain the attachment efficiency α_d under the hypothesis of clean bed filtration and considering blocking, ripening and straining mechanisms not important. Here, thanks to laboratory column studies performed using columns packed with granular material and injecting particles at a given concentration C_0 for a given time t_0 , it is possible to relate α_d to η_0 as follow:

$$\alpha_d = -\frac{2d_c}{3(1 - f)\eta_0 L} \ln(C/C_0) \quad (2.47)$$

where L is the filter medium packed length, f is the porosity of the bed, d_c is the grain diameter and C/C_0 is the column outlet normalized particle concentration at the initial stage of the particle breakthrough curve [89]. Besides, everything on the right-hand side of the Eq. 2.38 may be combined in a filter coefficient λ . This coefficient is often used to express the removal of particles in filter bed during a deep-bed filtration [89, 117, 118]. The filter coefficient is related to η_0 via [119]:

$$\lambda = \frac{3(1 - f)\alpha\eta_0}{2d} \quad (2.48)$$

2.6. DEPOSITION

Chapter 3

Material and Methods

This study aims to examine the transport behaviour of nTiO₂ under the influence of ionic strength (IS), natural organic matter (NOM), temperature, freezing, type of electrolyte and type of NP. Deposition and aggregation tests were conducted in order to understand the effect of NOM concentration and freezing on nTiO₂ mobility. In particular, column test with bare or NOM coated P25 and CoRI C nTiO₂, were performed through saturated sand column, along with size and surface charge characterizations. Two different kind of electrolyte, namely NaCl (above a wide range of IS) and moderately-hard reconstituted water (MHRW) were utilized. The effect of temperature were studied bearing in mind Canadian weather and environmental scenario. The whole work has been conducted in the department of chemical engineering at McGill University, Montréal (Canada). The efficiency of attachment α_d was calculated from the normalized effluent concentration C/C_0 thanks to the Equation 2.47. In turn, C/C_0 was obtained from an UV-visible spectrophotometer. The compounds were further characterize in terms of size and Electrophoretic mobility.

3.1 Preparation of nanoparticles suspensions

Two kind of nTiO₂ were tested, different from each other by composition. The nTiO₂ P25 was obtained from Evonik, Germany (P25 Aeroxide TiO₂ NPs). It contains anatase and rutile phases in a ratio of about 80/20 and has a declared mean diameter of 21nm. The specific surface area is 50m²/g measured by BET. The CoRI C nTiO₂ is, instead, from the Coating research institute, Belgium and it is usually present as ENP in hybrid organic/inorganic paint and coating [128]. Besides, it is formed by anatase alone and with a declared particle size of 5-15 nm. They have been chosen because of their different morphology but mostly because of their different applications. The P25 is widely characterized [129] and studied in terms of transport behaviour [80, 107, 130, 131] but is doesn't find any industrial application. Conversely, the CoRI C is a type of a family of nanoparticles with industrial purposes. A stock suspension of nTiO₂ (100mg/L) was prepared

3.1. PREPARATION OF NANOPARTICLES SUSPENSIONS

in the same way for both of them. The nanopowder was weighed in a microbalance in a tinfoil dish to minimize the presence of electrostatic charges. 20 mg of powder were transferred into a solution of 190 ml of deionized water (DI) and 10 ml of NOM and then probe sonicated (Qsonica Q700) for 6 minutes (12 seconds On and 3 seconds Off) according to NIST protocol [149]. The final concentration is 100mg/L nTiO₂ and 5mg/L NOM. At this stage the NOM is necessary to slightly stabilize the suspension and allow the NP to be dispersed. nTiO₂ suspensions were prepared by diluting the stock suspension into a number of NaCl (Sigma-Aldrich) solution of different concentration (IS = 1, 10, 100 mM) or into a MHRW solution. Immediately prior to each experiment, an aqueous suspension of containing a final nTiO₂ concentration of 5 mg/L, a desired concentration of NOM and the given solution chemistry, was prepared. Since every column test was performed at temperature of 10°C into a fridge (Danby 36 Bottle Freestanding Wine Cooler), each electrolyte solution was prepared, stored in the same fridge and buffered to pH 7, 9 ± 0, 1 with NaOH and HCl (Sigma-Aldrich). The temperature of 10°C was chosen to a representative groundwater temperature of warmer seasons in Canada [132–134]. The Suwanee River humic acid (SRHA, Standard II, International Humic Substances Society) was used as a model for naturally occurring humic substances. Humic substances represent a relevant fraction of organic carbon present in aquatic environment [150] and are usually present in natural waters at concentration of 0, 1 - 30 mg/L [136]. Natural organic matter stock solution (100 mg/L) was prepared by dissolving the SRHA in DI water and stirring overnight away from light sources. The final concentration mentioned above, of 1; 0, 5; 10; 20 mg/L NOM were obtained further diluting the NOM stock solution with the TiO₂ suspensions, immediately prior each column test. The sample solution of nTiO₂ and, eventually, NOM, was pH adjusted to pH = 7, 9 ± 0, 1 prior to each run with NaOH and HCl. Before each test, the stock solutions of P25 and CoRI C were further sonicated 1 min and 6 minutes, respectively. This process was necessary to resuspend the nanoparticles before adding them to the electrolyte and the NOM in the sample solution. However, the CoRI C, unlike the P25, because its intrinsic instability due to its composition, required another sonication. For this reason, after preparing the CoRI C sample solutions, they were sonicated again for 6 minutes. High purity quartz sand (-50 +70 mesh size, $d_{50} = 256 \mu m$, Sigma-Aldrich) was utilized as a model granular material to fill the column. Although it doesn't properly represent a natural soil, it is still a good compromise to minimize unintended external interaction and at same time, focus on the transport due to energetical (DLVO, non-DLVO, *etc.*) and physical (straining) mechanisms. Prior to use, the sand was cleaned according to the procedure proposed by Litton and Olson [137]. This process includes acid washing with 12 M HCl followed by pH adjustment until ~ 5, 6 and furnace baking at 800 °C for 5 h. The goal is to ensure that the media is completely free of impurities (especially metal or organic ones). The moderately-hard reconstituted water is a synthetic freshwater that aims to simulate typical groundwater conditions. It was prepared following the EPA (United States Environmental Protection Agency) Protocol [138]. Table 3.1 shows the chemical

composition of this media.

Table 3.1: Nominal chemical composition of MHRW.

Compounds(units)	MHRW
K ⁺ (mg/L)	2, 1
Na ⁺ (mg/L)	26, 3
Ca ₂ ⁺ (mg/L)	17, 6
Mg ₂ ⁺ (mg/L)	12, 1
SO ₄ 2 ⁻ (mg/L)	90, 2
CL ⁻ (mg/L)	1, 9
HCO ₃ - (mg/L)	69, 7
Hardness (mg/L as CaCO ₃)	94
Ca/Mg (molar ratio)	0, 88
pH	7, 9
Conductivity (S/cm)	295

3.2 Column Tests

Nanoparticles transport and deposition behaviour was studied performing laboratory-scale column tests, using a glass column packed with the clean quartz sand. Before each experiment, the required amount of sand was soaked in electrolyte (NOM eventually included) and stored over the night in the fridge at 10 °C. The reason is to both minimize fluctuation of temperature on the system and speed the future equilibration of the column up. the conditioned sand was then wet-packed into a glass column (8,5 cm packed length and 0,8 cm of radius). The porous medium was supported on a Nylon Spectra/Mesh filter (pore size: 70 μm, thickness: 70 μm) for the purpose of keeping the sand from going into the tubes through the bottom of the column. A porosity of 0,43 was obtained using a vibrator that ensure no air is trapped and the packing is uniform. Next, to equilibrate the collector surface, at least 12 pore volumes (one PVs is the volume of free space in the column unoccupied by media) of electrolyte was pumped through the column. This pre-equilibration of the column is essential in producing consistent results [139]. The electrolyte was at the desired condition of IS, NOM concentration and pH. The flow was induced by a syringe pump with a screw drive (Kd Scientific) with an approaching velocity U of 7,5E-05 m/s. The effluent from the column was collected by a 1 cm flow-through cell (Agilent), which was in turn part of an UV-visible spectrophotometer (Agilent 8453) system. Monitoring at $\lambda = 270$ nm, the UV-vis was used to obtain both real-time influent C_0 and effluent C particle concentration measurements. In particular, the influent concentration C_0 came from a NP column by-pass measurement. In other words, after the pre-equilibration, the run got started and around 1,3 PVs more of electrolyte were injected. At this point, 3,7

3.3. NANOPARTICLES CHARACTERIZATION

PVs of NP were introduced, followed by a NP-free background electrolyte solution (ca. 2,5 PVs). All the tests were run at $10\text{ }^{\circ}\text{C}$ in the fridge, as mentioned above. All background electrolyte solutions were prepared using the above stock solutions. All the sample were run at 5 ppm , regardless the type of nTiO_2 . In order to avoid cross-contamination among transport data, after each test, the tubes were rinsed thoroughly with a $0,1\text{M}$ NaOH, followed by a copious amount of DI and finally air. Figure 3.1 illustrates a layout of the system.

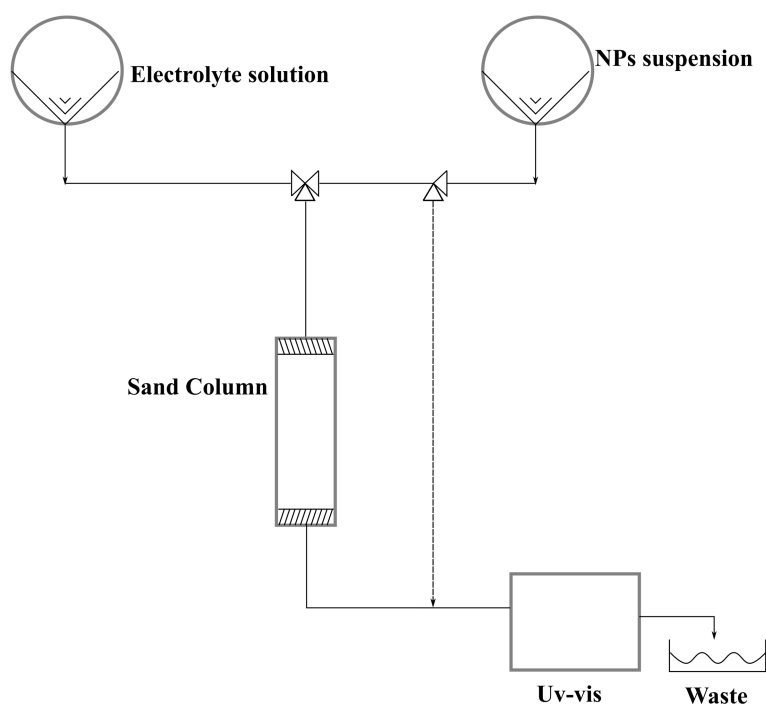


Figure 3.1: Column Test, system layout.

3.3 Nanoparticles Characterization

In order to both strengthen and corroborate the deposition data, every working condition investigated during the column tests, was supported with a further characterization of mean diameter and electrokinetic properties of the particles. The effluent from the column in between 2 and 2,6 PVs (The pore volumes are commonly used as volume but also as time units) was collected and immediately analyzed. The same was done for approximately the same volume of the final by-pass suspension.

The ranges of time have been chosen to respectively take in account the so-called clean bed filtration zone of the breakthrough curve and, of course, that volume representative of the influent NPs. The measurements were conducted in a Zetasizer Nano ZS and the samples were placed in a disposable 1-cm polystyrene cuvette for measurement. The hydrodynamic diameter along with the polydispersity of the suspension were verified over the range of solution chemistries investigated (in the presence and absence of NOM) by dynamic light scattering (DLS). DLS is a process performed by the Zetasizer that measures the change in scattering intensity over time due to Brownian motion and relates this to the size of the particles [140]. The Brownian motion causes the suspended particles to be in constant motion because of the random collisions with the molecules of the liquid that surround the particle. The Zetasizer illuminates the particles with a laser and then analyzes the light intensity fluctuation. The relationship between particle size and its speed due to Brownian motion is, to be more specific, defined by the Stokes-Einstein equation. DLS provides size distributions by intensity, and so mean intensity and average diameter. Each measurement was repeated at least three times. The electrokinetic properties, such as zeta potential and electrophoretic mobility (EPM), were investigated by laser Doppler velocimetry (LDV) at 25 °C, with an applied electrical field (E) of 4, 9. The tests were conducted using the exact same sample as the size characterization data. The instrument calculates the zeta potential, ψ_δ , the potential at the outer edge of the diffuse electrical double layer (Figure 3.2). The magnitude of the zeta potential gives an insight of the potential stability of the suspension. If all the particles in suspension have a large negative or positive zeta potential then repulsive forces will dominate the behaviour of the colloidal system. However, if the particles have low zeta potential values then there is no electrostatic force to prevent the particles coming together and aggregating. The general dividing line between stable and unstable suspensions is generally taken at either $+30mV$ or $-30mV$ [140]. When a charged particle is in an electric field, it will tend to move and then reaching a stationary velocity, this velocity is commonly referred to as Electrophoretic mobility of the particle. The Zeta potential is related to Electrophoretic mobility through the Henry equation [141]:

$$U_E = \frac{2\epsilon\psi_\delta f(ka)}{3\mu} \quad (3.1)$$

where ϵ is the dielectric constant, μ is the viscosity of the clean liquid and $f(ka)$ is the Henry's function, approximated with the Smoluchowsky equation [142]. The LDV technique measures the velocity of particles moving through a fluid in an electrophoresis experiment. When a laser beam is incident onto the Folded Capillary cell, it is scattered. Then, a receiving optics and a digital signal processor, together can relate the rate of scattered beam intensity fluctuation with the speed of the particles. Figure 3.3 gives an insight of the process. Each measurement was repeated at least three times for LDV tests. Finally, time resolved DLS (TRDLS) experiments were conducted to both have further information about the stability over time, but also to confirm the feasibility of the column tests. Namely, a TRDLS

3.3. NANOPARTICLES CHARACTERIZATION

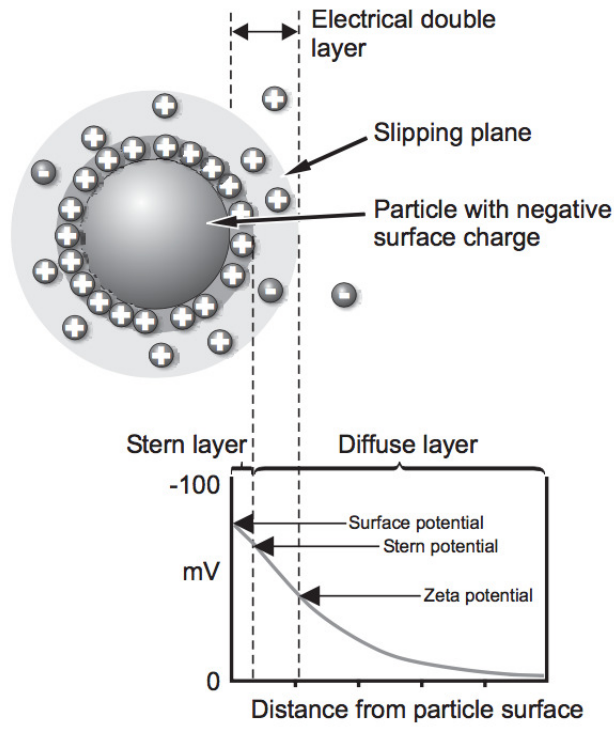


Figure 3.2: Zeta potential. From Malvern manual [140].

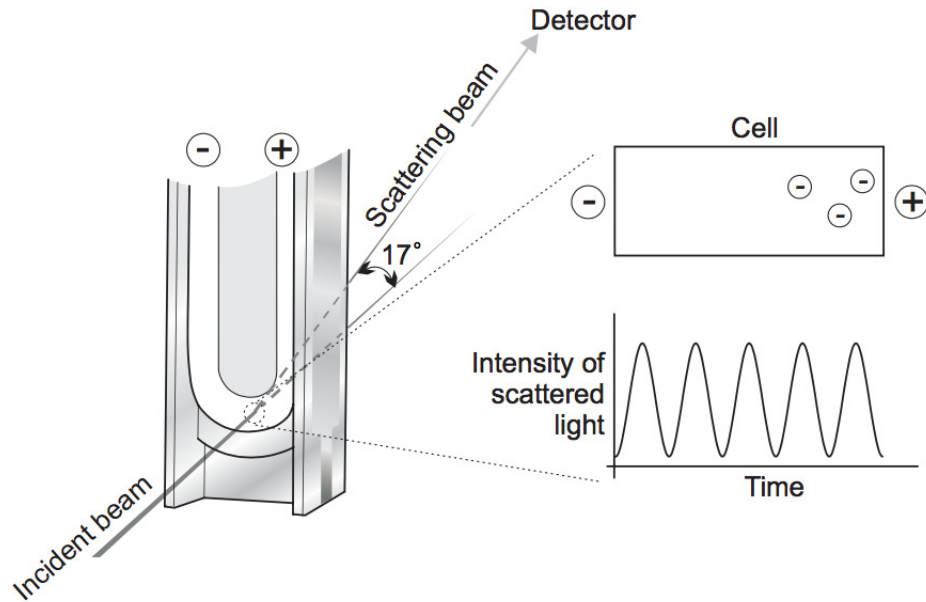


Figure 3.3: LDV technique. From Malvern manual [140].

consists of a series of DLS measurements conducted over a given time period, with scheduled measurements each 15 minutes. The goal of this test is to check how the particles behave in a given solution chemistry, i.e., whether they aggregate or not, how fast they do that, *etc.*. Furthermore, the particles, according to the time required to conduct the column tests, should be dispersed into the suspension for almost 90/120 minutes. To identify whether the particles aggregate even before entering to the column, altering the deposition data, the TRDLS was essential. The TRDLS also illustrated the inherent difference in P25 and CoRI C stability.

3.4 Freeze/Thaw

Along with the 10 °C deposition test, other column test were conducted. To simulate the temperature condition of a "mild" Canadian winter, the particles were subjected to a Freeze/Thaw test. This test was conducted in a recirculating chiller (Julabo 200F) filled with a mixture of Water/propylene glycol 70/30. All particle suspensions used in F/T studies were prepared in the same manner as those used in colloid filtration studies and NPs characterization. Therefore, following the standard nTiO₂ preparation procedure explained above, each sample each sample was split into two 50 mL falcon tubes, sealed with parafilm, and placed in the chiller. There, the sample was fixed on a styrofoam support in a way that every falcon tube would equally immersed in the bath, avoiding preferential cooling. The test is run over 24 hours from -10 °C to +10 °C, as shown in Fig.3.4. This test aims to understand how the particles could react to freezing and whether their behaviour changes or not because of that. To only take in account the effect of freezing/thawing and not the combined one of freezing and aggregation due to the temperature/time interplay, another sample was prepared as control: made in the same way but stored in the fridge at 10 °C. It is made under the same identical conditions, in the same way, but it is stored in fridge at 10 °C. After 24 hours, when the test is over, the two samples, the F/T and control, are run. Since, as we will see, the TRDLS data show that after 24 hours, the suspension have stabilized and there is a little, if any, continuing aggregation. The F/T were always run first, as soon as possible after finishing the F/T cycle. Prior to each deposition experiment, the falcon tubes were gently flipped once, in order to resuspend them without breaking up the aggregates, and then run.

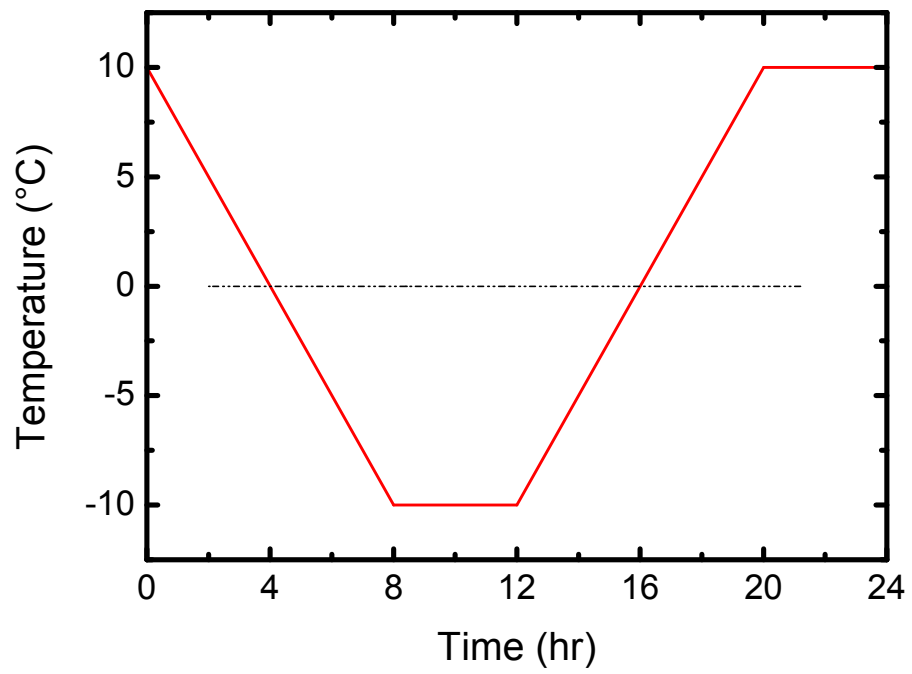


Figure 3.4: F/T test. Temperature over time.

Chapter 4

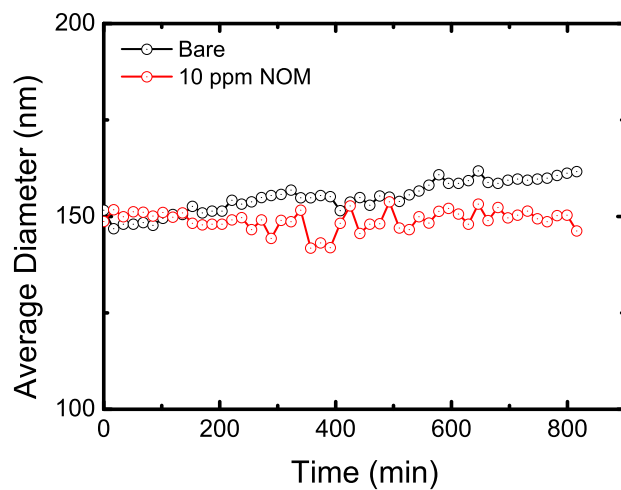
Results and Discussion

4.1 Nanoparticle properties: Size, Zeta, Stability (TRDLS)

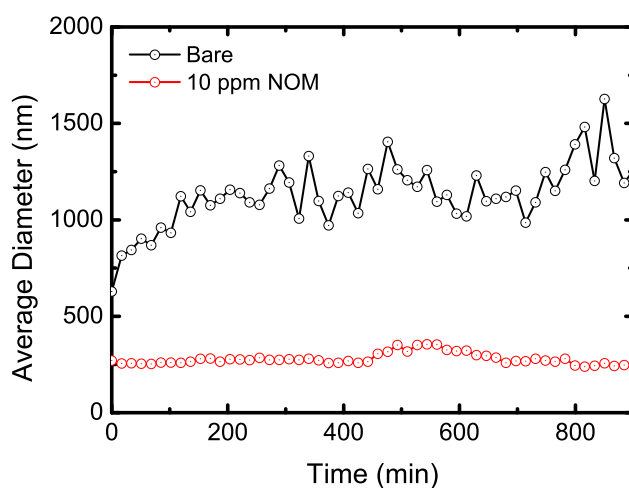
4.1.1 10°C experiments

As widely acknowledged [79, 80, 143], particle size is a key factor influencing the NP transport behaviour in granular aqueous systems. Besides, when the particles are suspended, because of the chemistry of the solution and the surrounding natural environment [98], their actual diameter is far greater than declared nominal sizes [144]. Keeping in mind that also the composition of the particles has been found to influence aggregation [143], a series of experiments were performed to characterize the materials used in the study as support in the interpretation of data obtained from the colloid deposition tests. First of all, TRDLS tests were conducted to provide an overview of the stability of the suspensions over time. The tests run for almost 16 hours and show the stabilization role of the NOM. As explained in Chapter 2.2.4, the presence of NOM may lead to a electrosterical stability, enhancing the repulsion forces. This mechanism has been suggested from many quarters [131, 145–148, 151]. Moreover, NOM has also known to alter the surface characteristics of NPs by changing surface charges, reactivity, and aggregation behaviour [152]. The NOM is composed of thousands of organic compounds, both high and low molecular weight substances (e.g. organic acids, sugars and other carbohydrates, cellulosic materials, alginate, proteins, lipids, *etc.*) for this reason there is still some uncertainty about its mechanism of stabilization. However, it is usually accepted that NOM can adsorb on the surface of NPs, negatively charge them and increase repulsive energy of the electrostatic double layer (EDL). Its addition may so lead to the stabilizing of the NPs and to their smaller aggregate size. Besides, NPs can be stabilized by NOM through complexation between the acidic functional groups (mainly carboxylic acid) [153]. The Figure 4.1 shows TRDLS data for P25, bare and coated with 10 ppm NOM respectively in 1mM NaCl and 100mM NaCl. The particles seem to be stabilized by the presence of NOM. Aggregation is much greater at higher IS. The reason for this could be that by increasing the IS of the solution, the NOM should become more coiled and more

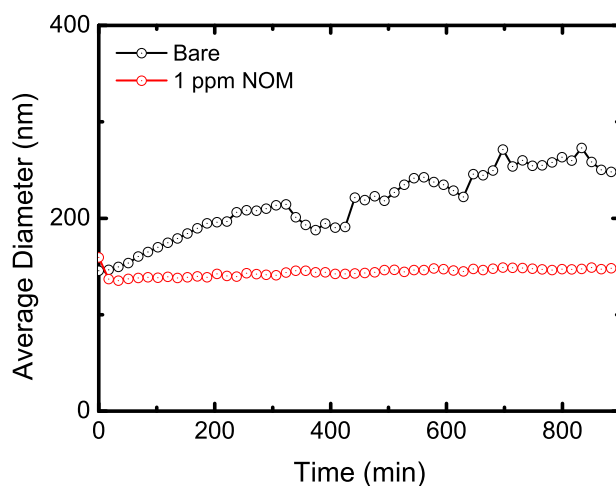
4.1. NANOPARTICLE PROPERTIES: SIZE, ZETA, STABILITY (TRDLS)



(a)



(b)



(c)

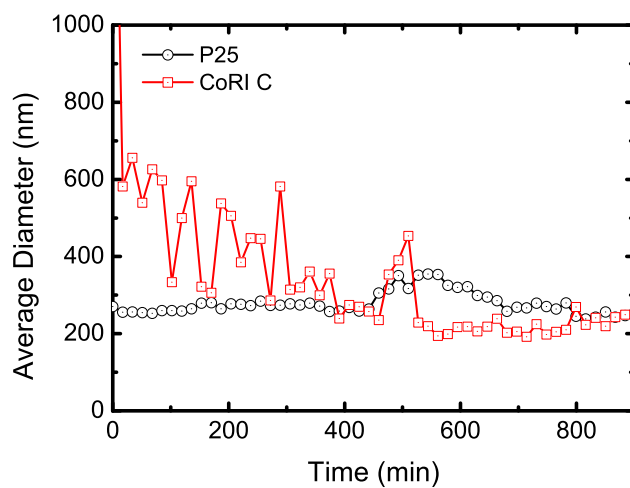
Figure 4.1: Time resolved DLS measurements. (a) P25 suspended in 1 mM NaCl, coated with 10 mg/L NOM and bare. (b) P25 suspended in 100 mM NaCl, coated with 10 mg/L NOM and bare. (c) P25 suspended in MHRW, coated with 1 mg/L NOM and bare. Every suspension contains 5 mg/L P25 and the pH is $7,9 \pm 0,1$.

4.1. NANOPARTICLE PROPERTIES: SIZE, ZETA, STABILITY (TRDLS)

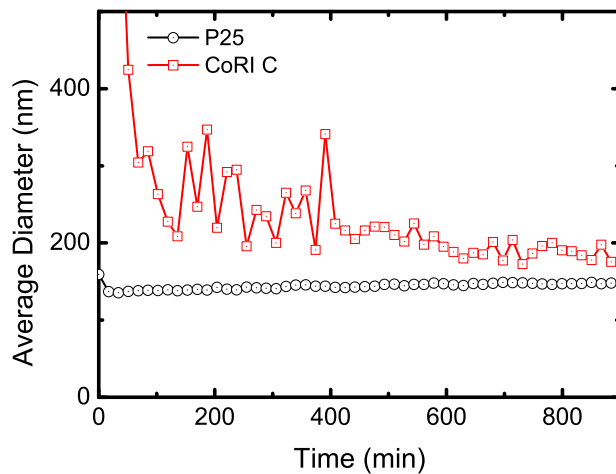
compact likely changing its shape from linear to spherical [150], allowing a larger amount of NOM onto the $n\text{TiO}_2$ surface [151]. In other words, higher IS compress the EDL around the $n\text{TiO}_2$, leading to a reduction in electrostatic repulsion between NOM and $n\text{TiO}_2$, allowing more NOM to cover the same surface area of the nanoparticles due to neutralization of the surface charge of $n\text{TiO}_2$ [151, 154]. Moreover, Figure 4.1 also suggests that the absorption of NOM onto the $n\text{TiO}_2$ surface largely depends on the specific ions present in solution, as suggested by [151]. In fact in MHRW, even a lower concentration of NOM, can have a significant effect on the colloidal stability. Finally, Figure 4.2 displays the structural difference between P25 and CoRI C. The CoRI C always aggregates in larger particles, in both MHRW and 100 mM. This gives us an insight about the difference in deposition behaviour between the two particles, as will be explained below. It would also be helpful to note what is shown in Figure 4.3. They are the size distribution profiles from 0 to 120 minutes. On the opposite of P25, whose average diameter slowly increases over time, for CoRI C sometimes, after some point, the average diameter, decreases. An explanation for this is the inherent instability of the CoRI C. As we can see in Figure 4.3, from 90 to 120 minutes, the profile goes back to smaller diameter. That is due to the sedimentation of the larger aggregates onto the bottom of the cuvette, outside the instrument's path of detection. Therefore, every comparison between CoRI C and P25 over time, has to read keeping that in mind. As will be seen below, the difference between CoRI C and P25 is mainly in their stability. In fact, along with the hydrodynamic diameter, the size measurements report the Polydispersity index (PDI). The hydrodynamic diameter is presented in Figure 4.1 4.2 4.3, which is defined as "the size of a hypothetical hard sphere that diffuses in the same fashion as that of the particle being measured" [155] and is the broadest way to characterize the particle size. When collecting the size during and after the deposition study, it makes sense introduce the PDI index to characterize the particles' distribution in a colloidal suspension. When the index is lower than 0,05, it means the particles are very highly monodispersed. Instead, if it greater 0,7, it means that the suspension has a very broad size distribution. As will be explained, except under very specific conditions, the PDI for suspensions of P25 was always in between this range of 0,05 - 0,7. Conversely, the CoRI C was always very polydispersed. This emphasises, once again, that for given conditions of pH, IS and NOM concentration, the P25 will always be more stable. Table 4.1 and Figure 4.2 provide a summary of PDI and hydrodynamic diameter of the column effluent. However, no significant differences were found between effluent and influent scenarios.

It has been widely stressed that an high absorption of NOM produces vast negative charge on the $n\text{TiO}_2$ [131]. In particular, since our pH has been set around 8 to be representative of a natural environment, [138], the $n\text{TiO}_2$ is already slightly negatively charged. In that light, the electrophoretic mobility (EPM) data find consistency. Figure 4.4 shows the electrophoretic mobility for both CoRI C and P25. The data equally refer to influent or eluent suspension, since no difference was observed in electrokinetic properties between the injected particles and those filtered

4.1. NANOPARTICLE PROPERTIES: SIZE, ZETA, STABILITY (TRDLS)



(a)



(b)

Figure 4.2: Time resolved DLS measurements: P25 & CoRI C. (a) $n\text{TIO}_2$ suspended in 100 mM NaCl, coated with 10 mg/L NOM. (b) $n\text{TIO}_2$ suspended in MHRW, coated with 1 mg/L NOM. Every suspension contains 5 mg/L P25/CoRI C and the pH is $7,9 \pm 0,1$.

4.1. NANOPARTICLE PROPERTIES: SIZE, ZETA, STABILITY (TRDLS)

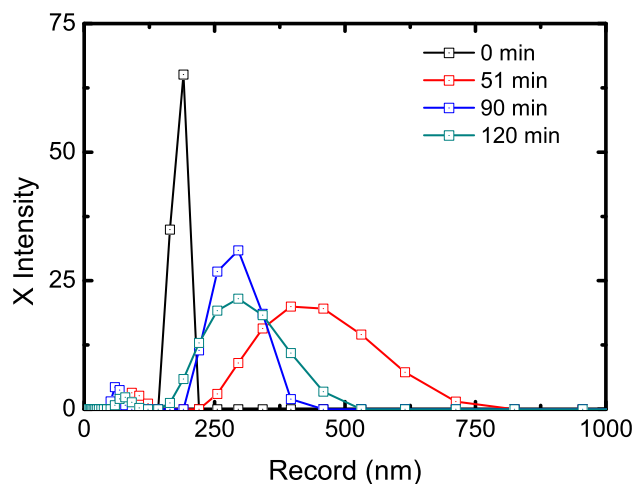
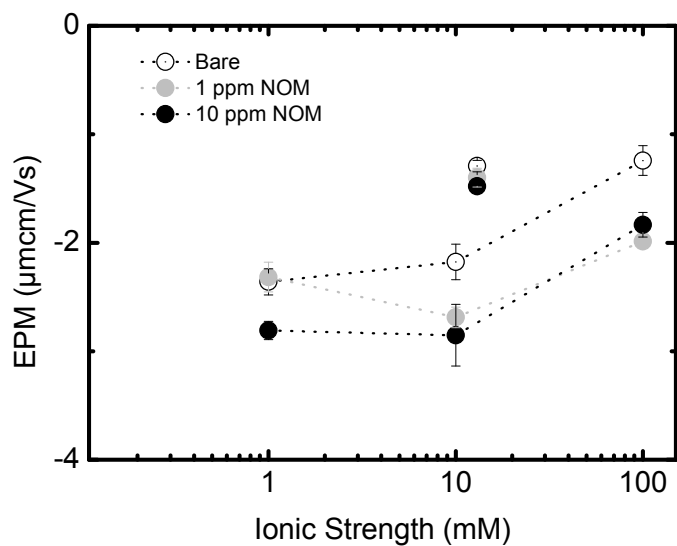


Figure 4.3: Size distribution over time 5 mg/L CoRI C in 100 mM NaCl, coated with 10 mg/L NOM. The the pH of the suspension is $7,9 \pm 0,1$.

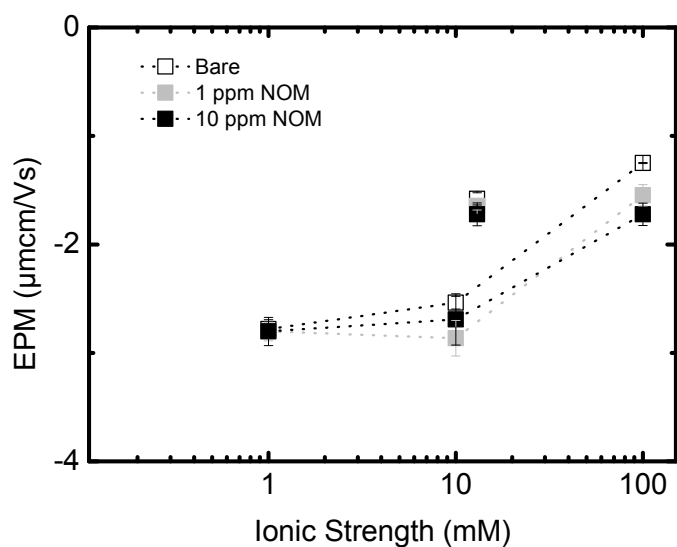
through the column. As would be expected, the IS greatly influences the surface charge of the particles. Regardless their morphological nature (Anatase, Rutile), enhancing the IS of the solution, means shortening the Debye length and so allowing the particles to draw closer to each other. Besides, the NOM both adsorbs on the particles and stand in their aggregation. Moreover, as pointed above, this effect is much evident at higher IS. Some recents studies, for instance [151], explained the interplay pH-IS on the NOM adsorption on nTiO₂. The pH usually hinders the NOM attachment because increasing the pH also increases the negative charge on both nTiO₂ and NOM [156]. Moreover, the higher the pH, the higher the solubility of NOM in the solution due to more extensive dissociation of carboxylic and phenolic groups, present in NOM. Therefore, there would be a greater tendency for NOM to remain in solution at high pH [156, 157]. Besides, at this pH it seems reasonable to suppose that the unfavourable effect of the relative high pH on kinetic absorption, may overcome the favorable effect of IS. However, adsorption studies [151] conducted under same condition of pH and concentration of both NOM and nTiO₂ have revealed that, even working with only 1 mg/L and 5 mg/L should be theoretically enough to have the particles almost completely covered. All things considered, the EPM trend is not linear with IS and probably, after a certain concentration of NaCl in solution, the particles are fully covered and to continue to increase the IS only leads to greater double layer compression.

Figure 4.4 also draws attention on at least two other key points: The role of the ionic valence and the P25-CoRI C difference. Yet in section 2.4.3 the importance of the valence z was pointed out. Moreover, according to the Hofmeister series [158] an ion of a given valence has a tendency to adsorb in direct proportion to its unhydrated size. Hence, at a given IS, the behaviour of the MHRW suspension is

4.1. NANOPARTICLE PROPERTIES: SIZE, ZETA, STABILITY (TRDLS)



(a) P25



(b) CoRI C

Figure 4.4: Electrophoretic mobility for P25 and CoRI C at $T = 10\text{ }^{\circ}\text{C}$ (a) nTiO_2 P25 in 1, 10, 100 mM NaCl and MHRW; bare and coated with 1 and 10 mg/L NOM. (b) nTiO_2 CoRI C in 1, 10, 100 mM NaCl and MHRW; bare and coated with 1 and 10 mg/L NOM. The pH of the suspension is $7,9 \pm 0,1$.

4.1. NANOPARTICLE PROPERTIES: SIZE, ZETA, STABILITY (TRDLS)

ruled by Ca^{2+} and Mg^{2+} . This is the reason why, for both CoRI C and P25, the the binding of the polyvalent ions on the particles surface effects more efficient charge neutralization.

Regarding the difference between the two kinds of particles, it seems clear that trend and values are pretty straightforward. But still, because at 100 mM NaCl the CoRI C EPM is somewhat "less negative", that would suggest, along with the huge size and polydispersity at those conditions (Tables 4.1,4.2), that something different is going on.

4.1.2 Freeze/Thaw Data: EPM

Figure 4.5 illustrates the EPM after the Freezing/Thawing test and Table 4.3 summarizes the related size and deposition data. This time, the EPM data are difficult

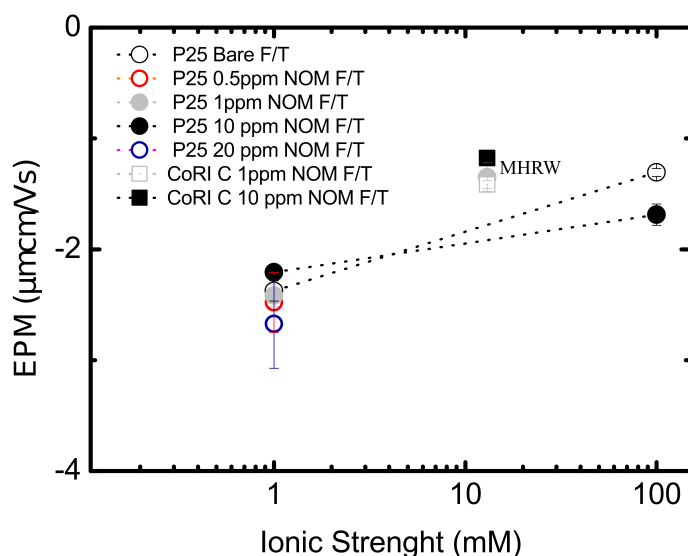


Figure 4.5: EPM data for CoRI C and P25 treated with F/T. P25 in 1 or 100 mM NaCl and MHRW, coated with 0,5 to 20 mg/L NOM or uncoated. CoRI C in MHRW, coated with 1 or 10 mg/L NOM. The the pH of the suspension is $7,9 \pm 0,1$ and the temperature is 10°C .

to draw conclusions from. The freezing of the particles is something beyond the DLVO theory and the Guoy-Chapman model as well. The most influential factor here is the size of the particle. The freezing physically force them together, at a temperature that is above 0°C for 12 hours. That is something new, which aims to bridge from lab to natural environment scenario. For this reason, even though EPM is, on average, higher than the 10°C case, the gateway to truth is not in EPM data. Table 4.3 cointains size and polydispersity for each IS/NOM/nTiO₂ configuration. Even the P25 are now very polydispersed and their average diameter are far bigger than the 10°C situation. What we still don't know is what exactly keeps the particles attached after the freezing. It is very likely they fall in an energy well where

4.1. NANOPARTICLE PROPERTIES: SIZE, ZETA, STABILITY (TRDLS)

they cannot go out from because the low temperatures. But we do know that the macroscopical phase transition from liquid to solid, really alters even the smallest boundary condition of the problem. The idea was to focus the attention at the ends of our NOM/IS range, to be sure to picture it in the best possible way. For this reason the point of Figure 4.5 could appear very scattered. Since the P25 appeared to be, as we will see in the deposition section, the most suitable to duplicate the results, a wide range of IS and NOM were then investigated. The attention was focused on the cases of large amount of NOM but low IS and viceversa. But then, as the Figure 4.5 shows, an higher EPM was found in presence of 10 mg/L NOM than that of the bare particles. That is something unexpected but it matched with the deposition data. For this reason a wider range was examined. The P25 seemed to be more unstable in an NOM concentration from 1 to 10 mg/L and in an 1mM electrolyte. The CoRI C was studied only coated with NOM because of its difficulty in reproducing the data otherwise, due to the formation of huge aggregates (way over the μm). The CoRI C was found more stable in presence of a lower concentration of NOM in the 1-10 mg/L range and in MHRW. The reason why could be that, because of the low IS, during the freezing the NOM may become adsorbed unto two or more particles. However, because of the freezing the coated particles may be keep to stay very close one another. Therefore, during the thawing, they can lead to a bridging flocculation. Attachment efficiency trends, below, support this. Every EPM data, for both 10°C and F/T represents the average of two experiments. Every 24 h EPM control data was more stable than the related F/T, with a more negative EPM and usually smaller size, data not shown.

4.1.3 Size: Hydrodynamic diameter and Polydispersity

Looking at the Tables 4.1 and 4.2 it is possible to back up what just explained. At 10 °C the CoRI C are always polydispersed and forms very big aggregates under every suspension chemistry. It would helpful to remember that the DLS works well until 1-1,5 μm . For huge aggregates, every numerical data is starting losing importance, so basically 2 μm could easily be 2,5 μm and viceversa. What really matters is the order of magnitude and that is, for CoRI C, completely different than that of P25. Moreover, Tables 4.1 and 4.2 also contain, together with the Z-average, the Intensity mean of each measurements. The intensity mean represents the peak intensity of the size distribution. They are shown mostly for two reasons: it helps to understand how dramatically the particles are dispersed, but also because the intensity mean usually stands for the main diameter of the most stable aggregates. It is interesting to note this subtext because it aids to realize how differently the two kinds of particles behave. In fact, comparing the intensity means in a given condition of IS/NOM, it appears how the CoRI C are still bigger or at most equal in size. This points out that, even in the worst case scenario of CoRI C nTiO₂ dispersed into a natural environment, the mobility of that teensy stable fraction would likely be lower than that of a P25 nTiO₂ dispersed in the same ecosystem. Table 4.3 corroborates the EPM data above. As anticipated in case of Freez-

4.1. NANOPARTICLE PROPERTIES: SIZE, ZETA, STABILITY (TRDLS)

Table 4.1: P25 Aggregation and Deposition summary at $T = 10\text{ }^{\circ}\text{C}$. The size data generally refers to the effluent from the column, but either way, no significant difference was noted between effluent and influent data. These are average values of at least two measurements. Where the value of Alpha and C/C_0 are not present, the size data only refers to the influent suspension. * the Physical straining condition refers to [159].

Electrolyte	IS (mM)	EnP	NOM (mg/L)	C/C_0	α_d^{TE}	I. mean (nm)	PDI	z-avg (nm)	P. straining* $\frac{dp}{dc} > 0,003$
NaCl	1			0,97 ± 0,01	0,01 ± 0,01	176 ± 33	0,19 ± 0,03	165 ± 30	NO
	10	P25	0	-	-	172 ± 41	0,18 ± 0,04	162 ± 21	NO
	100			0,03 ± 0,01	0,41 ± 0,01	643 ± 129	0,72 ± 0,14	1622 ± 121	YES
MHRW	13	P25	0	0,20 ± 0,01	0,21 ± 0,01	163 ± 4	0,18 ± 0,01	153 ± 10	NO
NaCl	1			0,98 ± 0,01	0,01 ± 0,01	215 ± 4	0,24 ± 0,05	183 ± 3	NO
	10	P25	1	0,93 ± 0,01	0,01 ± 0,01	177 ± 30	0,15 ± 0,04	156 ± 7	NO
	100			0,31 ± 0,01	0,12 ± 0,02	242 ± 7	0,23 ± 0,03	243 ± 3	NO
MHRW	13	P25	1	0,82 ± 0,01	0,06 ± 0,02	152 ± 5	0,21 ± 0,03	155 ± 5	NO
NaCl	1			0,99 ± 0,02	0,00 ± 0,01	175 ± 6	0,18 ± 0,03	160 ± 5	NO
	10	P25	10	0,99 ± 0,01	0,01 ± 0,01	151 ± 8	0,20 ± 0,02	157 ± 11	NO
	100			0,42 ± 0,02	0,10 ± 0,02	255 ± 4	0,32 ± 0,03	265 ± 2	NO
MHRW	13	P25	10	0,96 ± 0,03	0,01 ± 0,01	163 ± 1	0,18 ± 2	154 ± 5	NO

4.1. NANOPARTICLE PROPERTIES: SIZE, ZETA, STABILITY (TRDLS)

Table 4.2: CoRI C Aggregation and Deposition summary at $T = 10\text{ }^{\circ}\text{C}$. The size data generally refers to the effluent from the column, but either way, no significant difference was noted between effluent and influent data. Where the value of Alpha and C/C_0 are not present, the size data only refers to the influent suspension. These are average values of at least two measurements. * the Physical straining condition refers to [159].

Electrolyte	IS (mM)	EnP	NOM (mg/L)	C/C_0	α_d^{TE}	I. mean (nm)	PDI	z-avg (nm)	P. straining* $\frac{dp}{dc} > 0,003$
NaCl	1			$0,91 \pm 0,01$	$0,01 \pm 0,01$	204 ± 22	$0,98 \pm 0,02$	2061 ± 600	YES
	10	CoRI C	0	-	-	175 ± 43	1 ± 0	2945 ± 828	YES
	100			-	-	225 ± 21	1 ± 0	2621 ± 432	YES
MHRW	13	CoRI C	0	$0,33 \pm 0,06$	$0,14 \pm 0,01$	150 ± 2	1 ± 0	2098 ± 200	YES
	NaCl	1		$0,91 \pm 0,01$	$0,01 \pm 0,01$	198 ± 15	$0,99 \pm 0,01$	1866 ± 200	YES
		10	CoRI C	1	$0,60 \pm 0,06$	$0,06 \pm 0,01$	225 ± 44	$0,96 \pm 0,03$	1501 ± 350
100			$0,08 \pm 0,02$	$0,60 \pm 0,2$	324 ± 76	$0,99 \pm 0,01$	2074 ± 288	YES	
MHRW	13	CoRI C	1	$0,58 \pm 0,02$	$0,07 \pm 0,01$	177 ± 11	1 ± 0	2157 ± 126	YES
NaCl	1			$0,75 \pm 0,1$	$0,02 \pm 0,01$	163 ± 3	1 ± 0	1594 ± 104	YES
	10	CoRI C	10	$0,77 \pm 0,08$	$0,03 \pm 0,08$	206 ± 32	$0,99 \pm 0,01$	1603 ± 129	YES
	100			$0,46 \pm 0,01$	$0,10 \pm 0,01$	142 ± 10	1 ± 0	1640 ± 1487	YES
MHRW	13	CoRI C	10	$0,76 \pm 0,01$	$0,03 \pm 0,01$	176 ± 6	1 ± 0	2029 ± 200	YES

4.1. NANOPARTICLE PROPERTIES: SIZE, ZETA, STABILITY (TRDLS)

Table 4.3: P25 and CoRI C Aggregation and Deposition summary for FIT. The size data generally refers to the effluent from the column, but either way, no significant difference was noted between effluent and influent data. Where the value of Alpha and C/C_0 are not present, the size data only refers to the influent suspension. These are average values of at least two measurements. * the Physical straining condition refers to [159]. ** Size distribution not available.

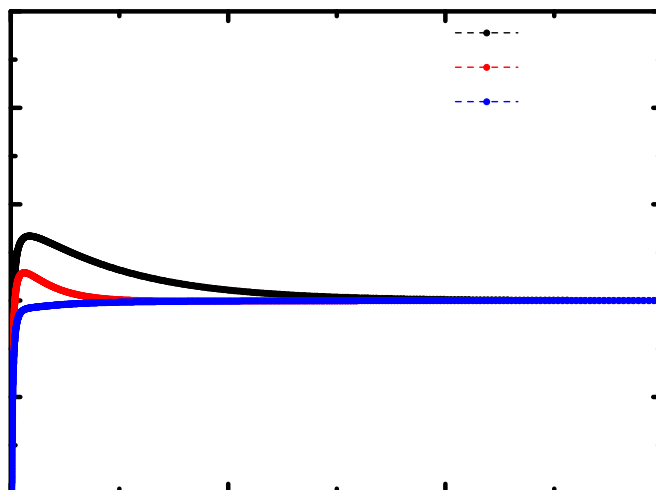
Electrolyte	IS (mM)	EnP	NOM (mg/L)	C/C_0	$\alpha_d^{T,E}$	I. mean (nm)	PDI	z-avg (nm)	P. straining* $\frac{dP}{dc} > 0,003$
NaCl	1	P25	0	0,98 ± 0,02	0,004 ± 0,002	166 ± 24	0,19 ± 0,01	148 ± 10	NO
	100			0,02 ± 0,01	0,438 ± 0,001	126 ± 158	1 ± 0	3657 ± 931	YES
NaCl	1	P25	0,5	0,94 ± 0,01	0,007 ± 0,001	219 ± 14	0,33 ± 0,01	249 ± 8	NO
NaCl		P25	1	0,83 ± 0,05	0,022 ± 0,007	152 ± 113	1 ± 0	4492 ± 2441	YES
MHRW	13	P25	1	0,82 ± 0,04	0,020 ± 0,003	156 ± 10	0,22 ± 0,08	155 ± 5	NO
NaCl	1	P25	10	0,71 ± 0,04	0,041 ± 0,005	182 ± 29	0,96 ± 0,07	1483 ± 336	YES
	100			0,02 ± 0,01	0,437 ± 0,001	248 ± 98	0,82 ± 0,177	1181 ± 398	YES
MHRW**	13	P25	10	0,73 ± 0,01	0,016 ± 0,001				-
NaCl	1	P25	20	0,92 ± 0,01	0,016 ± 0,001	225 ± 5	0,21 ± 0,02	225 ± 3	NO
MHRW	13	CoRI C	1	0,47 ± 0,01	0,095 ± 0,001	87 ± 20	1 ± 0	3225 ± 400	YES
MHRW	13	CoRI C	10	0,41 ± 0,01	0,104 ± 0,001	110 ± 30	1 ± 0	4651 ± 1000	YES

4.1. NANOPARTICLE PROPERTIES: SIZE, ZETA, STABILITY (TRDLS)

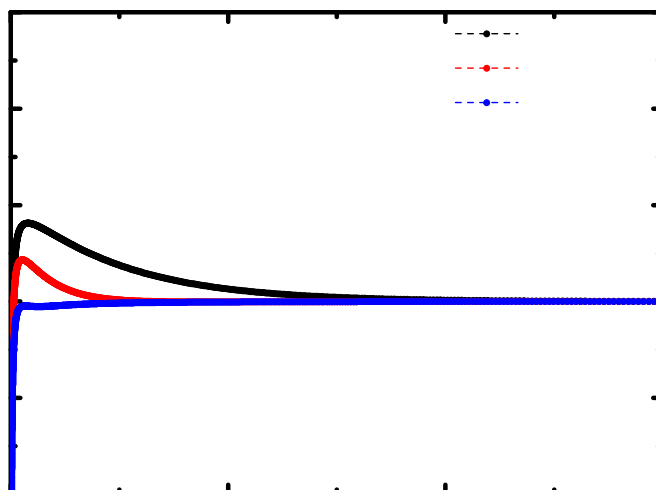
ing/Thawing cycles, even the P25 often appeared very polydispersed. The sizes are significantly higher than those at 10 °C, for every cases. Some data are evidently out of range (e.g., P25 1 mg/L NOM in 1mM NaCl) but are still reported to emphasize the magnitude of the phenomenon. The Z-average (hydrodynamic diameter) helps in determining how the particles behave as aggregate. Therefore, is not difficult to imagine that the focus is now switching from electrochemical causes of aggregation to physical causes of aggregation. It also has never to be forgot that the aim of all this aggregation data is to fully understand how the particles would move in an actual environment. How and to what extent does the temperature influence the mobility? How and to what extent the solution chemistry (IS, NOM) does?. Bearing in mind that this is something now, there will not be a comprehensive answer, but only insights and perspectives. For example, as already stressed before, the NOM seems to destabilize the suspension within a concentration of 1-10 mg/L and in presence of relative low IS. The size data converge to the same hypothesis. The 24h control data follow well enough the TRDLS and don't present such huge aggregates. The latter means that the aggregation is due to the interplay between freezing/NOM concentration and, at the same time, it doesn't depend on how long the samples are stored in fridge. What has been said perfectly matches with both P25 in 1 mM NaCl and CoRI C in MHRW. However, for the sake of accuracy, one last thing should be stressed. As matter of fact, the CoRI C, coated with 1 and 10 mg/L, suspended in MHRW, doesn't have very clear data. Here, if it's true that the 24h control size data (I.mean and hydrodynamic diameter as well) are lower than the F/T, it is also true that the difference is way outside the sensitivity of the equipment. We are talking about a Z-average of 3200 nm vs 1290 nm and 4650 nm vs 2900 nm respectively for F/T and control coated with 1 and 10 mg/L NOM. The particles stored in fridge for 24 hours are indeed much smaller and the tests were at least duplicated. But still, because of the very high PDI and the sensitivity of the DLS, the aggregation of CoRI C nTiO₂ during the F/T test, may also be somewhat influenced by the time of the test.

4.1.4 DLVO Profiles

DLVO interactions were calculated using the 2015 version of the MNMs - Micro - and Nanoparticles transport, filtration and clogging Model - Suite software. The Hamaker constants of P25 and CoRI C in vacuum, refers to [160] and [106], while molecular weight, density and molecular volume of NOM, respectively refer to [161], [162] and [163]. The interactions were investigated for the 10°C conditions and for both P25 and CoRI C in 1-100 mM NaCl. Figures 4.6 and 4.7 show the results. These, partially confirm what seen in Figure 4.4 and Tables 4.1 and 4.2. In fact, Figures 4.6 and 4.7 points out that the aggregation will be very likely in between 10 - 100 mM NaCl for P25 nTiO₂. In particular, as will be clear below, when the particles are suspended in 100 mM NaCl there is no repulsion force to keep them separated, since the IS is here too high and completely overcomes the repulsion force due to the EDL and, eventually, to the presence of NOM. Moreover,

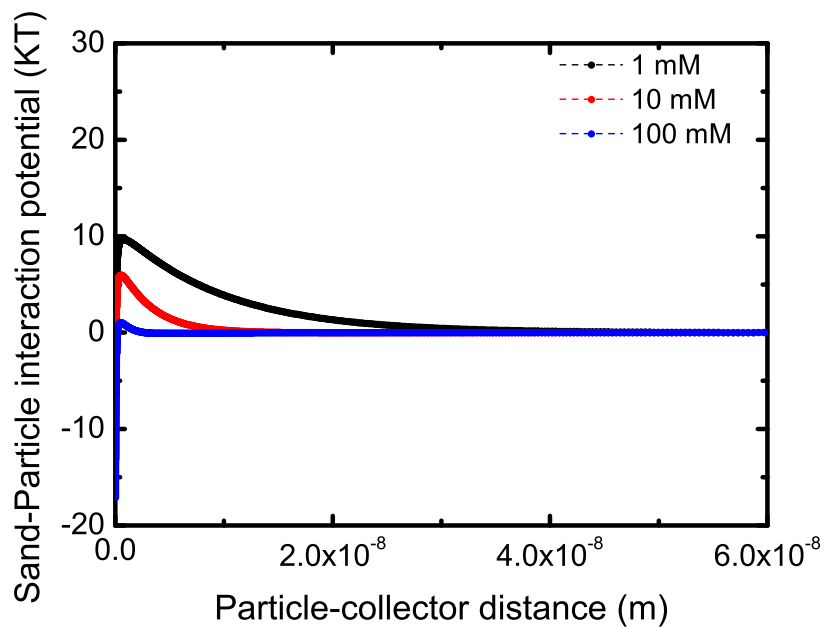


(a) Bare

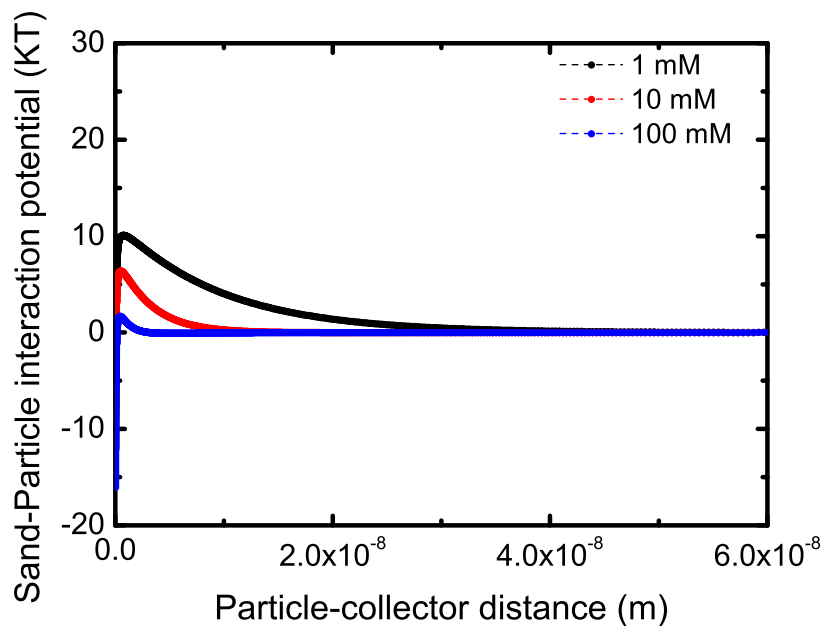


(b) 10 ppm NOM

Figure 4.6: Representative Φ_{Tot} profiles for P25 suspended in 1-100 mM NaCl, (a) bare and (b) coated with 10 ppm NOM, at $T = 10^\circ\text{C}$ and $\text{pH } 7,9 \pm 0,1$.



(a) Bare



(b) 10 ppm NOM

Figure 4.7: Representative Φ_{Tot} profiles for CoRI C suspended in 1-100 mM NaCl, (a) bare and (b) coated with 10 ppm NOM, at $T = 10^\circ\text{C}$ and $\text{pH } 7,9 \pm 0,1$.

the NOM stabilizing role on P25 nTiO₂ looking at the H_{barr} of Figure 4.6. In turn, just as seen in Figure 4.4, the CoRI C behaviour seems very less influenced by the presence of NOM. Hence, the energy profiles of both P25 and CoRI C singularly match with the DLVO theory and the EPM data as well. Increasing the IS, the total interaction shifts from repulsion to attraction, for the reasons already explained in the second chapter. Besides, P25 presents a secondary minimum when dispersed in 100 and 10 mM NaCl, in both Bare and coated cases. The depth of the minimum is around 0,3 KT for the bare particles and 0,2 for the coated ones at 10mM NaCl. Conversely, it is 0,2 and 0,1 at 100 mM NaCl for bare and 10 mg/L NOM coated, respectively. Therefore, this suggests how the aggregation as flocculation might be slightly important in these conditions. In Turn, CoRI C particles do not present a secondary minimum of energy. Finally, the theoretical interaction profiles, do not aid to find out the different between the two kinds of nTiO₂. Figure 4.8 illustrates the interactions profiles for P25 after freezing/Thawing cycle. As will be explained below, they stress the effect of NOM on transport of P25 after freezing. Namely, the NOM seems, in a concentration between 1 - 10 mg/L, to destabilize the suspension. The reasons why will be further explained below. The H_{barr} here is always considerable high ($> 10 k_B T$) and therefore the particles shouldn't aggregate easily in such conditions. No secondary energy minimum was here found.

4.2 Deposition Experiments

Two series of tests were conducted to examine the colloid transport behaviour in a column packed with silica sand. The first experiment was carried out using suspended nTiO₂ at $T = 10^\circ\text{C}$ and $\text{pH } 7,9 \pm 0,1$ and under a wide range of solution chemistries, i.e., IS 1-100 mM resulting from NaCl or MHRW and NOM 0-10 mg/L. The second set of column test was performed with F/T nTiO₂ at $T = 10^\circ\text{C}$ and $\text{pH } 7,9 \pm 0,1$ and under the same range of solution chemistries but a wider range of NOM (0-20 mg/L). P25 and CoRI C nTiO₂ were used in both of the series. The obtained particles breakthrough curves (BTc) are plotted as normalized particle concentration at the column effluent C/C_0 versus pore volumes. C/C_0 is calculated from the absorbance of column effluent under the clean-bed condition (1,9 to 2,1 PVs) divided by the column bypass at $\lambda = 290 \text{ nm}$. The pore volume is the volume needed to completely replace the water held in the saturated column or, in other hands, one pore volume is simply the total volume of water contained between the sand grains in the column. The number of pore volumes that have passed through a column is often utilized as dimensionless time [164]. PVs and C/C_0 usually permit the comparison of breakthrough curves from columns of different sizes since each column will be normalized to its own pore volume [165]. To quantify and compare the colloid transport behaviour under different experimental conditions, the attachment efficiency α_d was used, calculated using colloidal filtration theory (Eq.2.47). The value η_0 for each experimental condition were determined using the Tufenkji and Elimelech correlation (Eq.2.35).

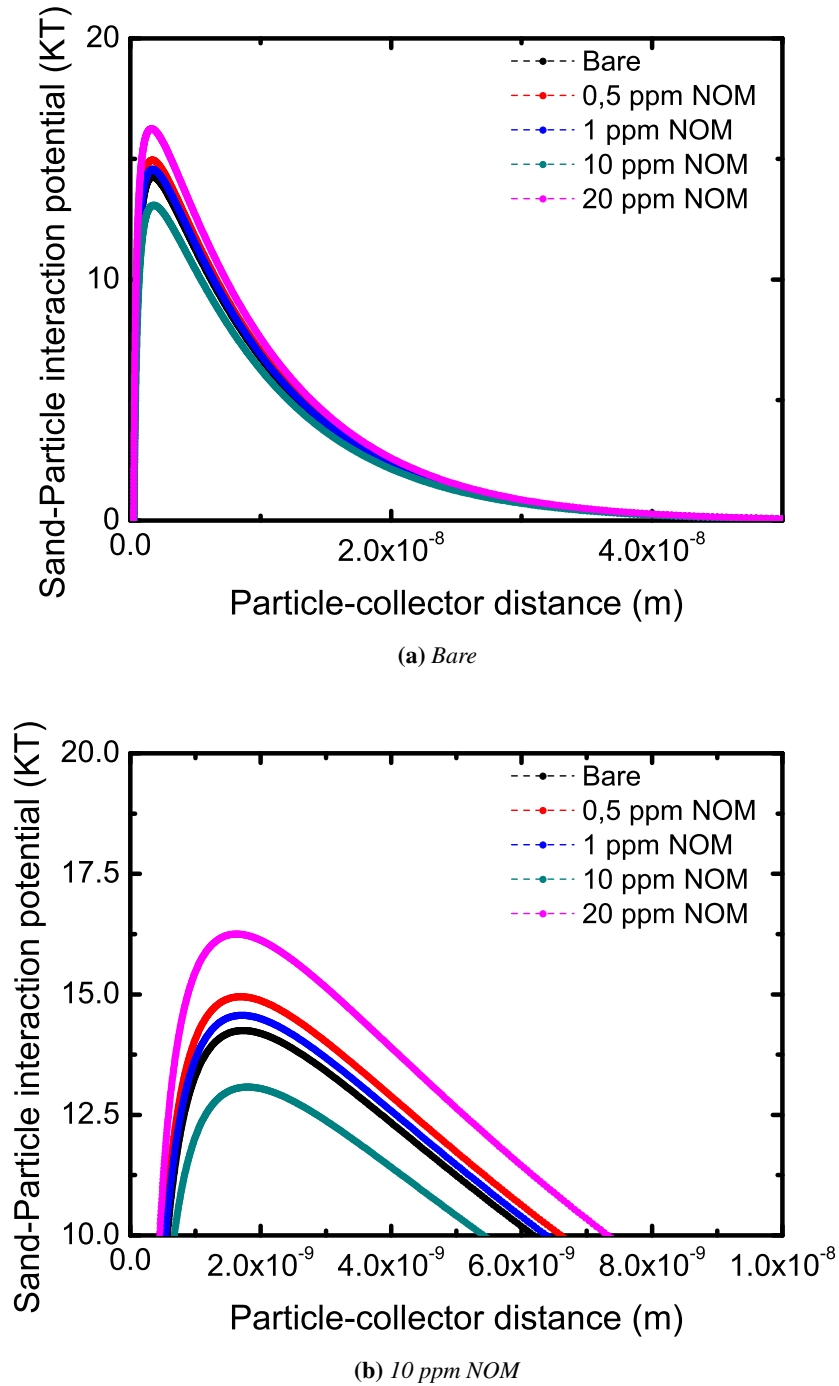


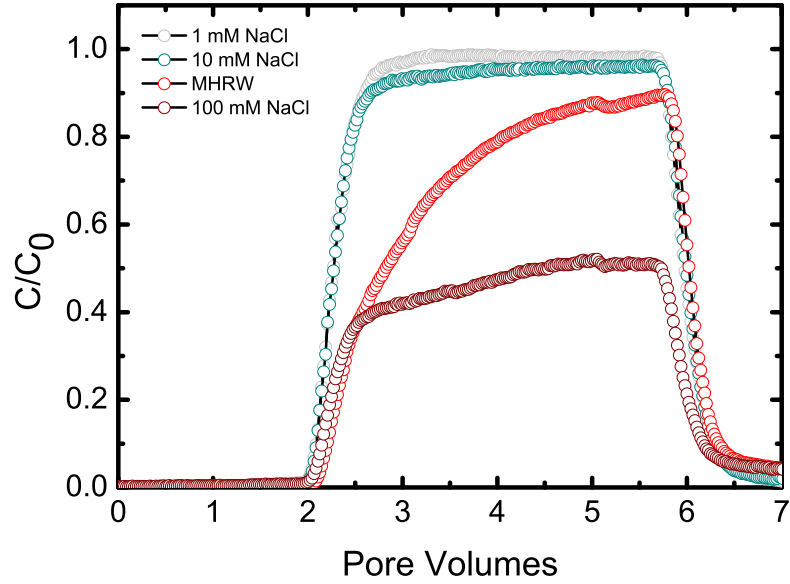
Figure 4.8: Representative Φ_{Tot} profiles for F/T P25 suspended in 1 mM NaCl with 0 - 20 mg/L NOM, (a) profiles and (b) zoomed image of the energy barrier. Tests conducted at $T = 10^\circ\text{C}$ and $\text{pH } 7,9 \pm 0,1$.

4.2.1 Role of Salinity and NOM at 10 °C

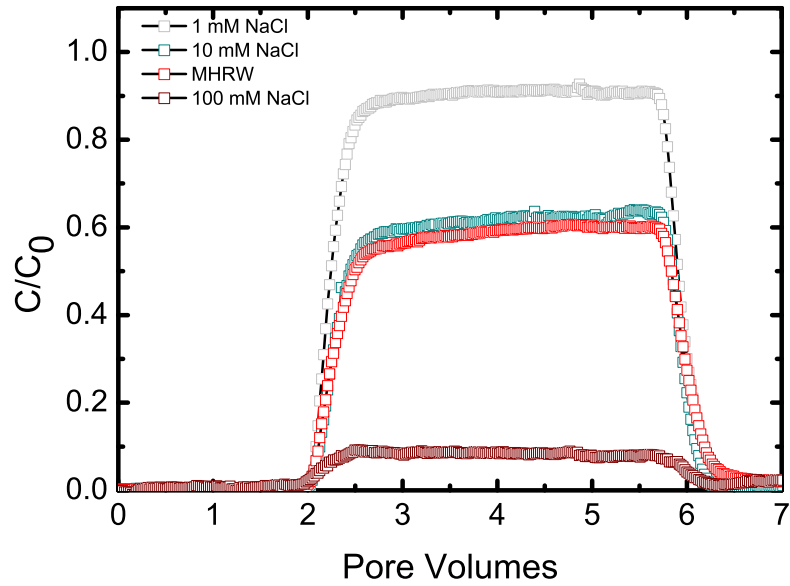
Figure 4.9 and 4.10 show some representative BTC and Figure 4.11 summarizes the calculated attachment efficiencies for each particle/solution chemistry condition analyzed. Figures 4.9 and 4.10 illustrate the interplay of NOM and IS on nTiO₂ stability. As would be expected from the classical DLVO theory of stability, at a given NOM concentration, enhancing the IS of the electrolyte results in compression of the electrostatic double layer. This would lead to both the sand and the nTiO₂ to be less negatively charged, namely a decrease in EPM, as can be seen in Figure 4.4. Consequently, an increase in the deposition rate of both P25 and CoRI C, and therefore an increase of the attachment efficiency α_d , are observed (Figure 4.11). Hence, the particle attachment behaviour observed in Fig. 4.11 is in qualitative agreement with the DLVO theory of colloidal stability (Figures 4.6 and 4.7) whereby the extent of physicochemical attachment increases with decreasing absolute zeta potential. However, data shown in Figure 4.9 do not completely match what would be expected from the EPM data (Figures 4.4 and 4.9). Differences in the EPM data for a given condition, are not so dramatic between P25 and CoRI C, but still the CoRI C α_d are, almost always, significantly higher than P25, meaning an higher retention of CoRI C over the range of solution analyzed. Several studies [159, 166, 167] stressed the impact of physical straining onto the nanoparticles filtration. As postulated by the traditional theory of filtration, the colloids may collide with grain surfaces, mainly via sedimentation, interception, and diffusion. Similar studies [80, 107] suggest the presence of an energy barrier preventing deposition into primary minima. In these conditions colloids that are weakly attached on the sand surface via secondary minima, can be carried along the grain surface by hydrodynamic shear to more favorable for deposition pore spaces. These may be small pore spaces that are formed adjacent to grain-to-grain contacts [159]. Deposition of nanoparticles in these straining locations is expected to be greater than other regions of the water-sand system due to chemical and physical considerations. DLVO attractive forces are greater between multiple solid-water interfaces [168], besides the fluid drag force is also decreased in the smallest region of the pore space because of lower fluid velocities [159]. It has been empirically found that when the critical diameter ratio of particles to median sand grains is greater than 0,003 [159], colloidal particles become trapped in the pore throats that are too small to allow their passage. Since the sand we used has a diameter of 256 μm , particles bigger than 768 nm, could be retained in this manner. Moreover, has been demonstrated [159, 166] that increasing the solution IS may lead to greater numbers of colloids that are directed to small pore spaces where straining occurs. Once colloids end up there, the morphology of the system (size of colloid and pore) along with the reduced fluid drag in these locations, prevent their releasing. The Tables 4.1 and 4.2 show whether the physical straining occurs or not. Effectively every CoRI C deposition was affected by this mechanism of filtration.

Figure 4.10 and Figure 4.11 show the NOM effect on the colloidal stability and

4.2. DEPOSITION EXPERIMENTS



(a) P25



(b) CoRI C

Figure 4.9: Representative particle breakthrough curves for 10°C series. Experiments conducted in a column packed with clean quartz sand, at $\text{pH } 7.9 \pm 0.1$, $T = 10^\circ\text{C}$, approach velocity $7.5 \times 10^{-5} \text{ m/s}$, mean grain diameter $d_c = 256 \text{ nm}$, porosity $f = 0.43$. (a) P25 coated with 1 mg/L NOM, suspended in 1, 10, 100 mM NaCl and MHRW. (b) CoRI C coated with 1 mg/L NOM, suspended in 1, 10, 100 mM NaCl and MHRW.

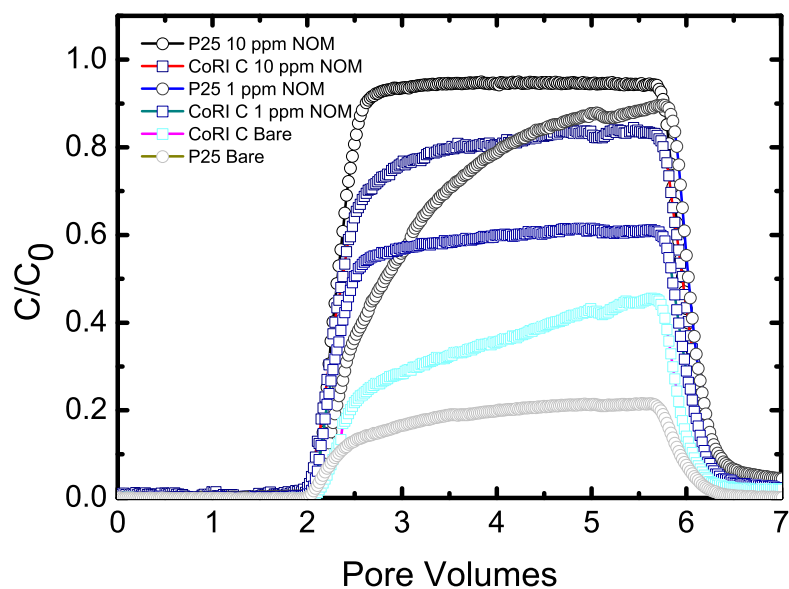
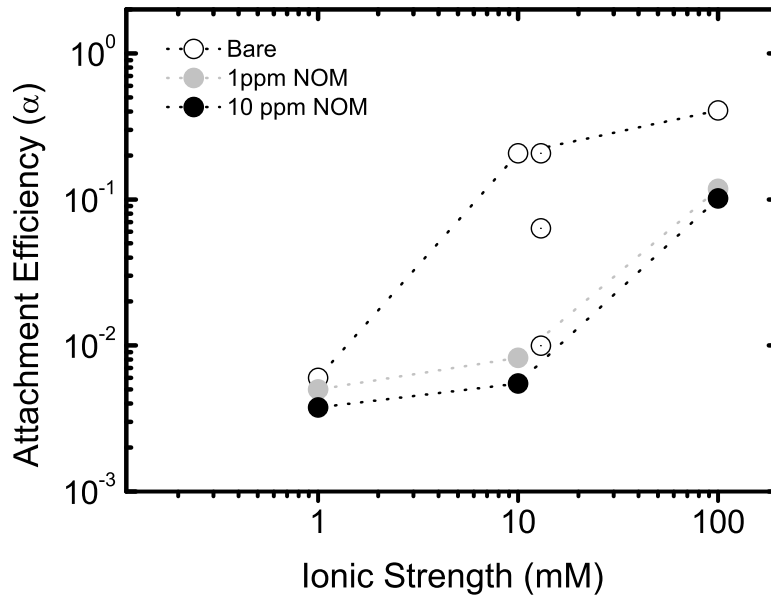
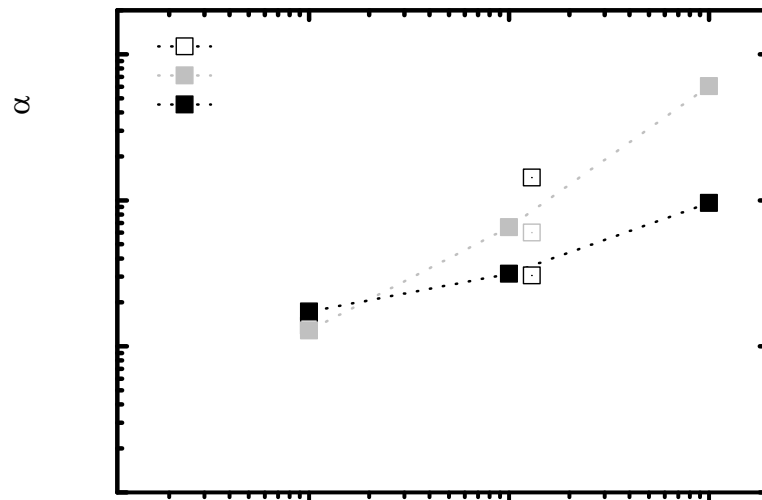


Figure 4.10: Representative particle breakthrough curve for 10°C serie. Experiment conducted in a column packed with clean quartz sand, at $\text{pH } 7,9 \pm 0,1$, $T = 10^\circ\text{C}$, approach velocity $7,5E-05 \text{ m/s}$, mean grain diameter $d_c 256 \text{ nm}$, porosity $f 0,43$. P25 and CoRI C coated with 0, 1, 10 mg/L NOM, suspended in MHRW.



(a) P25



(b) CoRI C

Figure 4.11: Attachment efficiencies for 10°C serie, calculated using Eq.2.47. (a) P25 and (b) CoRI C. The open symbols with dot, represent the MHRW. The experimental conditions are the same as Fig.4.9 and Fig.4.10.

also highlight the difference between CoRI C and P25 nTiO₂. As seen in Figure 4.9, the MHRW usually acts in between 100 mM and 10 mM NaCl, with a more enhanced effect on P25 than CoRI C. The attachment efficiencies of nTiO₂ are, in general, lower or equal to those measured in the absence of humics. Significant retention of the particles, with or without NOM, are observed at a salt concentration over 10 mM NaCl. However, equally important was the mobility enhancement resulting from increasing the NOM concentration. As repeatedly stated, NOM coating can give rise to electrosteric stabilization, which can prevent aggregation and deposition [80, 89, 107]. Moreover, more the particle are coated, smaller the aggregates will be, and that may also reduce the possibility of physical straining [159, 166, 169]. The stabilization in presence of NOM has traditionally been attributed to the effect of NOM on particle surface potential. The NOM has been known to increase the absolute value of colloid zeta potential for negatively charged colloids [131, 170, 171]. With that in mind, along with the EMP data (Figure 4.4), the attachment efficiencies seem now to be consistent. Besides, it also appears the NOM having a milder effect on CoRI C than P25. This could be related to the milder effect the NOM has onto the EPM of the particles. In the last years the attention has been focused to the type of nTiO₂ as well. As explained previously, the nominal difference between P25 and CoRI C is their composition, therefore their morphology. However, crystallinity and morphology were not found to be influential factor in determining the stability of Anatase and Rutile/Anatase nTiO₂ [143]. Nevertheless, a key factor governing the stability has been discovered to be the amount of extractable impurities (i.e., Si, P) in the pristine TiO₂ [143]. Since the CoRI C is a commercial product, we don't know the exact composition but we only know the declared composition of 100 % Anatase. This could be one reason why, at a same electrolyte concentration, the CoRI C surface is less negatively charged. Bearing in mind this aspect, it would be possible to link the different NOM stabilization effect on CoRI C and P25, imagining that the point of zero charge of the two particles is different and then even 10 ppm of NOM are not enough to sterically stabilize the CoRI particles. But still, the NOM may play a key role on the size of the CoRI C aggregates, and therefore onto their straining attitude. Actually, there is no literature about how the NOM adsorbs on the CoRI C particles, whether its adsorption trend may or may not be influenced by a greater amount of impurities, or even about the exact CoRI C composition. For this reason, an idea for a future work would be surely a further understanding in how the NOM adsorption onto the CoRI C, influences the EPM and attachment efficiencies curves slopes. In conclusion, the deposition behaviour at T = 10°C of nTiO₂ P25 and CoRI C has been studied in packed column test. The mobility of both P25 and CoRI C has been found dramatically influenced by IS, ionic valence and NOM concentration. In particular, a significant retention through the column was observed at IS of 100 mM, regardless the NOM concentration. In addition to that, the NOM has generally enhanced particles mobility and stability, in particular those of P25. Moreover, the MHRW, mostly composed of Mg²⁺ and Ca²⁺, has caused a steeper reduction into particles mobility. The CoRI C has been found to be more

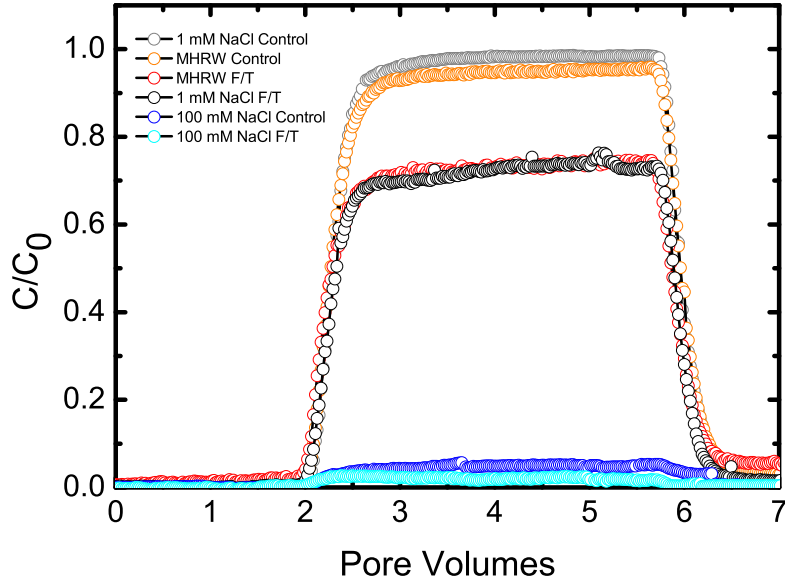
4.2. DEPOSITION EXPERIMENTS

retained because of its different kind of interaction with NOM and because of its intrinsic nature. The CoRI C mobility has been revealed widely influenced mostly by straining, but also aggregation and ripening, that is a rising in the nanoparticle elution profile. Straining, ripening and aggregation, may slightly change the calculated attachment efficiencies because they are not considered within the classical theory of filtration. Hence, the α_d values are here reported with the main purpose of qualitative interpretation of experimental observations.

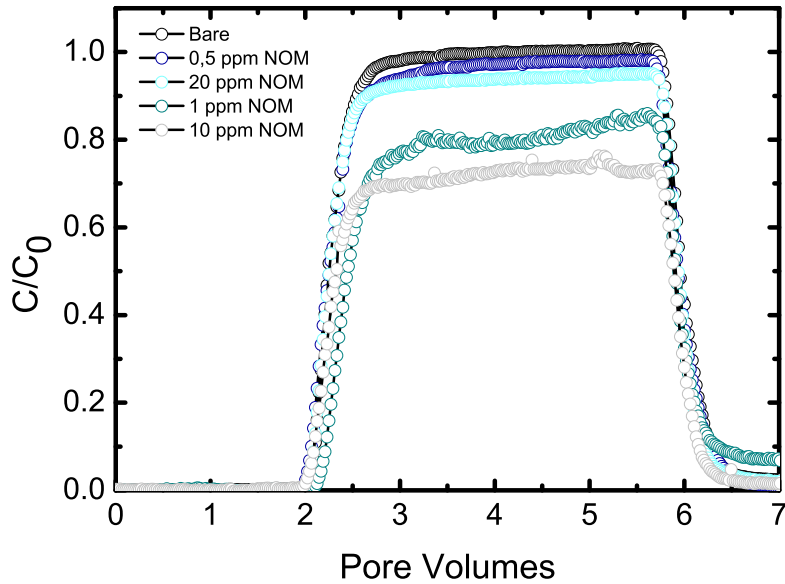
4.2.2 Freeze/Thaw Deposition study

Figures 4.12 and 4.13 display the interplay of NOM, IS and Freezing/Thawing, under CoRI C and P25. Because of very low values of absorbance, only MHRW column experiments were conducted for CoRI C nTiO₂. The replicability for CoRI C was very difficult and even small changes in nTiO₂ concentration or time delays, were found to compromise the results. For this reason, aiming to the greatest possible attention, the only electrolyte examined was the MHRW because of its scientific interest. The F/T generally largely affected and reduced the mobility of the particles, for both CoRI C and P25. There is basically no elution for the P25 suspended in 100 mM NaCl, regardless of the NOM concentration. The retention was always found to be greater after the F/T, compared to the Control test and the related counterpart test at 10 °C. Due to the average size of the aggregates (Table 4.3), the straining was here a relevant filtration mechanism for both P25 and CoRI C. The compression of the double layer in the thawed suspension in higher IS electrolyte, was more important than the freezing point depression by the same electrolyte. That is the reason why an increasing of IS leads to an increasing in retention, in a very similar trend to that of 10 °C experiments. Besides, from the available data, the CoRI C still appears more unstable and its mobility is smaller than P25. The combined time temperature effect may cause first the formation of the biggest cluster and then, because of the freezing, their further growth. We do know the freezing plays a key role into the deposition behaviour for two main reasons. In the first place, the control deposition data are consistently closer to those of 10 °C experiment than the F/T ones. Besides, If was only matter of time, the controls sizes should be the same order of magnitude as the TRDLS ones. So, if it is true that the TRDLS are conducted at T = 25 °C and the control test at T = 10 °C, it is also true that during the F/T, the nanoparticles form far bigger aggregates than those of both Control and TRDLS. This aspect is particularly significant in interpreting the α_d trends for CoRI C and P25. Figure 4.13 effectively shows that the P25 is much more influenced by an IS changing than the CoRI C. In fact, the α_d increases much steeper for P25 than CoRI C. At first reading, this could be misunderstood as the CoRI being less destabilized by double layer compression. However, what I would suggest is that for CoRI C the straining filtration becomes dominant. Since the α_d are calculated according to the classical theory of filtration, they don't take in account the straining role.

The NOM has here an uncertain effect. For nTiO₂ suspended in MHRW and 100



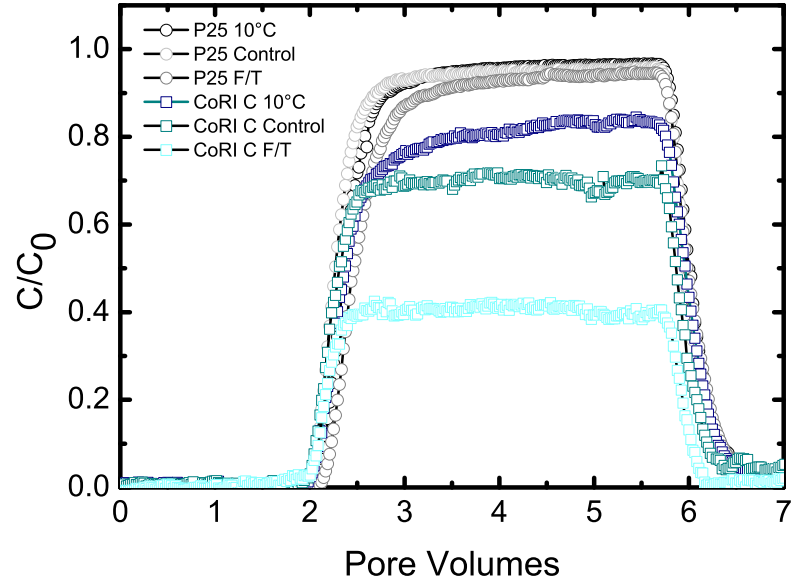
(a)



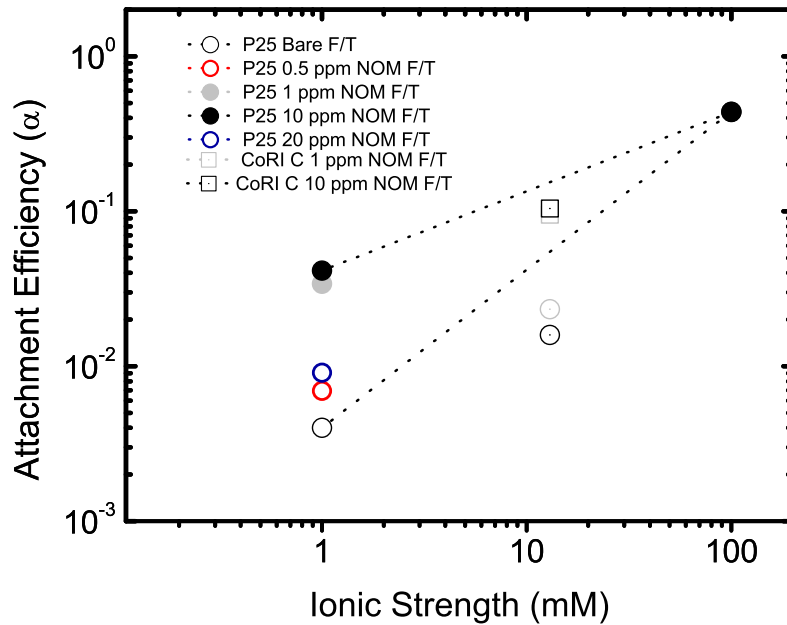
(b)

Figure 4.12: Representative particle breakthrough curves for F/T series. Experiments conducted in a column packed with clean quartz sand, at $\text{pH } 7,9 \pm 0,1$, $T = 10^\circ \text{C}$, approach velocity $7,5E-05 \text{ m/s}$, mean grain diameter $d_c 256 \text{ nm}$, porosity $f 0,43$. (a) P25 coated with 10 mg/L NOM , suspended in $1, 100 \text{ mM NaCl}$ and MHRW; Test and Control. (b) P25 in 1 mM NaCl , coated with $0 - 20 \text{ mg/L NOM}$. Control not reported.

4.2. DEPOSITION EXPERIMENTS



(a)



(b)

Figure 4.13: Representative particle breakthrough curves for F/T series and Alpha summary. Experiments conducted in a column packed with clean quartz sand, at $pH 7,9 \pm 0,1$, $T = 10^\circ C$, $U 7,5E-05 m/s$, mean grain diameter $d_c 256 nm$, porosity $f 0,43$. (a) P25 and CoRI C in MHRW, coated with 10 mg/L NOM; Test, Control and 10 °C Run. (b) Attachment efficiencies F/T test: P25 and CoRI C. Open symbols with dot as MHRW.

mM NaCl, the NOM seems to slightly enhance their mobility. However, when suspended in 1 mM NaCl, the presence of NOM has a peculiar role. Fig.4.13 shows that the P25 nTiO₂ appears to be destabilized in a NOM concentration in between 0,5 - 20 mg/L. The retention follows the order: 10 > 1 ≫ 20 > 0,5 ≫ 0 mg/L NOM. Unexpectedly, in 1 mM NaCl, the colloidal system seems to be more stable without any NOM, with a greater retention in presence of NOM into the range 1-10 mg/L. Both calculated α_d and BTC confirm this aspect. In normal conditions, as we have seen, the NOM would shield the aggregation effect due to the increasing of the IS. In turn, here, it seems to contribute in reducing the effectiveness of the Coulombic repulsion, leading to increased aggregation. As anticipated in section 4.1.3, this may be due to the NOM bridging. We suppose that the NOM adsorbs on the nTiO₂ more and more, until have all the particles covered, within a concentration of 0,5 - 10 mg/L. Decreasing the temperature, the NOM should theoretically adsorb even more, but with a slower kinetic. But when the system starts to freeze, everything moves more and more slower, until everything is frozen. Therefore, it would seem reasonable to suppose that, because of the kinetic of the process, the particles are not completely coated by NOM. Hence, when the system is kept still because of the change in its state of matter, two or more particles partially coated may come in contact. We know from theory that when this happens, namely two partially coated particles coming in contact, the electrosterical NOM layers can bind together. At these NOM concentration, the bridging flocculation appears to be consistent with an increasing in molecular rigidity, as explained elsewhere [152]. As pointed out in the second chapter, this mechanism likely occurs in the presence of low concentrations of a polyelectrolyte. In this particular case, the trend of retention with NOM concentration, would suggest that the bridging starts at 0,5 mg/L NOM. That is a very low concentration and therefore lead to have few and weak bridge-spots. The phenomenon is more pronounced as NOM concentration increases to 10 mg/L. However, when the NOM concentration is over 10 mg/L, despite the slow rate of adsorption, the concentration is high and all the particles are covered. For this reason the particles starts to be sterically stabilized, just as happened at 10 °C with 1 and 10 mg/L NOM. This result is very interesting because, under the NOM concentration range of a natural aquatic system, the NOM may decrease the mobility when the environment is frozen. This mechanism does not occur when the IS is higher because of the already cited contribution of IS in adsorption rate. As previously described, the adsorption rate depends on the IS and increase with IS increasing. Thus, with MHRW and 100 NaCl, the favourable effect of the IS dominates on the unfavourable effect of the low temperature, and so it governs the adsorption rate and therefore, the deposition behaviour. If the particles are totally coated with NOM, what we would expect from theory is that within a certain range of concentration, the thickness of the steric barrier prevents the particles from approaching.

4.3 Conclusion and future work

4.3.1 Environmental Impact

Clearly, in the natural environment, the fate, mobility, and bioavailability of nTiO₂ will be deeply influenced by particle size and charge. In this study, nTiO₂ were generally sterically stabilized in presence of NOM at T = 10°C. This was evident with smaller aggregates, more elution and more negatively charged particle surfaces. These findings suggest that in a natural aquatic system, the dispersion and mobility of nTiO₂ might be much greater than what is predicted by laboratory tests. On average, the P25 were more mobile than their CoRI C counterparts, which were more likely to be retained into the soil under the same physiochemical conditions. For both of them, the role of IS, divalent ion contents and pH under the deposition, were consistent with previous literature. Conversely, the nTiO₂, after Freezing/Thawing were both stabilized and destabilized by the NOM, depending on its concentration. This means that the mobility of the colloidal suspension into a natural environment is considerably influenced by weather, temperature and the chemical composition of the aquatic environment they are moving in. For this reason these factors should be taken into account to decide whether dispose or not of nTiO₂ and eventually where. I am confident this work might bring to light the critical importance of the boundary conditions into a such delicate topic.

4.3.2 Future work

I would like to think this work being only the cornerstone of a full understanding of nTiO₂ transport and fate into the actual environment. All the previous studies are based on P25 nanoparticles, simple to handle at laboratory scale but basically not used for industrial purpose. Besides, there still isn't clarity about the NOM role under every working conditions. Another aspect that would merit further focus is the sand. The sand we used is an extra fine quartz sand, same that is often used run column tests. However, it only pretends to simulate a real soil. Next steps should move in that direction. Furthermore, the F/T data showed how still uncertain is the mobility when several physiochemical condition are combined, and act together. Moreover, they also pointed out the necessity of a worldwide model to determine the fate into several possible scenarios. The nTiO₂ are spread everywhere and the slightest change in environmental condition (weather, temperature, pH of the water source, *etc.*) has an enormous impact on nanoparticles mobility. A series of deposition F/T test examining different scenarios, in order to collect a large number of data, may aid to develop a semi-empirical model. Finally, would be surely useful to continue in moving on the path we opened. We saw that the mobility dramatically changes between CoRI C and P25, and this is likely the case with other particles. Besides, in this particular case, the exact adsorption mechanism and kinetic of NOM onto the CoRI C, it is necessary to entirely explain the fate of this particle. Testing several types of commercial ENP might be the very next step.

Acknowledgements

First and foremost to my supervisor Nathalie Tufenkji. Thank you for the opportunity you gave me to work with you. Your passion for research is catching and your caring about students is heartfelt. To work in your lab was the best academic experience I've ever had.

Secondly, to Jeff(rey) for teaching me a lot about science, and life. Thank you for helping me out with my english (still working on, sorry) but most of all, thank you for your friendship. I'm sure you'll be an awesome professor, because you are a good person, that means a lot. To Laura, for your support when things were going bad and thank you for aiding me, always. I will be eternally grateful to you for the great time we had together. I wish you the best because you deserve it. To Emeric, my dear friend, who seamlessly faces everything plain and simply. Thank you for listening to me and always cheering me up. You'll get how to make a real italian pizza...just not in this life. To Rachel, who should get the credit for at least half of the data of this project. I'm glad you became twice the scientist I've never been. To all my friends in Montreal, for never letting me feel alone.

Ringraziamenti

Ai miei genitori ed a mio fratello, per aver sempre visto la versione migliore dell'uomo che sarei potuto diventare. Grazie ai miei compagni di corso, ed amici, Andrea, Baldo, Mariangela, Maria, Roberta, Giulia, Katia, Sasi, Alessandro, ed a tutto il Drinchimteam. La vostra amicizia è una cartina al tornasole di quest'avventura. Per quello che abbiamo costruito, grazie. A Lorenzo, non riesco ad immaginare quanto più insignificante sarebbe stato tutto questo senza di te, ti voglio bene. Ad Elisa e Gianluca, per avermi sopportato, grazie. Ed ancora, a Salvatore, per esserci stato, da sempre, per conoscere la mia parte peggiore, e non aver mai smesso di volermi bene. A Peppe Summa, un amico sincero ed un fiero conducente delle macchine più belle del mondo. A Soccorso e Carlo per aver allietato tantissime serate in questi cinque anni. A Rocco Marino per il calcio e le nostre infinite conversazioni sulla pizza. A te Alessandro, per aver condiviso con me ogni istante di questo percorso, ed avermi capito, compreso, sopportato, senza mai perdere di vista la persona che sono veramente. Ti ringrazio per essere la forza motrice della mia quotidianità.

Ed Infine, grazie a Benedetta, la cui fede incrollabile nel fatto che potessi farcela, è probabilmente la ragione per la quale sono qui. Ti ringrazio per aver creduto in me più di quanti facessi io stesso, per essere sempre stata presente ai miei traguardi, ma soprattutto aver condiviso le mie tante cadute. Molto di quello che sono, e queste mie piccole vittorie, sono indubbiamente in debito con la tua forza ed il tuo coraggio.

Bibliography

- [1] Lead J.R., Wilkinson K.J., 2006, Environmental chemistry 3.
- [2] Hough R.M., Noble R.R.P., Reich M., 2011. *Natural gold nanoparticles*. Ore Reology Reviews 42(55).
- [3] Colomban P., 2009. *The Use of Metal Nanoparticles to Produce Yellow, Red and Iridescent Colour, from Bronze Age to Present Times in Lustre Pottery and Glass: Solid State Chemistry, Spectroscopy and Nanostructure*. Journal of Nano Research, Vol.8.
- [4] Sciau P., 2012. *The Delivery of Nanoparticles*. Intech,Rijeka, Croatia.
- [5] Heiligtag Florian J., Niederberger Markus, 2013. *The fascinating world of nanoparticle research*. Materialstidday, Vol.16, Issues 7-8, 262-271
- [6] Henglein A., 1989. *Small-Particle Research: Physicochemical Properties of Extremely Small Colloidal Metal and Semiconductor Particles*. Chemical Reviews, 89(8), 1861-1873.
- [7] Burda C., Chen X., Narayanan R., El-Sayed Mostafa A., 2005 *Chemistry and Properties of Nanocrystals of Different Shapes*. Chemical Reviews, 105(4), 1025-1102.
- [8] Roco, M.C.; Bainbridge, W. S., 2011. *Societal Implications of Nanoscience and Nanotechnology*. National Science Foundation Arlington, VA
- [9] Robichaud, C.O., Tanzil, D., Weilenmann, U., Weisner, M.R., 2005. *Relative risk analysis of several manufactured nanomaterials: an insurance industry context*. Environmental Science and Technology 39 (22), 8985-8994.
- [10] RNCOS Business Consultancy Services, Nanotechnology Market Outlook 2020. 2015.
- [11] Berg John C., 2010. *An introduction to Interfaces and Colloids: The Bridge to Nanoscience*. 1st ed., World Scientific Publishing: Hackensack, NJ.
- [12] Ray, P. C., Yu, H. and Fu, 2009. *Toxicity and environmental risks of nano-materials: challenges and future needs*. J Environ Sci Health C Environ Carcinog. Ecotoxicol. Rev., 27, 1-35.

BIBLIOGRAPHY

- [13] ISO TS 80004-1:2010 Nanotechnologies-Vocabulary-Part 1: Core terms.
- [14] Horikoshi N. and Serpone N., 2013. *Microwaves in Nanoparticle Synthesis: Fundamentals and Applications*. 1st ed., Wiley-VCH.
- [15] Hett A., 2004. *Nanotechnology: small matters, many unknown*. Swiss Re Report.
- [16] European Commission, *Types and uses of nanomaterials, including safety aspects*. Brussels, 2012.
- [17] Fahlman B.D., 2007. *Materials Chemistry* Springer.
- [18] Krug HF, Wick P., 2011. *Nanotoxicology: an interdisciplinary challenge*. *Angew. Chem. Int. Ed*, 50, 1260-1278
- [19] Santos Càtia S.C., Gabriel B., Blanchy M., Menes O., García D., Blanco M., Arconada N., Neto V. 2015. *industrial application of nanoparticles - a prospective overview*. 5th International conference of Advanced Nano Materials, Materials today.
- [20] Ostiguy C., Lapointe G., Mènard L., Cloutier Y., Trottier M., Boutin M., Antonoun, M. and Norman, C. 2006. *Nanoparticles: Actual Knowledge about Occupational Health and Safety Risks and Prevention Measures*. IR-RST Report R-445.
- [21] Batley, G. E. and Mclaughlin, M. J. 2010. *Fate of Manufactured Nanomaterials in the Australian Environment*. CSIRO Niche Manufacturing Flagship Report.
- [22] Dufour, E.K., Kumaravel, T., Nohynek, G.J., Kirkland, D., Toutain, H., 2006. *Mutation Research Genomics Toxicology and Environmental Mutagenesis*. 607 (2), 215-224.
- [23] Englert, B.C., 2007. *Journal of Environmental Monitoring* 9 (11), 1154-1161.
- [24] Mueller, N.C., Nowack, B., 2008. *Environmental Science and Technology* 42 (12), 4447-4453.
- [25] Sayes, C.M., Wahi, R., Kurian, P.A., Liu, Y., West, J.L., Ausman, K.D., Warheit, D.B., Colvin, V.L., 2006. *Toxicology Science* 92 (1), 174-185.
- [26] Mah C, Zolotukhin I, Fraites TJ, Dobson J, Batich C, Byrne BJ, 2000. *Microsphere-mediated delivery of recombinant AAV vectors in vitro and in vivo*. *Mol Therapy*.

- [27] Panatarotto D, Prtidos CD, Hoebeke J, Brown F, Kramer E, Briand JP, Muller S, Prato M, Bianco A., 2003. *Immunization with peptide-functionalized carbon nanotubes enhances virus-specific neutralizing antibody responses*. Chemistry and Biology.
- [28] Tomalia DA, Reyna LA, Svenson S., 2007. *Dendrimers as multipurpose nanodevices for oncology drug delivery and diagnostic imaging*. Biochem Soc Trans.
- [29] Roy I, Ohulchanskyy TY, Pudavar HE, Bergey EJ, Oseroff AR, Morgan J, Dougherty TJ, Prasad PN., 2003. *Ceramic-based nanoparticles entrapping water-insoluble photosensitizing anticancer drugs: a novel drug-carrier system for photodynamic therapy*. J Am Chem Soc.
- [30] Vance Marina E., Kuiken T., Vejerano Eric P., McGinnis Sean P., Hochella Michael F. Jr., Rejeski David and Hull Matthew S., 2015. *Nanotechnology in the real world: Redeveloping the nanomaterial consumer products inventory*. Beilstein J. Nanotechnol., 1769-1780.
- [31] *Project on Emerging Nanotechnologies*. 2013. Consumer Products Inventory.
- [32] Piccinno F.; Gottschalk F.; Seeger S.; Nowack 2012. B. J. Nanopart. Res., 14, 1109.
- [33] Keller A.A., McFerran S., Lazareva A., Suh S., 2013. *Global life cycle releases of engineered nanomaterials*. Journal of Nanoparticle Research, 15(6), 1692..
- [34] The Global Market for Nanomaterials 2002-2016: Production Volumes, Revenues and End Use Markets; Future Markets, Inc.: 2012; p 371
- [35] Hendren C. O., Mesnard X., Dröge J., Wiesner M. R., 2011. *Estimating Production Data for Five Engineered Nanomaterials As a Basis for Exposure Assessment*. Environ. Sci. Technol., 45, (7), 2562-2569.
- [36] Gottschalk F., Sonderer T., Scholz R. W. Nowack B., 2010. *Possibilities and limitations of modeling environmental exposure to engineered nanomaterials by probabilistic material flow analysis*. Environ. Toxicol. Chem. 29, (5), 1036-1048.
- [37] Kelly L. Coronado E., Zhao L.L. and Schatz George C., 2002. *The Optical Properties of Metal Nanoparticles: The Influence of Size, Shape, and Dielectric Environment*. J. Phys. Chem. B, 107, 668-677.
- [38] Astruc D., Lu F., Aranzaes J.R., 2005. *Nanoparticles as Recyclable Catalysts: The Frontier between Homogeneous and Heterogeneous Catalysis*. Angew. Chem. Int. Ed., 44, 7399.

BIBLIOGRAPHY

- [39] Astruc, 2007. *Palladium Nanoparticles as Efficient Green Homogeneous and Heterogeneous Carbon-Carbon Coupling Precatalysts: A Unifying View*. Inorg. Chem., 46 (6), pp 1884-1894.
- [40] Weinheim, 2004. *Nanoparticles*. (Ed.: G. Schmid), Wiley-VCH.
- [41] Finke R.G., 2002. *Metal Nanoparticles. Synthesis, Characterization and Applications*. (Eds.: D. L. Feldheim, C. A. Foss, Jr.), Marcel Dekker, chap. 2, p.17
- [42] Weinheim, 1998. *Nanoparticles and Nanostructured Films. Preparation, Characterization and Applications*. (Ed.: J. H. Fendler), Wiley-VCH.
- [43] Astruc D., 2008 *Nanoparticles and Catalysis*. WILEY-VCH Verlag GmbH & Co. chap. 1.
- [44] Naugle D. G., Glover, R. E., 1969. *Size dependence of the superconducting transition temperature*. Physics Letters A, 28(9), 611-612.
- [45] Luo X.L. et al., 2006. *Application of nanoparticles in electrochemical sensors and biosensors Electroanalysis*. 18 319-26.
- [46] Guo D., Xie G., Luo J., 2013. *Mechanical properties of nanoparticles: basics and applications*. Journal of Physics D: Applied Physics, 47, 1
- [47] Liu W.M., Wang X.B., 2012. *Nanoparticle-Based Lubricant Additives*. (SpringerReference).
- [48] Rohatgi P. K., Schultz B., 2007 *Lightweight metal matrix nanocomposites-stretching the boundaries of metals*. Mater. Matters 2.4 16.
- [49] Hanemann T., Vinga Szabó D., 2010 *Polymer-nanoparticle composites: from synthesis to modern applications*. Materials 3 3468-517
- [50] Englert B.C., 2007. Journal of Environmental Monitoring 9 (11), 1154-1161.
- [51] Mueller N.C., Nowack B., 2008. Environmental Science and Technology 42 (12), 4447-4453.
- [52] Sayes C.M., Wahi R., Kurian P.A., Liu Y., West J.L., Ausman K.D., Warheit D.B., Colvin V.L., 2006. Toxicology Science 92 (1), 174-185.
- [53] Diebold U., 2003. *The surface science of titanium dioxide*. Surface science reports, 48(5), 53-229.
- [54] Aitken R.J., Chaudhry M.Q., Boxall A.B.A., Hull M., 2006. *Occupational Medicine-Oxford* 56 (5), 300-306.

- [55] Tseng W.J., Lin K.C., 2003. *Materials Science and Engineering*. A 355 (1-2), 186-192.
- [56] Maness P.C., Smolinski S., Jacoby W.A., 1999. *Appl. Environ. Microbiol.*, 65, p. 4094.
- [57] Paz Y., Luo Z., Rabenberg L., Heller A.J., 1995. *Mater. Res.*, 10 (1995), p. 2842.
- [58] Sakai H., Baba R., Hashimoto K., Kubota Y., Fujishima A., 1995. *Chem. Lett.* 185.
- [59] Budarz J.M.F., 2016. *Lights, Camera, Reaction! The Influence of Interfacial Chemistry on Nanoparticle Photoreactivity*. Doctoral dissertation, Duke University.
- [60] Han F., Kambala V.S.R., Srinivasan M., Rajarathnam D., Naidu R., 2009. *Tailored titanium dioxide photocatalysts for the degradation of organic dyes in wastewater treatment: a review*. *Applied Catalysis A: General*, 359(1), 25-40
- [61] Lu M., Pichat P., 2013. *Photocatalysis and water purification: from fundamentals to recent applications*. John Wiley & Sons.
- [62] Wiesner M.R., Bottero J.Y., 2007. *Environmental Nanotechnology*. The McGraw- Hill Companies, New York.
- [63] Huang C.C., Aronstam R.S., Chen D.R., Huang Y.W., 2010. *Toxicology in Vitro* 24 (1), 45-55.
- [64] Moos P.J., Chung K., Woessner D., Honegger M., Cutler N.S., Veranth J.M., 2010. *Chemical Research in Toxicology* 23 (4), 733-739.
- [65] Schanen B.C., Karakoti A.S., Seal S., Drake III D.R., Warren W.L., Self W.T., 2009. *ACS Nano* 3 (9), 2523-2532.
- [66] Sharma V., Shukla R.K., Saxena N., Parmar D., Das M., Dhawan A., 2009. *Toxicology Letters* 185 (3), 211-218.
- [67] Duan Y., Liu J., Ma L., Li N., Liu H., Wang J., Zheng L., Liu C., Wang X., Zhao X., Yan J., Wang S., Wang H., Zhang X., Hong F., 2010. *Biomaterials* 31 (5), 894-899.
- [68] Hu R., Gong X., Duan Y., Li N., Che Y., Cui Y., Zhou M., Liu C., Wang H., Hong, F., 2010. *Biomaterials* 31 (31), 8043-8050.
- [69] Ma L., Liu J., Li N., Wang J., Duan Y., Yan J., Liu H., Wang H., Hong F., 2010. *Biomaterials* 31 (1), 99-105.

BIBLIOGRAPHY

- [70] Warheit D.B., Webb T.R., Reed K.L., Frerichs S., Sayes C.M., 2007. *Toxicology* 230 (1), 90-104.
- [71] Bai W., Zhang Z., Tian W., He X., Ma Y., Zhao Y., Chai Z., 2010. *Journal of Nanoparticle Research* 12 (5), 1645-1654.
- [72] Federici G., Shaw B.J., Handy R.D., 2007. *Aquatic Toxicology* 84 (4), 415-430.
- [73] Hao L., Wang Z., Xing B., 2009. *J. Environmental Science* 21 (10), 1459-1466.
- [74] Fang X., Yu R., Li B., Somasundaran P., Chandran K., 2010. *Journal of Colloid and Interface Science* 348 (2), 329-334.
- [75] Ge Y., Schimel J.P., Holden P.A., 2011. *Environmental Science and Technology* 45 (4), 1659-1664.
- [76] Roh J.Y., Park Y.K., Park K., Choi J., 2010. *Environmental Toxicology and Pharmacology* 29 (2), 167-172.
- [77] Valant J., Drobne D., Sepcic K., Jemec A., Kogej K., Kostanjsek R., 2009. *Journal of Hazardous Materials* 171 (1-3), 160-165.
- [78] Lowry G.V., Gregory K.B., Apte S.C., Lead J.R., 2012. *Transformations of nanomaterials in the environment*.
- [79] Petosa A.R., Jaisi D.P., Quevedo I.R., Elimelech M., Tufenkji, N., 2010. *Environmental Science and Technology* 44 (17), 6532-6549.
- [80] A.R., Brennan S.J., Rajput F., Tufenkji N., 2012 *Water research* 46, 1273-1285.
- [81] Choy C.C., Wazne M., Meng X., 2008. *Chemosphere* 71 (9), 1794-1801.
- [82] Fatisson, J., Domingos R.F., Wilkinson K.J., Tufenkji N., 2009. *Langmuir* 25 (11), 6062-6069.
- [83] Verwey E.J.W., Overbeek J.T.G., 1948. *Theory of the Stability of Lyophobic Colloids*. Elsevier, Amsterdam.
- [84] Hamaker H.C., 1937, *Physica*, 4, 1058.
- [85] Gregory J., 1975 *Interaction of unequal double layers at constant charge*. *Journal of Colloid and Interface Science* 51(1), 44-51.
- [86] Gregory J., 1981. *Approximate expressions for retarded van der waals interaction*. *Journal of Colloid and Interface Science* 83(1), 138-145.

- [87] Byrd T.L., Walz J.Y., 2005. *Interaction force profiles between Cryptosporidium parvum oocysts and silica surfaces*. Environ. Sci. Technol. 39 (24), 9574-9582.
- [88] De Gennes P. G., 1987. *Polymers at an interface; a simplified view*. Adv. Colloid Interface Sci. 27 (3-4), 189-209.
- [89] Elimelech M., Gregory J., Jia X., Williams R.A., 1995. *Particle Deposition and Aggregation: Measurement, Modeling, and Simulation*. Butterworth-Heinemann: Oxford.
- [90] Bergström L., *Hamaker constants of inorganic materials*. Adv. Colloid Interface Sci. 70, 125-169.
- [91] Ross S., Morrison I.D., 1988. *Colloidal Systems and Interfaces*. John Wiley & Sons, Inc.: New York.
- [92] Auffan M., Rose J., Chanéac C., Jolivet J.P., Masion A., Wiesner M.R., Bottero J.Y., 2011. *Surface reactivity of manufactured nanoparticles*. Nanoeethics and Nanotoxicology (pp. 269-290). Springer Berlin Heidelberg.
- [93] Kosmulski M., 2011. *The pH-dependent surface charging and points of zero charge: V. Update*. Journal of colloid and interface science, 353(1), 1-15.
- [94] Parks G.A., 1965. *The isoelectric points of solid oxides, solid hydroxides, and aqueous hydroxo complex systems*. Chemical Reviews, 65(2), 177-198.
- [95] Stern O., 1924. *Zur theorie der elektrolytischen doppelschicht*. Berichte der Bunsengesellschaft für physikalische Chemie. 30(21-22), 508-516.
- [96] Pilon L., Wang H., D'Entremont, A. (2015). *Recent advances in continuum modeling of interfacial and transport phenomena in electric double layer capacitors*. Journal of The Electrochemical Society, 162(5), A5158-A5178.
- [97] Ruckenstein E., Prieve D.C., 1976. *Adsorption and desorption of particles and their chromatographic separation*. AIChE Journal, 22(2), 276-283.
- [98] Hotze E.M., Phenrat T., Lowry G.V., 2010. *Nanoparticle aggregation: challenges to understanding transport and reactivity in the environment*. Journal of environmental quality, 39(6), 1909-1924.
- [99] Fritz G., Schädler V., Willenbacher N., Wagner, N.J., 2002. *Electrosteric stabilization of colloidal dispersions*. Langmuir, 18(16), 6381-6390.
- [100] Phenrat T., Saleh N., Sirk K., Tilton R. D., Lowry G.V., 2007. *Aggregation and sedimentation of aqueous nanoscale zerovalent iron dispersions*. Environmental Science & Technology, 41(1), 284-290.

BIBLIOGRAPHY

- [101] Chen K. L., Elimelech M. 2007. *Influence of humic acid on the aggregation kinetics of fullerene (C 60) nanoparticles in monovalent and divalent electrolyte solutions*. Journal of Colloid and Interface Science, 309(1), 126-134.
- [102] Asakura S., Oosawa F. 1958. *Interaction between particles suspended in solutions of macromolecules*. Journal of Polymer Science Part A: Polymer Chemistry, 33(126), 183-192.
- [103] Healy T.W., Homola A., James R.O., Hunter, R.J. 1978 *Coagulation of amphoteric latex colloids: reversibility and specific ion effects*. Faraday Discussions 65, 156-163.
- [104] Fischer E. W., 1958. *Elektronenmikroskopische untersuchungen zur stabilität von suspensionen in makromolekularen lösungen*. Colloid & Polymer Science, 160(2), 120-141.
- [105] Chan D.Y., Henderson D., 1984. *The orientation-averaged interaction of a pair of magnetic dipolar spheres in an external magnetic field*. Journal of Colloid and Interface Science, 101(2), 419-423.
- [106] Israelachvili J. N., 1992. *Intermolecular and surface forces: with applications to colloidal and biological systems (Colloid Science)*, London: Academic.
- [107] Chen G., Liu X., Su C., 2012. *Distinct effects of humic acid on transport and retention of TiO₂ rutile nanoparticles in saturated sand columns*. Environmental science & technology, 46(13), 7142-7150.
- [108] Tufenkji N., Elimelech M., 2004. *Correlation equation for predicting single-collector efficiency in physicochemical filtration in saturated porous media*. Environmental science & technology, 38(2), 529-536.
- [109] Luo M., Huang Y., Zhu M., Tang Y. N., Ren T., Ren J., Li, F. 2016. *Properties of different natural organic matter influence the adsorption and aggregation behavior of TiO₂ nanoparticles*. Journal of Saudi Chemical Society.
- [110] Von Smoluchowski M., 1916. *Drei vortrage uber diffusion. Brownsche bewegung und koagulation von kolloidteilchen*. Z. Phys., 17, 557-585.
- [111] Fuchs V.N., 1934. *Über die stabilität und aufladung der aerosole*. Zeitschrift für Physik A Hadrons and Nuclei. 89(11), 736-743.
- [112] Reerink, H., Overbeek, J. T. G. 1954. *The rate of coagulation as a measure of the stability of silver iodide sols*. Discussions of the Faraday Society, 18, 74-84.
- [113] Trefalt G., Szilagyi I., Borkovec M., 2013. *Poisson-Boltzmann description of interaction forces and aggregation rates involving charged colloidal particles in asymmetric electrolytes*. J. Colloid Interf. Sci. 406, 111-120.

-
- [114] Yao K.M., Habibian, M. T., O'Melia C.R., 1971. *Water and waste water filtration. Concepts and applications*. Environmental science & technology, 5(11), 1105-1112.
- [115] Messina F., Marchisio D. L., Sethi R. 2015. *An extended and total flux normalized correlation equation for predicting single-collector efficiency* Journal of colloid and interface science, 446, 185-193.
- [116] Levich V.G., 1962. *Physicochemical hydrodynamics*. Prentice hall.
- [117] Yao K.M., 1968. *Influence of Suspended Particle Size on the Transport Aspect of Walter Filtration* (Doctoral dissertation, University of North Carolina at Chapel Hill).
- [118] Tien C., Ramarao B.V., 2011. *Granular filtration of aerosols and hydrosols*. Elsevier.
- [119] Ives K.J., 1960. *Rational design of filters. Proceedings of the Institution of Civil Engineers*. 16(2), 189-193.
- [120] Elimelech M., 1994. *Particle deposition on ideal collectors from dilute flowing suspensions: Mathematical formulation, numerical solution, and simulations*. Separations Technology, 4(4), 186-212.
- [121] Spielman L. A., Fitzpatrick J.A., 1973. *Theory for particle collection under London and gravity forces*. Journal of Colloid and Interface Science, 42(3), 607-623.
- [122] Spielman L.A., 1977. *Particle capture from low-speed laminar flows*. Annual review of fluid mechanics, 9(1), 297-319.
- [123] Happel J., 1958. *Viscous flow in multiparticle systems: slow motion of fluids relative to beds of spherical particles*. AIChE Journal, 4(2), 197-201.
- [124] Prieve D.C., Ruckenstein E., 1974. *Effect of London forces upon the rate of deposition of Brownian particles*. AIChE Journal, 20(6), 1178-1187.
- [125] Nelson K.E., Ginn T.R., 2011. *New collector efficiency equation for colloid filtration in both natural and engineered flow conditions*. Water Resources Research, 47(5).
- [126] Song L., Elimelech M., 1992. *Deposition of Brownian particles in porous media: Modified boundary conditions for the sphere-in-cell model*. Journal of colloid and interface science, 153(1), 294-297.
- [127] Nelson K.E., Ginn T.R., Kamai T., 2013. *Comment on "Extending applicability of correlation equations to predict colloidal retention in porous media at low fluid velocity"*. Environmental science & technology, 47(14), 8078-8079.

BIBLIOGRAPHY

- [128] www.nanora.eu/cori
- [129] Ohno T., Sarukawa K., Tokieda K., Matsumura M., 2001. *Morphology of a TiO₂ photocatalyst (Degussa, P-25) consisting of anatase and rutile crystalline phases*. Journal of Catalysis, 203(1), 82-86.
- [130] Kim C., Lee S., 2014. *Effect of seepage velocity on the attachment efficiency of TiO₂ nanoparticles in porous media*. Journal of hazardous materials, 279, 163-168.
- [131] Thio B.J. R., Zhou D., Keller A.A., 2011. *Influence of natural organic matter on the aggregation and deposition of titanium dioxide nanoparticles*. Journal of hazardous materials, 189(1), 556-563.
- [132] Hackbarth D.A., 1978. *Groundwater temperatures in the Athabasca oil sands area, Alberta*. Canadian Journal of Earth Sciences, 15(11), 1689-1700.
- [133] Drury M.J., Jessop A.M., Lewis T.J., 1984. *The detection of groundwater flow by precise temperature measurements in boreholes*. Geothermics, 13(3), 163-174.
- [134] Drake J., Bradford A., Joy D., 2010. *Application of HEC-RAS 4.0 temperature model to estimate groundwater contributions to Swan Creek, Ontario, Canada*. journal of hydrology, 389(3), 390-398.
- [135] Thurman E.M., 1985. *Amount of organic carbon in natural waters*. In *Organic geochemistry of natural waters* (pp. 7-65). Springer Netherlands.
- [136] Thurman E.M., Malcolm R.L. 1981. *Preparative isolation of aquatic humic substances*. Environmental Science & Technology, 15(4), 463-466.
- [137] Litton G.M., Olson T.M., 1993. *Colloid deposition rates on silica bed media and artifacts related to collector surface preparation methods*. Environmental science & technology, 27(1), 185-193.
- [138] U.S. Environmental Protection Agency, Office of Water (4303T), 2002. *Methods for Measuring the Acute Toxicity of Effluents and Receiving Waters to Freshwater and Marine Organisms*. Fifth edition.
- [139] Amirbahman A., Olson T.M., 1993. *Transport of humic matter-coated hematite in packed beds*. Environmental Science & Technology, 27(13), 2807-2813.
- [140] Instruments, M., 2004. Zetasizer nano series user manual. MAN0317, 1.
- [141] Henry D.C.. 1931, September. *The cataphoresis of suspended particles. Part I. The equation of cataphoresis*. In *Proceedings of the Royal Society of London A: Mathematical, Physical and Engineering Sciences* (Vol. 133, No. 821, pp. 106-129). The Royal Society.

- [142] Masliyah J.H., Bhattacharjee S., 2006. *Electrokinetic and Colloid Transport Phenomena*, Wiley-Interscience.
- [143] Liu X., Chen G. Su C., 2011. *Effects of material properties on sedimentation and aggregation of titanium dioxide nanoparticles of anatase and rutile in the aqueous phase*. Journal of colloid and interface science, 363(1), 84-91.
- [144] Lecoanet H. F., Bottero J.Y., Wiesner M.R., 2004. *Laboratory assessment of the mobility of nanomaterials in porous media*. Environmental science & technology, 38(19), 5164-5169.
- [145] Zhang Y., Chen Y., Westerhoff P., Crittenden J., 2009. *Impact of natural organic matter and divalent cations on the stability of aqueous nanoparticles*. Water research, 43(17), 4249-4257.
- [146] Li Y., Yang C., Guo X., Dang Z., Li X., Zhang Q., 2015. *Effects of humic acids on the aggregation and sorption of nano-TiO₂*. Chemosphere, 119, 171-176.
- [147] Romanello M. B., de Cortalezzi M. M. F., 2013. *An experimental study on the aggregation of TiO₂ nanoparticles under environmentally relevant conditions*. Water research, 47(12), 3887-3898.
- [148] Ren M., Horn H., Frimmel F.H., 2017. *Aggregation behavior of TiO₂ nanoparticles in municipal effluent: Influence of ionic strength and organic compounds*. Water research, 123, 678-686.
- [149] Taurozzi J. S., Hackley V.A., Wiesner M.R., 2011. CEINT/NIST PROTOCOL.
- [150] Thurman E.M., 1985. *Amino acids*. In *Organic geochemistry of natural waters* (pp. 151-180). Springer Netherlands.
- [151] Erhayem, M., Sohn, M. (2014). *Stability studies for titanium dioxide nanoparticles upon adsorption of Suwannee River humic and fulvic acids and natural organic matter*. Science of the Total Environment, 468, 249-257.
- [152] Domingos R. F., Tufenkji N., Wilkinson K. J., 2009. *Aggregation of titanium dioxide nanoparticles: role of a fulvic acid*. Environmental Science & Technology, 43(5), 1282-1286.
- [153] Hajdú A., Illés E., Tombác E., Borbáth I., 2009. *Surface charging, polyanionic coating and colloid stability of magnetite nanoparticles*. Colloids and Surfaces A: Physicochemical and Engineering Aspects, 347(1), 104-108.
- [154] Chibowski E., Holysz L., Terpilowski K., Wiacek A.E., 2007. *Influence of ionic surfactants and lecithin on stability of titanium dioxide in aqueous electrolyte solution*. Croatica Chemica Acta, 80(3-4), 395-403.

BIBLIOGRAPHY

- [155] Worldwide M.I., 2011. *Dynamic light scattering, Common terms defined. Inform white paper*. Malvern Instruments Limited, 2011, 1-6.
- [156] Yang K., Lin D., Xing B., 2009. *Interactions of humic acid with nanosized inorganic oxides*. *Langmuir*, 25(6), 3571-3576.
- [157] Vermeer A.W.P., Van Riemsdijk W.H., Koopal, L.K., 1998. *Adsorption of humic acid to mineral particles. I. Specific and electrostatic interactions*. *Langmuir*, 14(10), 2810-2819.
- [158] Hofmeister F., 1888. *Zur lehre von der wirkung der salze*. *Naunyn-Schmiedeberg's Archives of Pharmacology*. 25(1), 1-30.
- [159] Bradford S. A., Torkzaban S., Walker S.L., 2007. *Coupling of physical and chemical mechanisms of colloid straining in saturated porous media*. *Water Research*, 41(13), 3012-3024.
- [160] Gómez-Merino A. I., Rubio-Hernández F. J., Velázquez-Navarro J. F., Galindo-Rosales F. J., Fortes-Quesada P., 2007. *The Hamaker constant of anatase aqueous suspensions*. *Journal of colloid and interface science*. 316(2), 451-456.
- [161] Chin Y. P., Aiken G., O'Loughlin E., 1994. *Molecular weight, polydispersity, and spectroscopic properties of aquatic humic substances*. *Environmental Science & Technology*, 28(11), 1853-1858.
- [162] Leenheer J. A., Brown P. A., Noyes T. I. 1989. *Implications of mixture characteristics on humic-substance chemistry*.
- [163] Averett R. C., Leenheer J. A., McKnight D. M., Thorn K. A., 1994. *Humic substances in the Suwannee River, Georgia; interactions, properties, and proposed structures* (No. 2373). USGPO; US Geological Survey, Map Distribution.
- [164] Cameron D.R., Klute A., 1977. *Convective?dispersive solute transport with a combined equilibrium and kinetic adsorption model*. *Water Resources Research*, 13(1), 183-188.
- [165] Dunnivant, F. M., Olsen, R. (2007). A simple sand column laboratory exercise to illustrate pollutant hydrology in groundwater systems. *Journal of Geoscience Education*, 55(1), 51-55.
- [166] Bradford S.A., Yates S.R., Bettahar M., Simunek J., 2002. *Physical factors affecting the transport and fate of colloids in saturated porous media*. *Water Resources Research*, 38(12).
- [167] Foppen J. W., Van Herwerden M., Schijven J., 2007. *Measuring and modelling straining of Escherichia coli in saturated porous media*. *Journal of Contaminant Hydrology*, 93(1), 236-254.

- [168] Hoek E.M., Agarwal G.K., 2006. *Extended DLVO interactions between spherical particles and rough surfaces*. Journal of Colloid and Interface science, 298(1), 50-58.
- [169] Bradford S.A., Simunek J., Bettahar M., van Genuchten M.T., Yates, S. R. (2003). *Modeling colloid attachment, straining, and exclusion in saturated porous media*. Environmental science & technology, 37(10), 2242-2250.
- [170] Franchi A., O'Melia C.R., 2003. *Effects of natural organic matter and solution chemistry on the deposition and reentrainment of colloids in porous media*. Environmental science & technology, 37(6), 1122-1129.
- [171] Wang Y., Li Y., Kim H., Walker S. L., Abriola L. M., Pennell, K.D., 2010. *Transport and retention of fullerene nanoparticles in natural soils*. Journal of environmental quality, 39(6), 1925-1933.